Use of small angle X-ray scattering in investigations of leather and the cornea

A thesis presented in partial fulfilment of the requirements for the degree of
Doctor of Philosophy in Engineering at Massey University, Manawatū, New Zealand.

S.J.R. Kelly

2018

Abstract

Collagen is the most abundant protein in the body and the major structural component of skin and the cornea, where it provides strength and is an important physical and chemical barrier against the environment. The biological function of collagen lies predominantly in its mechanical properties where its structural arrangement greatly influences the tissue characteristics. Understanding collagen structure, its properties and how these are affected by processing, is essential for the manufacture of skin products with superior function and when considering collagen in abnormal corneal tissue.

Leather is derived from skins of various animals, providing aesthetically pleasing products that are strong and hard wearing because of their collagen structure. Collagen is comprised of fibrils which have been studied here in leather produced from skins of ovine (sheep), bovine (cattle) and cervine (deer) origins. Small angle X-ray scattering (SAXS) was used to evaluate the collagen fibril structure and alignment in leather, processed normally and by stretch-tanning, along with tear and bend testing. The average collagen fibril direction at standard sampling points in all species was perpendicular to the backbone, with the average fibril orientation relative to the backbone being 44° in cervine, 66° in bovine and 79° in ovine. The orientation index (OI) suggests the relative alignment of the fibrils, where 1 is perfectly aligned and 0 is randomly aligned. The OI was lowest in cervine (0.24), suggesting a more mesh-like arrangement, increasing in bovine (0.38) and highest in ovine (0.44) where fibrils lay more parallel to one another. There was considerable and unpredictable variability in collagen arrangements in each species but a significant difference in tear strength with ovine leather (21 N/mm) being weakest, and cervine leather (53 N/mm) stronger than bovine leather (43 N/mm), making ovine leather not suitable for high value applications like footwear. Previous correlations between leather strength and fibril alignment suggest greater alignment led to greater strength. When fibrils were aligned artificially by stretch-tanning, the OI in ovine leather increased from 0.48 to 0.79 as did the strength from 27 to 43 N/mm, making it comparable to bovine leather strength. Measurements of the bend modulus of stretch-tanned ovine leather, which was stiffer than the non-stretch tanned leather (15 vs. 34 kPa), when conditioned under increasing relative humidity environments, during which water was incorporated into leather's collagen structure, resulted in a 66% reduction in stiffness.

Examination of clinically normal sheep corneas were used to determine effects of common preservatives on collagen structures using SAXS. Compared to the control, frozen cornea, there was a significant increase in the fibril diameter and D-spacing of collagen in corneas stored for 5 days in all the preservatives studied (5% glutaraldehyde, 10% formalin, Triton X and phosphate buffered saline). Corneas from cats with corneal opacities (Florida spots) that were studied using histology, transmission electron microscopy (TEM) and SAXS showed that there was less collagen in the stroma of the lesions. Here collagen fibrils had larger and more variable diameters (32 nm vs. the normal 27 nm), and a greater relative alignment (OI) compared to normal corneas (0.43 vs. 0.29, respectively). These changes explain the opacity of the lesions as corneal transparency depends on regular small fibril diameters which are aligned orthogonally.

The above studies have demonstrated the usefulness of SAXS in characterizing collagen in natural, pathological, and mechanically and chemically altered collagen-based samples.

Acknowledgements

First and foremost I want to thank my supervisor Professor Richard Haverkamp. It has been a great honour to be one of you PhD students. Thank you to my co-supervisors Dr Katie Sizeland and Dr Hannah Wells for showing me the ropes and for your on-going support.

The Australian Synchrotron and the SAXS/WAXS Beamline in Melbourne, Australia have provided a significant portion of the results presented in the publications from this thesis. To the beamline scientists Dr Nigel Kirby, Dr Stephen Mudie and Dr Tim Ryan, you were fundamental in data collection and processing, for that I thank you.

The work on leather in Chapters 3 to 6 was made possible through the support of Dr Richard Edmonds, Dr Geoff Holmes and Dr Sue Cooper at the New Zealand Leather and Shoe Association. Your advice and expertise in the leather industry have been indispensable for these chapters.

Chapters 5 & 6 were supported by Dr Richard Weinkamer, Dr Luca Bertinetti and Prof Peter Fratzl at the Max Planck Institute for Colloids and Interfaces in Potsdam, Germany. Working alongside you has been a memorable highlight. I have appreciated the camaraderie and local expertise of Mrs Ingrid Zenke in using the Nanostar and Mr Klaus Bienert for building a custom humidity cell. In my attempted measurements of leather collagen structures using Raman Spectroscopy, Dr Clemens Schmitt is thanked for his time and curiosity.

In my later work investigating collagen structures in the cornea, presented in Chapters 7 & 8, thank you to Prof Patrick Kelly and Dr Pompeii Bolfa from Ross University School of Veterinary Medicine in St Kitts, West Indies for the collaboration, Dr Fernanda Castillo from the School of Veterinary Science at Massey University for the samples and Ms Jordan Taylor of the Manawatū Microscopy Centre for her assistance in electron microscopy sample preparation and imaging.

For this dissertation I would like to thank my proof readers for their time, interest and helpful comments. Also thanks to the members of my oral defence committee for their insightful questions.

I gratefully acknowledge the funding sources that made my PhD work possible. Thank you to the New Zealand Leather and Shoe Research Association for co-funding the project through the LSRX1301 Ministry of Business, Innovation and Employment grant and to the New Zealand Synchrotron Group for providing travel funding for the various synchrotron trips.

Thank you to Mum, Sean and my friends for your sanity checks and a special thank you to my Dad for all his insights and support.

Contents

List of Figures

INTRODUCTION

Collagen-based materials are fibre composites with a hierarchical structure. Their exceptional mechanical properties are believed to be due to functional structural adaptations at all levels of hierarchy. Understanding natural collagen structures and how they impart particular characteristics in native tissue and in leather manufacturing will provide insights into how desirable properties can be artificially enhanced by mechanical and chemical processing.

The research aims for this dissertation were to understand how collagen arrangements influence mechanical properties in leather and optical properties in the cornea. The following research questions were established to enable these to be met:

- What is the variation in collagen alignment and strength across the skins used for leather and does this change between species? Are the variations significant enough that certain species or regions within a skin are better suited to specific applications? Findings presented in Chapter 3.
- Highly aligned collagen fibres have been correlated with leather of high strength. In weak leather the alignment is low which poses the question: is it possible to artificially align collagen fibres in skins known to produce weak leather and what effect does this have on the leather strength? Findings presented in Chapter 4.
- Strength and stiffness are intertwined properties. During stretch-tanning we increase the leather's strength while also increasing the stiffness. Water is known to mitigate stiffness in collagen-based materials. What is the effect of water on leather stiffness? Findings presented in Chapters 5 & 6.
- Corneal collagen has a very precise arrangement allowing for optical transparency. Examined tissue has often been preserved which has a notable effect on tissue transparency. How do common preservatives interfere with the collagen structure in the cornea? Findings presented in Chapter 7.
- Tropical Keratopathy is a corneal disease that causes opaque lesion in the cornea. Can we characterize the collagen structures in both normal and opaque sections of a cornea? Are the collagen structures comparable and can structural changes be linked to opacity? Findings presented in Chapter 8.

These questions have formed the research incentives behind the publications presented in this thesis. The approach to answering these questions utilized a combination of techniques to form structure/function relationships in leather and the cornea. X-ray techniques for small and wide angle X-ray scattering and transmission electron microscopy have provided nano-structural information, while industry defined mechanical testing standards for leather were used to measure mechanical performance.

Chapter 1. Collagen Structure and Function

Collagen is the most abundant fibrous protein in animals where it provides strength and structure to a variety of soft and hard tissues. The key structural elements of collagen are its component fibres which are anisotropic, that is, they can impart different properties to tissues depending on the manner in which they are arranged[1, 2, 3]. When all are of uniform size, they confer optical transparency to the cornea[4], if aligned side-by-side they provide exceptional strength as in tendon and leather[5, 6]. When randomly arranged they provide resistance to tear propagation and flexibility for example in skin[7]. In the following two chapters, the collagen structure of the skin, leather and the cornea are reviewed and the experimental methods used to analyse collagen structure are described.

Collagen Structure

About one third of the protein in the body consists of collagen[8, 9] which is the major structural component of many tissues including tendons, ligaments, skin, the cornea, cartilage, bone, dentin and blood vessels[10]. There are 28 different types of collagen, each having distinct polypeptide chain components. The most abundant is type I collagen which is responsible for strength and flexibility in the skin and leather[6, 11-16], and the structure and optical transparency of the cornea[4, 17, 18]. The amino acid sequence and fibril and fibre structure of type I collagen is described below.

The Collagen Molecule (Tropocollagen)

Collagen is composed of polypeptides containing repeating units of three amino acids ($(Gly\text{-}Xx\text{-}Yy)_n$), primarily glycine (Gly) with proline, hydroxyproline or alanine[16, 19]. These repeating units (n = 337 to 343) are arranged sequentially in a left hand spiral to form an alpha (α) chain. Each α chain is tightly coiled (3.3 amino acids per twist) and held in this position by hydrogen bonds between the more peripheral amino acids[20] (Figure 1). Glycine with its small side chain, a single hydrogen molecule, is located at the centre of the helix.

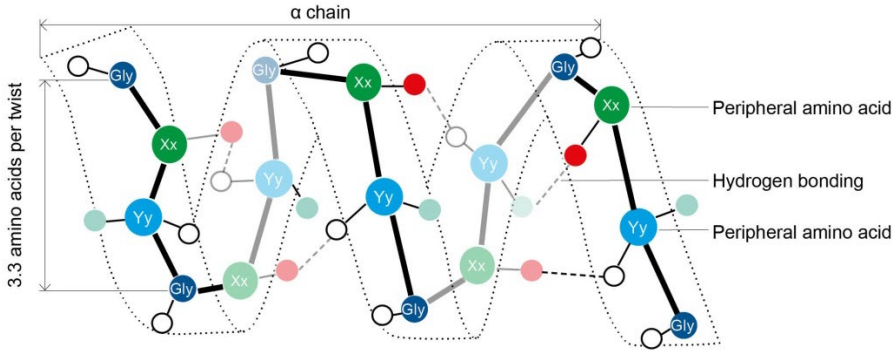

Figure 1. Hydrogen bonding between sequential peripheral amino acid side chains (Xx, Yy) maintaining the helical structure of the alpha (α) chain.

Hydrogen bonding between amino acids in adjacent α chains and with surrounding water molecules results in three α chains coiling together to form a right handed triple helix which is the basic collagen molecule (also known as tropocollagen). Each collagen molecule contains 1050 amino acids[21] and is approximately 300 nm in length with a diameter of approximately 1.6 nm[22, 23] (Figure 2).

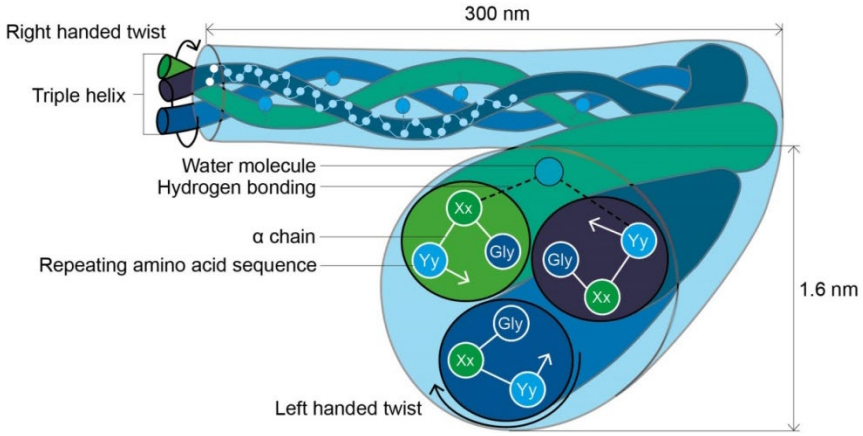

Figure 2. The collagen molecule triple helix. There are three α chains comprising around 340 repeating amino acid sequences $((Gly\text{-}Xx\text{-}Yy)_n)$ wound together in a right handed twist. The small glycine (Gly) amino acid is located in the centre of the helix with larger amino acids in the Xx and Yy positions. Molecules are about 1.6 nm wide and 300 nm long. Hydrogen bonds between amino acid side chains (Figure 1) and hydrogen bonds with surrounding water molecules maintain the structure.

Collagen Fibrils

Collagen molecules are secreted into the extracellular matrix[24] where they self-assemble[25] side-by-side to form collagen fibrils of around 50 – 200 nm in diameter (Figure 3). Although the collagen molecules lie parallel to the length of the fibril they are aligned in a staggered pattern, each molecule being offset from its neighbour by approximately 67 nm. The collagen molecules are held together in this staggered pattern by aldol cross-linkages of lysine, hydroxylysine or arginine at the ends of the collagen molecules[26-28]. The areas of the collagen fibril where there is complete overlap of the adjacent component collagen molecules appear as dark bands microscopically, while areas where there is no overlap between some molecules appear as pale bands. The distance between a dark band, that is the area where all collagen molecules in a fibril overlap, and a pale band, where all the collagen molecules do not overlap, is termed the D-spacing[29, 30] (or D-period). This varies with the types of amino acids in the fibrils and can be used to characterise the different types of collagen. Typically type I collagen in the skin normally has a D-spacing of 67 ± 0.5 nm[31].

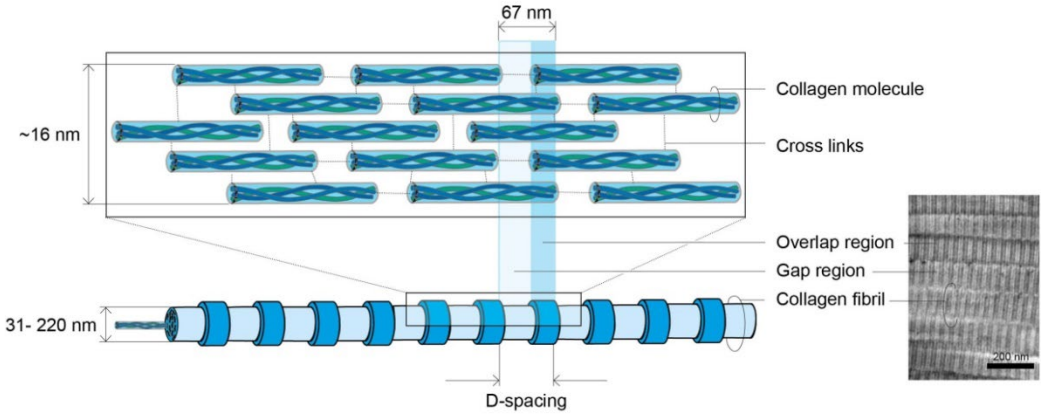

Figure 3. Collagen fibril assembly. Cross links between collagen molecules cause a staggered arrangement creating overlap and gap regions resulting in the characteristic banding pattern along the collagen fibril when viewed microscopically. The combination of an overlap and gap region is termed the D-spacing which is approximately 67 nm in type I fibrillar collagen.

The D-spacing is also influenced by hydrogen bonding between amino acids in the fibrils and the surrounding water molecules, hence the hydration state of the collagen. In this way the D-spacing in type I collagen found in the skin can vary from approximately 68 nm when the tissue is fully hydrated to 64 nm when dehydrated[32]. A greater variation in D-spacing exists across all type 1 collagen tissue, such as cornea, tendon and bone[33]. The diameters of the collagen fibrils vary, depending on the number of collagen molecules stacked side-by-side, influencing the properties of the tissues in which they are found: corneal collagen fibril diameter is around 31 nm for optical transparency[4] while fibrils in tendons are larger at 31 to 220 nm for elasticity and strength[34].

Collagen Fibres

Collagen fibres are approximately 10 µm in diameter (in leather[35]) and are made up of bundles of fibrils that are arranged in parallel. The ultimate mechanical and transparency properties of tissue containing collagen fibres are partly determined by the ways in which fibrils are arranged[5, 36-39]. The distances separating the fibrils in a collagen fibre are largely determined by the matrix that surrounds them. This matrix contains proteoglycans that regulate the water content and also attach to the fibrils in the gap region (Figure 4). Electrostatic forces between proteoglycans lead to the fibrils being maintained at optimal distances for transparency, as in the case of the stroma, and mechanical strength in tendons, skin and other connective tissue[4].

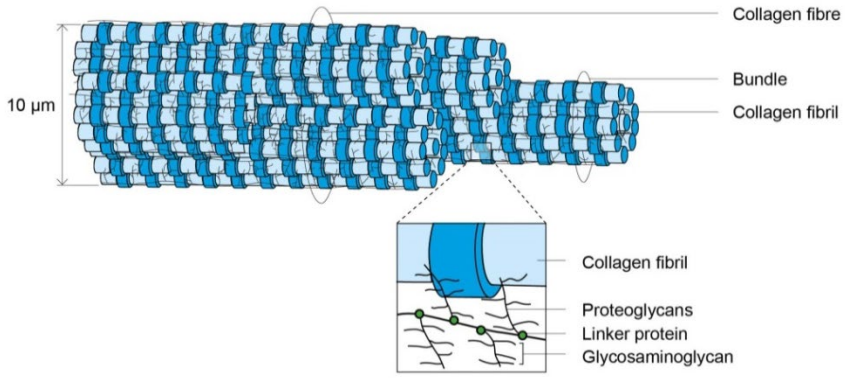

Figure 4. Collagen fibrils bundled together into fibres through cross-linkages with proteoglycans in the extracellular matrix.

Mechanical Properties

The properties of tissues containing collagen vary according to the arrangement of their collagen fibrils and fibres. For example, collagen fibres are found parallel to the direction of force in tendons, which provides maximal physical strength and resistance to rupture. At the same time the collagen fibres can act as shock absorbers, dissipating applied forces to some extent as fibrils and fibres slide passed one another. In the skin, the collagen fibres are generally more randomly arranged providing mechanical resistance to tearing in multiple directions. The ability of the fibrils and fibres to slide passed one-another in all directions also gives flexibility[16].

The number of cross-links between adjacent fibrils determines their ability to slide passed one another. More cross-linking between fibrils increases the stiffness of a tissue while less cross-linking facilitates sliding and gives flexibility and elasticity before permanent deformation occurs[40]. Cross-links can be artificially created

between collagen molecules[41-44] with aldehydes being widely used in tanning to impart mechanical strength to leather products[45] and in histology to impart rigidity to soft tissue samples[46].

The ability of collagen fibrils to slide passed one another depends on the amount of contact they have with one another. The more contact a fibril has with its neighbour, the higher the internal friction generated when forces are applied and fibres are forced to slide passed one another. A parallel arrangement, or high relative alignment, of fibres generates the greatest internal friction due to high fibril-to-fibril contact. This means that tissues with highly aligned fibrils and fibres, such as tendon, have greater longitudinal strength due to both the physical strength of the collagen itself and also the internal friction between adjacent fibres. In the leather industry, areas of skin with highly aligned collagen are selected for tanning and manufacture of leather products that need to be able to resist linear forces such as belts, straps and harnesses[6, 47].

Tissues with collagen fibrils that have a more random arrangement, or low relative alignment, can be more easily stretched in all directions and therefore are more flexible. Similarly, the low relative alignment means the tissue is more resistant to tearing forces in any direction. Areas of skin that contain less aligned collagen fibres are selected for leather products that need to be flexible and tear resistant, for example gloves and clothes[7]. The alignment of collagen in different animals used in leather production varies, with cattle generally having greater alignment of collagen in their skins than sheep[47].

Various methods have been developed to measure the mechanical properties of skin.

Stress and Strain

Application of force (stress: tensile and/or compression) to materials while continuously recording the strain (deformation) provides insights into the materials mechanical properties. Stress (σ) represents an applied force over an area, while strain (Ɛ) represents the length of elongation relative to the original length of the material (Equation 1).

$$\sigma = \frac{F}{A} \quad ; \quad \varepsilon = \frac{(L - L_o)}{L_o}$$

Equation 1. Stress (σ) and strain (Ɛ) where F is the applied force, A is the area over which the force is applied, L is the length of elongation and L_O is the original length of the sample.

A plot of stress versus strain reveals the thresholds for elastic and plastic deformation by the yield strength and fracture point respectively, as well as other parameters such as the Young's modulus, (discussed below) and ultimate strength that is the maximum force the sample can withstand.

Analysing changes in collagen structure under varying stress has provided important information on how forces are dissipated by collagen-based materials (Figure 5). Initially, mechanical stress applied to a collagen containing tissue results in elastic deformation where knots in fibrils (so called fibrillar crimps which are seen to a greater extent in tendon due to an additional undulation of molecules[48]) are straightened out. This dissipates some of the applied strain resulting in only a slow increase in stress seen at the start of the stress-strain curve, also known as the heel region (Figure 5 (a-b)) which is characteristic of entropic elasticity. After the crimping is removed, additional stress causes fibres to rotate and align in the direction of the strain[49]. The

greater order/alignment of fibres relative to one another results in a more tightly packed fibre arrangement (Figure 5 (b-c))[2]. This creates a greater resistance to stress due to the greater internal friction between the more aligned fibres and the stretching of the cross-links resulting in linear elastic behaviour[50]. The 'yield strength' is the maximum stress that can be applied before the collagen structure is permanently altered, that is, with stresses up to the yield strength the collagen remains elastic and can return to its original shape when the stress is removed. Beyond this elastic deformation phase the effects of applied forces are no longer reversible and plastic deformation occurs. Here the collagen fibrils become stretched as a result of inter- and intra-fibrillar sliding with permanent elongation of the helical structure shown by an increase in the D-spacing (Figure 5 (d)). Above the ultimate strength, the fibrils and fibres rupture and ultimately the tissue fails at the fracture point (Figure 5 (e)).

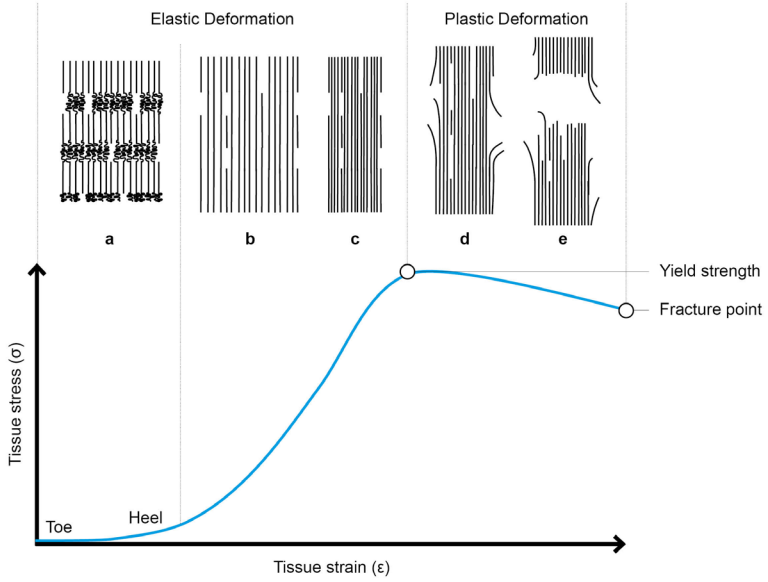

Figure 5. Stress – Strain curve for a relatively aligned collagen-based tissue during five stages of tensile loading and their relation to a schematic representation of the collagen fibres over the two major stages of elastic and plastic deformation. Applied strain is in the vertical direction. (a) Material at rest; (b) after fibril crimps are removed, marking the end of the heel region, the collagen fibres begin to straighten in the direction of strain; (c) fibres continue to straighten as more fibres orientate along the axis of strain making the material more tightly packed; (d) fibres begin to stretch; (e) fibres fracture.

Flexibility (Young's Modulus)

The Young's modulus, also referred to as the 'elastic' or 'tensile' modulus, is an intrinsic property of a material, which is a measure of material flexibility along the axis of strain in Pascal's. This mechanical property is defined as the relationship between stress and strain in the linear elastic region of the stress-strain curve according to the factor of proportionality in the linear region under bend forces (Equation 2).

$$\frac{dF}{dx} = \frac{4\,E\,a^3 b}{L^3}$$

Equation 2. Young's Modulus (E) for a beam where L is the length of the beam, F is the force applied to the middle of the beam, a and b are the width and height of the beam, and x is the beam deflection due to the force applied.

The Young's modulus of a material tells us how much the material can be expected to deform along an axis when opposing forces are applied. Typical Young's modulus values range from > 1 GPa in flexible materials like

rubber and low-density polyethylene, to values of > 10 GPa in stiffer materials like wood and bone. The Young's modulus for collagen has been studied extensively under various methods resulting in a range of values for the same tissue. For example, hydrated individual fibrils have a Young's modulus of approximately 0.9 GPa[51], collagen from rat tail tendon has a range of values from 3 - 20 GPa and bovine Achilles tendon of 2 - 7 GPa, depending on the experimental method used, cross-linkages between fibrils and tissue hydration state[14, 52]. Flexural testing using a three-point bend test, applying a force perpendicular to ovine leather samples reveals its anisotropic two layer structure where the Young's modulus values vary depending on the sample orientation. The difference between the Young's modulus grain side up and corium side up is approximately 1.5 GPa[16, 53] suggesting the grain to be more resistant to compression and/or the corium being less resistant to tension.

The linear portion of a stress-strain curve, when bend forces are applied, is used to determine the materials bend/ flexural modulus (Equation 3). Data is collected from a three-point bend test, applying forces perpendicular to the sample (technique discussed in Section 2). The bend modulus is a measure of the materials stiffness under flexural deformation where the materials surface is submitted to the greatest values of stress.

$$\mathrm{E_{bend}} = \frac{dF}{dx}\,\frac{1}{4w}$$

Equation 3. Bend Modulus (E_{bend}) F is the force applied to the middle of the beam; w is the width of the beam, and x is the beam deflection due to the force applied.

Poisson's ratio

When comparing a material's ability to resist distortion under a mechanical load, rather than altering its volume, Poisson's ratio offers a measure to compare performance when a material is strain elastically under tensile forces. Materials under tensile forces experience elongation in the direction of the applied force and often contraction in the orthogonal direction, hence a negative strain in the direction perpendicular to the elongation strain. This relationship is summarized into the Poisson's ratio (Equation 4) which can help to differentiate between materials that are isotropic or anisotropic (Figure 6). In a stable isotropic material, where the material has the same properties regardless of measurement direction, we expect a theoretical upper limit of 0.5 for Poisson's ratio with a lower limit of -1. When a material has a negative Poisson's ratio they are regarded as Auxetic materials since they become thicker perpendicular to the applied force. In an anisotropic material, where there are direction specific properties, it is possible for the Poisson's ratio to exceed 0.5. However anisotropic materials can still exhibit a Poisson's ratio below 0.5[54].

$$\nu = -\frac{\varepsilon_{\,\mathrm{lateral}}}{\varepsilon_{\,\mathrm{axial}}} = \frac{\dfrac{\mathrm{L_y} - \mathrm{L_{o,y}}}{\mathrm{L_{o,y}}}}{\dfrac{\mathrm{L_x} - \mathrm{L_{o,x}}}{\mathrm{L_{o,x}}}}$$

Equation 4. Poisson's ratio (ν) where $\varepsilon_{lateral}$ is the strain in the direction of the applied force, ε_{axial} is the strain orthogonal to the applied force, L_y is the length after elongation, $L_{o,y}$ is the original sample length in the lateral direction, L_x is the length after contraction and $L_{o,x}$ is the original sample length in the axial direction.

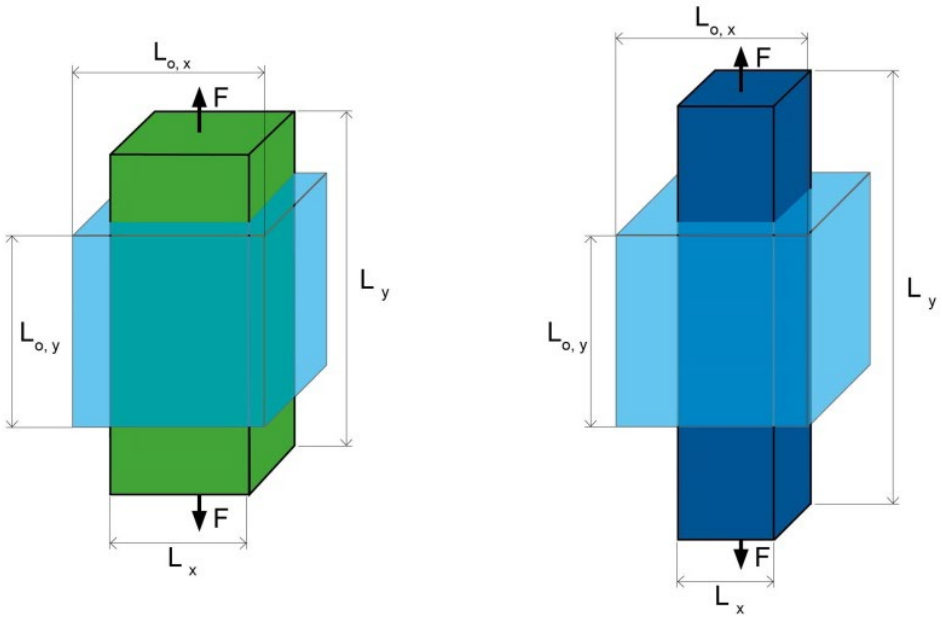

Figure 6. Isotropic (*left*) and anisotropic (*right*) materials ($L_{o,x}$, $L_{o,y}$) under tensile forces (F) resulting in elongation, lateral to the applied force direction, L_y and contraction orthogonal to the applied force in the axial direction, L_x.

Collagen-based materials are anisotropic in that the properties are direction specific, tailored to suit their function in living tissue, for example, tendons require direction specific strength and elasticity for performance. Since collagen is anisotropic, it is possible to get a Poisson's ratio of > 0.5, suggesting the volume of the collagen fibrils decreases with strain. A range of collagen-based materials have been investigated. The Poisson's ratio of the individual collagen fibrils, when the material is under tension, have been measured and values have been determined for bovine pericardium ($\nu = 2.1$)[55], human patella cartilage ($\nu = 1.3$)[56] and tendon fascicles ($\nu = 4$)[57].

Skin

The skin is a major organ in the body with three main functions: protection, temperature and moisture regulation and sensation[58]. It consists of three main layers, the epidermis which is the outer most layer, the dermis and the subcutaneous layer (Figure 7). The epidermis is the thin tough outer layer which is composed mainly of keratinocytes providing waterproofing and some protection for the thick fibrous dermis layer. The dermis is mostly made up of type I collagen and elastin and is the main protection for the body against external trauma. The subcutaneous layer sits below the dermis and enables the skin and underlying muscles to move independently[59]. It also acts as a site of energy storage (fat), to insulate the body, and it is the site where blood vessels, nerve endings and hair follicles are found.

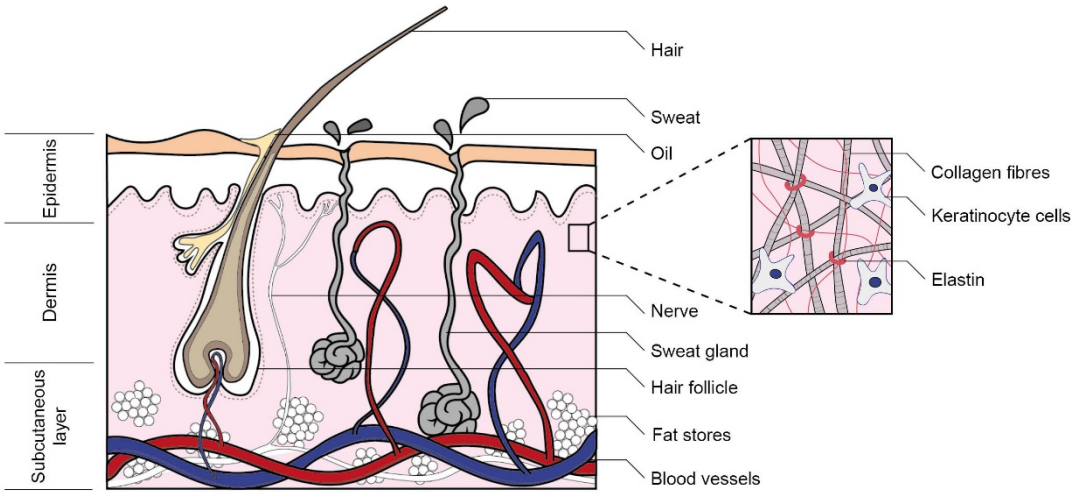

Figure 7. Three primary layers of skin: the epidermis, dermis with its collagen and elastin network and subcutaneous layer embedded with blood vessels, hair follicles, sweat glands and fat.

Mechanical Properties of Skin

The protective function of skin is largely provided by its mechanical properties of flexibility and strength. Flexibility is a material's ability to reversibly deform in response to an applied force while strength is a material's ability to withstand an applied force until it ruptures. In skin, flexibility and strength are mainly due to interweaved and interlaced collagen and elastic fibres in the dermis[60, 61]. The elastin fibres contribute primarily to the elasticity of the skin while the collagen primarily provides strength. Tear resistance is an important measure of skin strength and depends on collagen fibre arrangement in the dermis. It indicates the ability of skin to resist an introduced tear front under tensile loading[62]. Tear resistance is widely used in the leather industry as a measure of the strength of various areas of skin from different species following tanning.

Leather

Tanning is the process used to transform skins into leather that has greater strength and is suitable for protective and hardwearing products, such as shoes, saddles and harnesses. Tanning can also impart flexibility to the final leather product making it more suitable for products such as gloves. During the tanning process, various mechanical and chemical processing steps are used to preserve the collagen network responsible for strength and flexibility, while some skin components are removed. The latter include proteins, and fats and carbohydrates that can be acted upon by spoilage bacteria leading to putrefaction and undesirable changes to the collagen network. Leather consists mainly of the collagen rich dermis that remains after tanning. It is characterized by two structurally different layers, separated by a transition zone (Figure 8). The upper surface is called the grain, which consists of small (0.1 µm diameter) densely packed collagen fibres that represent the remains of the sub-epithelial skin tissues and give leather its surface texture and appearance. Below the grain is the corium which is made up of larger (100 µm diameter) collagen fibres and is largely responsible for the bulk strength of leather[63]. The fibrils that make up these two distinct layers are similar, and it is the way these fibrils assemble into fibres that accounts for the differences in the physical properties of these layers[16].

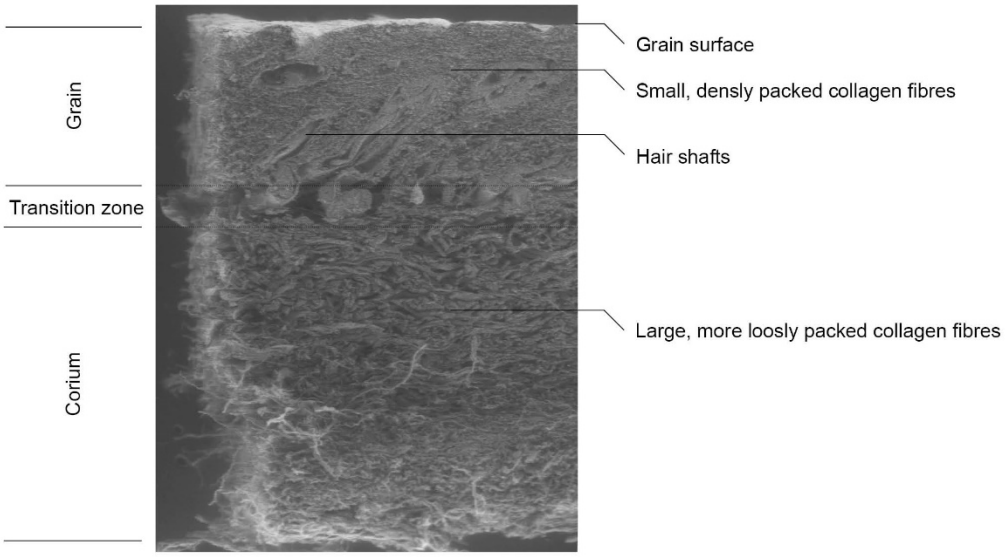

Figure 8. A cross section of ovine leather showing two distinct layers, separated by a transition zone: the grain with small densely packed fibres and the corium with larger, more loosely packed fibres.

Leather Production

To create leather with desirable properties, targeted chemical processing steps are used in tanning to alter specific skin components (Table 1). For example, the addition of calcium hydroxide during the unhairing stage targets cystine bonds found exclusively in keratin, allowing just the hair to be removed[64]. Approximately 70% of the protein in skin is made up of type I collagen and it is the principal concern of the tanner to leave this collagen intact while removing the remaining proteins and other skin structures[65, 66].

Table 1. Bovine skin composition, the relevant tanning stage and the resulting composition of hides at the official sampling position (OSP). Created from Sharphouse et al (1971)[67].

Skin Component	Tanning Stage	Composition of Hide at the OSP
Collagen	Entire process	70%
Keratin	Unhairing	2%
Albumins/Globulin	Liming, De-liming and Bating	1%
Glycoproteins/ Proteoglycans	Fleshing, Liming, De-liming and Bating	1%
Fats	Fleshing, Liming, De-liming and Bating	2%
Water	Skin preparation and Curing	24%

Leather Production Process

Beamhouse operations, that is all the processes from curing to tanning, are reviewed below.

Curing. Since slaughterhouses and tanneries are usually at separate sites, skins are salted to prevent putrefaction during storage before tanning. This curing process results in loss of water from the skins, which then need to be rehydrated by soaking in water. The process also helps to remove surface contaminants such as soil.

Tanning.

Step 1: **Liming and Unhairing.** This step is to remove the epidermis and the other structural proteins, mainly hair composed of keratin. During unhairing the skins are immersed in an alkaline solution, typically lime

(calcium hydroxide) or soda ash (sodium carbonate), which causes chemical degradation of the hair shaft. More specifically the chemicals break down cystine linkages, a primary structural component of keratin, which allows the hair to be released from the hair follicle. The liming stage also results in the removal of unwanted material, such as grease and fats, and the matrix between collagen fibres which leads to an influx of water into the skin. Penetration of water into the collagen fibres causes them to swell and burst, thereby exposing collagen fibrils to subsequent chemical treatments resulting in better tanning and dyeing.

Step 2: Fleshing. Residual flesh is removed from the skin with a fleshing machine that helps to mechanically expel excess water from the skin and at the same time even out variations in thickness. Skins of even thickness are important for the later processing stages to allow for uniform chemical penetration.

Step 3: Deliming and Bating. Deliming is performed by adding acid salts to neutralize the alkaline solutions in the skins. The lowered pH encourages rapid protonation of basic groups in the collagen fibres and further opening out of the collagen structure. The lower pH also facilitates bating which is the addition of proteases to remove collagen fibrils that have degraded and disintegrated. This leads to the production of a softer leather[68].

Step 4: Pickling. The skins are acidified in citric acid that stops the bating and facilitates the penetration of mineral tanning agents added in the next step.

Step 5: Tanning. This involves the addition of tanning agents that often cause complex chemical reactions that lead to crosslinking of collagen fibrils to produce the final leather product. There are a variety of tanning agents available, with each producing characteristic cross-linkages. These agents stabilize the collagen and prevent its degradation while at the same time maintaining flexibility and introducing colour and texture. The major tanning methods, and in turn resulting leather types, are listed below:

- Vegetable-tanned leather is produced with tannins extracted from vegetable matter. It is not stable in water and tends to discolour as well as lose its flexible, smooth texture if soaked and left to dry.
- Chrome-tanned leather is made by adding chromium sulphate and other chromium salts which produce a more supple and pliable leather when compared to vegetable tanned leather. This leather is known as wet blue, as the chromium imparts a blue colour.
- Aldehyde tanned leather is produced by the addition of glutaraldehyde or oxazolindine compounds and is referred to as wet white leather due to its pale cream appearance. Marketed as chrome-free leather, it can typically be found in infant shoes and car interiors. Under the aldehyde tanned leather category there is a further classification depending on the source of the tannin. This is as follows:
    - Formaldehyde tanned leather is produced by a form of aldehyde tanning which is beginning to be phased out due to people's sensitivity to formaldehydes and toxicity concerns.
    - Brain tanned leather undergo a labour intensive process during which animal brains are emulsified to extract oils used as the tannin. These leathers are known for their exceptional softness and their ability to be washed.
    - Chamois leather is processed in a similar way to brain tanned leather but cod liver oil is used as the tannin.

Step 6: Neutralizing and Dyeing. Here a sodium bicarbonate solution is applied to raise the skin pH to neutral, which enables the leather dyes to more readily penetrate the leather and ensure more even colouration. Leather dyes are anionic and come in a variety of colours. The intensity and evenness of the final colouration can be varied by pre-treatment with various fixatives and multiple applications of different dyes.

Step 7: Drying. Removing the remaining water in the leather facilitates the stabilization of the chemical properties of the leather. Drying can be achieved through toggling where skins are stretched over a vertical frame and allowed to either air dry in a well-ventilated room or in a blast oven for a short period of time.

Step 8: Finishing. Once most of the water has been removed from the leather, the final stages of the process can begin. The leather is re-dampened and left to equilibrate at room temperature. When a residual moisture content of around 10-20% is reached, the leather is staked by passing it through a set of weighted rollers. Staking relaxes the structure by loosening any tight fibres and softens the leather. Surface coatings can then be applied to improve the colour or even out the texture.

Mechanical Properties of Leather

Various mechanical characteristics of leather have been defined in a series of ISO Standards creating a normalized method for comparing properties of leather between species (Table 2).

Table 2. The mechanical characteristics of bovine and ovine leather at the official sampling position (OSP).

Parameter	Bovine Leather at the OSP	Ovine Leather at the OSP	Reference
Tear strength (N/mm)	63	20 - 40	[69]
Tensile Strength (N/mm^2)	22	10	[70, 71]
Young's Modulus (GPa)	10	2	[72, 16]
Orientation Index	0.49	0.42 - 0.46	[47]
D-spacing (nm)	63.5	64.2	[47]
Fibril diameter (nm)	59 - 62	61 - 63	[69]
Fiber diameter (μm)	0.1 (grain) 100 (corium)	0.1 (grain) 100 (corium)	[35]

Cornea

The cornea is the outer clear layer of the eye that meets the surrounding opaque sclera at a region called the limbus. The cornea is around 0.5 mm thick and performs a number of functions including protection and focusing light onto the lens and retina for vision. These functions are intimately related to the macro- and microscopic structure of the cornea that are described below.

Cornea Structure

The cornea is made up of five parallel layers (Figure 9). The outermost is the epithelium which is coated in a tear film and consists of around 6 to 12 layers of epithelial cells. Beneath, and supporting the epithelium, is Bowman's layer which is made up of various types of collagen (types I, III, V and VII). Bowman's layer merges with the stroma which is a dense layer of type I collagen making up 90% of the thickness of the cornea. On the inside of the cornea, against the vitreous humor in the anterior chamber, is Descemet's layer which is a thin layer of connective tissue and an endothelium, a single layer of non-dividing cells that maintains the hydration status of the cornea.

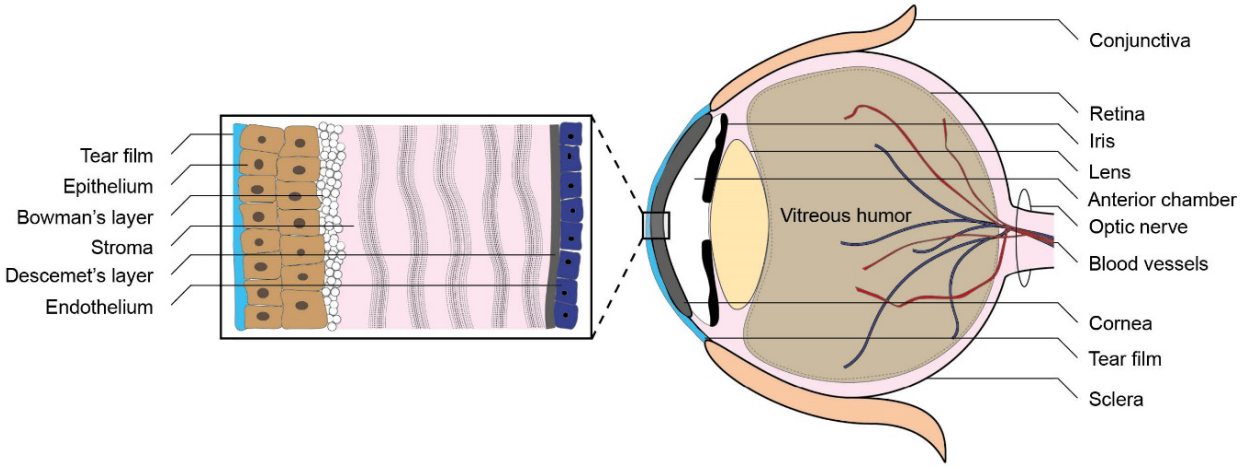

Figure 9. A cross section of the eye showing the location of the cornea, anterior chamber, vitreous humor and sclera. The cornea is composed of five parallel layers, from the outer most epithelium to the deeper Bowman's layer, stroma, Descemet's layer and endothelium.

Epithelium

As the outer most layer of the eye, the epithelium forms a barrier between the environment and the inner eye structures. It is also important for absorbing ultraviolet (UV) radiation, protecting the underlying structures from the harmful effect of UV rays[73, 74]. The epithelium is about 50 µm thick and consists of several layers of rapidly growing and easily regenerated epithelial cells which are anchored to Bowman's layer.

Bowman's Layer

Bowman's layer lies between the epithelium and the underlying stroma. It constitutes a 10 µm thick layer of randomly oriented collagen fibrils that merge with the collagen lamellae of the stroma and anchor the overlying epithelial cells.

Stroma

This thick (about 0.2 mm) fibrous layer consists of collagen fibrils (mainly type I but also some type V) and an inter-fibrillar matrix consisting mainly of proteoglycans (PGs) (Figure 10a) which are produced by keratocytes that are interspersed between lamellae (collagen fibrils arranged in flat sheets). The keratocytes can also repair damaged tissue by changing into fibroblasts which replace damaged tissue with scar tissue[75]. The lamellae are made up collagen fibrils that lie parallel to one another in sheets that then interweave and interlace with adjoining lamellae (Figure 10). There are over 300 layers of lamellae in the stroma[17] with most interweaving found in the anterior cornea, where the stroma inserts into the Bowman's layer. It is thought that this increase in interweaving contributes to the stability and shape of the anterior cornea[76, 77]. In cross-section, the collagen fibrils within the lamellae have a quasi-regular hexagonal lattice arrangement with a centre-to-centre interfibrillar distance of 40 to 65 nm[78] (Figure 10b).

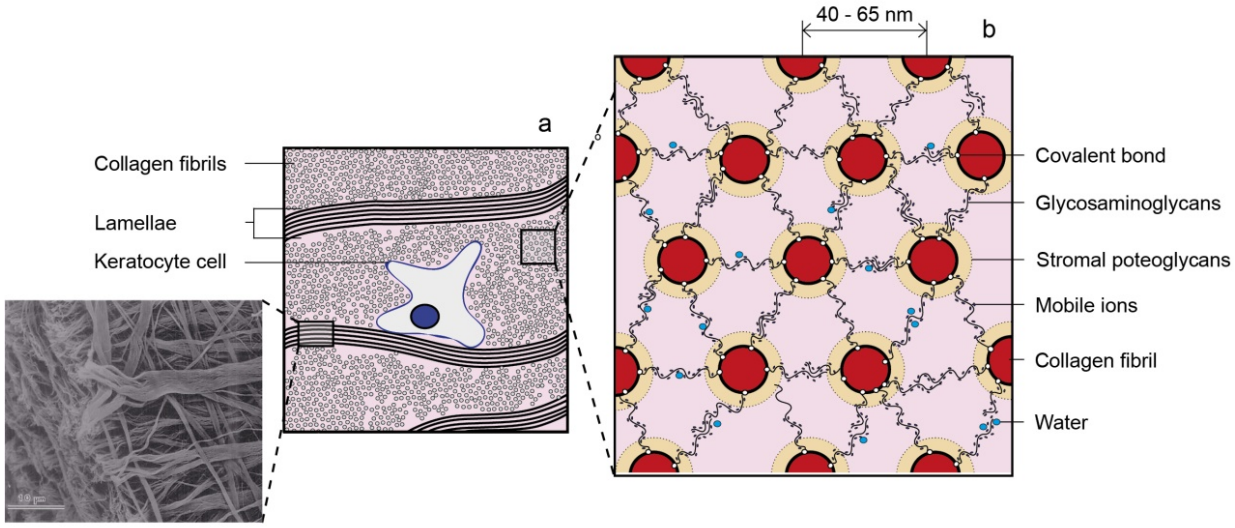

Figure 10. (a) Stroma collagen fibrils organized in parallel arrays in lamellae seen in cross section and transverse section. Keratocytes are interspersed between adjacent lamellae. Image of collagen fibril arranged into lamellae in the human cornea (taken from Komai and Ushiki 1991[79]). (b) Collagen fibrils seen in cross section are arranged in a quasi-hexagonal lattice by ionic forces between fibrils, proteoglycans, and water and ions in the matrix.

The regular spacing of the fibrils depends on complex ionic forces between adjacent fibrils and also between the fibrils and the proteoglycans in the matrix (PGs)[80, 81, 82]. These forces are influenced by the hydration state of the stroma. Proteoglycans and ions in the matrix create an osmotic pressure which draws water into the stroma from tears and the anterior chamber. The hydration state, however, ultimately depends on active transport mechanisms in the endothelial cells which effectively remove water from the stroma[83]. Disruption of the hydration control mechanisms results in fluid accumulation in the stroma that disrupts the quasi-regular hexagonal lattice which is required for optical transparency[83].

Descemet's Layer

This thin layer, 8 to 10 µm thick, provides a barrier between the anterior chamber of the eye and the cornea. It consists of type IV and VIII collagen and supports the endothelium.

Endothelium

The endothelium is a single layer of non-dividing of cells which controls the exchange of ions and water between the cornea and the vitreous humor. It maintains the cornea in a slightly dehydrated state which is important for the optimal spacing of collagen fibrils and transparency[84].

Properties of the Cornea

The collagen of the cornea provides support and maintains the cornea in the shape required to focus light onto the retina with minimal scatter[85]. At the same time, it prevents changes in the shape when the extra ocular eye muscles exert forces on the globe during eye movement.

Transparency

The cornea must be transparent to allow light to pass onto the retina with minimal reflection and refraction. The epithelium is transparent because the refractive indices of the cytoplasm and cell organelles are within a

range that does not produce scattering of light. This is due to the presence of specialized crystalline proteins and high levels of enzymes such as aldehyde dehydrogenase and transketolase in the cytoplasm of the epithelial cells[86]. The transparency of the stroma is mainly due to the precise arrangement of its component collagen fibrils [78] which comes about because of ionic forces between adjacent fibrils, and between fibrils and the proteoglycans and water molecules in the matrix[80].

Collagen Arrangement for Transparency

The collagen fibrils found in the stroma of the cornea are much smaller and have more uniform diameters and D-spacing than those found in other areas such as the skin and tendons (approximately 31 to 34 nm and 65 nm respectively)[17, 87]. Although it has been calculated that 95% of incident light is transmitted through the cornea, how these light waves pass through the myriad of fibrils in the cornea is unknown[4]. It is known, however, that the size and spacing of the corneal stromal collagen fibrils is critical for transparency. It is thought that fibril diameters need to be constant to ensure that there is perfect destructive interference between incident light and the light that encounters fibrils and is reflected (back-scatter)[4]. Also, the distances between adjacent collagen fibrils need to be restricted, with the stromal fibrils having a short-range order[4] (Figure 11).

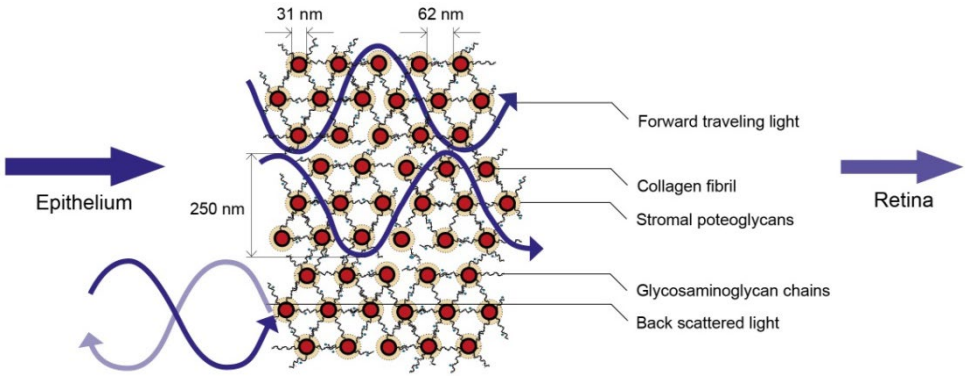

Figure 11. Collagen lamellae short-range order for transparency of visible light where all fibrils have the same diameter of about 31 nm and no fibrils are closer than 62 nm from centre-to-centre. Incoming light is traveling from left to right with a wavelength of 500 nm.

Where there is damage to the epithelium or endothelium and Descemet's layer, water flows into the cornea (oedema) and disrupts the normal interfibrillar distances with a loss of transparency and resulting in opacity of the cornea (Figure 12).

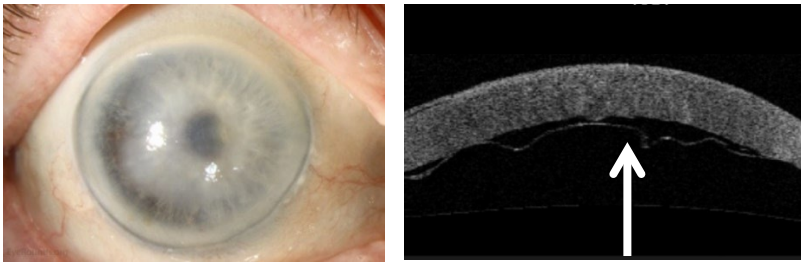

Figure 12. Corneal oedema in a human after the Descemet's layer and the endothelial cells that control stromal hydration have been detached (indicated by the white arrow) and is no longer functional. Photograph by Brice Critser from the Department of Ophthalmology at the University of Iowa.

Chapter 2. Characterizing Collagen Structures

Collagen is the most abundant protein in mammalian bodies and its mechanical properties are largely due to its hierarchical structure (Figure 13). The component amino acids of collagen are assembled to form triple helices that combine in a staggered array to form fibrils that are bundled together to form fibres. To thoroughly evaluate collagen's hierarchical structure and properties, analytical techniques are required.

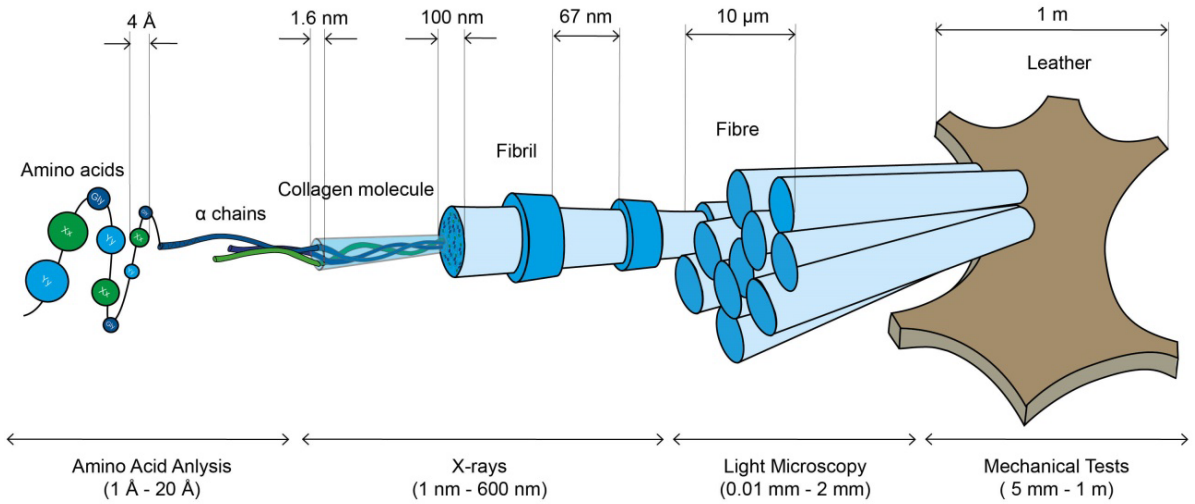

Figure 13. Hierarchical structure of collagen and the techniques used to view its structural features and mechanical properties at length scales from Angstroms to millimetres.

Below follows a description of two X-ray techniques, small and wide angle x-ray scattering (SAXS and WAXS), which were used to investigate collagen structure on the nano-scale in leather and the cornea. Further, mechanical tests are described, including tensile, tear and three-point bend tests, which were used to characterize the mechanical properties of collagen in leather.

Imaging at the Nano-level

The nano-structure of collagen containing materials has been widely studied using analyses by means of SAXS and WAXS[5, 47, 55, 88-92]. SAXS and WAXS are X-ray techniques which provide structural detail on the nano-scale based on intensities of the scattering diffraction patterns made by the X-rays when scattered by atoms in the sample[93]. In diffraction studies, the structural resolution that can be obtained depends on the wavelength of the incident radiation. The X-rays used in SAXS and WAXS have wavelengths between 0.01 and 0.2 nm which have been found to be suitable for providing structural detail on the nano-scale in a wide range of biological samples[63, 89, 90, 92, 94].

Synchrotrons

Initially an unwanted by-product of particle accelerators, synchrotron radiation has become a multidisciplinary tool for investigating nano-scaled structures across a range of fields from medical imaging and forensic science, to basic and applied research in a variety of fields including protein structure and mineral composition and more recently, manufacturing techniques for nano-scaled lithography for micro-electronics[95-98]. Currently

there are over 50 synchrotron facilities in operation across the world. The closest to (and partially funded by) New Zealand is the Australian Synchrotron, located in Melbourne, which accelerates electrons in a circular orbit to produce extremely bright light. The term synchrotron is in fact short for synchrotron light source. It has six basic components namely; the electron gun, linear accelerator (linac), booster ring, storage ring, beam lines and workstations (Figure 14).

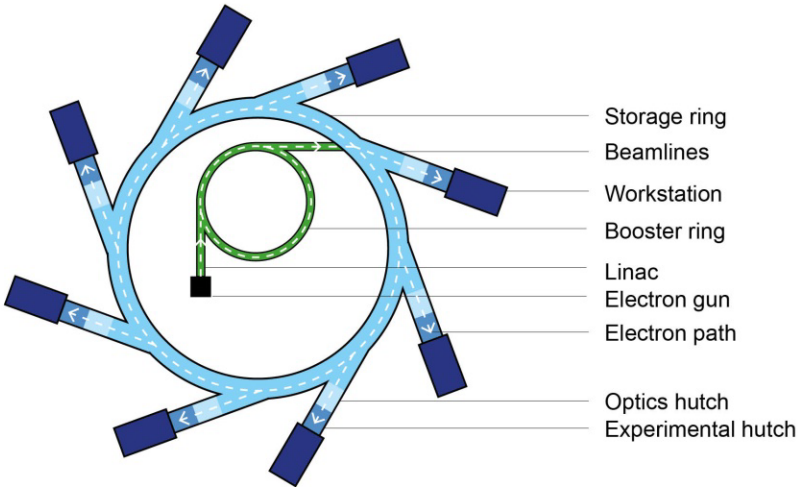

Figure 14. The basic components of a synchrotron.

At the Australian Synchrotron the electron gun (the cathode at the beginning of the linac) contains a barium compound that is heated to 1000 degrees Celsius to enable electrons to be emitted (thermionic emission). These electrons are directed in a stream about the thickness of a human hair towards an anode at the end of the linac in bunches of around 100 million electrons spaced just two nano-seconds apart, at almost 60% the speed of light. There is a very high voltage between the electron gun cathode and anode (90 kV) causing the electrons to reach speeds close to the speed of light, roughly 100 billion km/h, 99.9987% the speed of light. The linac feeds into the booster ring where magnetic fields direct the electron beam around the ring. Here radio frequency cavities microwaves are used to add energy to the electrons each time they go passed the cavities. After 600 milliseconds and 1.38 million laps, the electrons bunches have 30 times the energy they had when they left the linear accelerator, and now travel at 99.99998% the speed of light. They are then moved into their final home, a long vacuum chamber operating at a similar pressure to the moon's atmosphere, called the storage ring. Rather than a true circle, the storage ring is more of a multisided shape covering an area of approximately 100 m across. Within the storage ring are a series of magnets and insertion devices (wigglers, undulators and bending magnets) that cause the electron beam to bend and travel in a snaking path around the circumference of the ring. As the electron beam bends, radiation/synchrotron light is emitted[*]. The tightness of the bend depends on the strength of the magnetic field applied and influences the wavelength of the radiation emitted. A tight bend produces short wavelength radiation, such as X-rays, while a gentler curve

[*] For energy to be exchanged between the electron beam and a light wave, an undulator is needed. The undulator consists of alternating dipole magnets which cause the electron beam to oscillate. They add a velocity component to the electron beam in the transverse direction. The transverse component of the electron velocity and the vector of the light wave must point in the same direction to get an energy transfer from the electron to the light wave. The light wave, traveling at the speed of light, then has to shift by half an optical wavelength in a half period of the electron trajectory in order not to get ahead of the large, slower traveling electron beam. This is important for sustaining a steady energy transfer from the electron beam to light wave along the entire undulator. A slip of this magnitude allows the transverse velocity and the electromagnetic field of the light wave to remain parallel.

produces wider wavelength radiation such as infrared rays. In this way, specific radiation can be produced in the storage ring by the placement of insertion devices across the beam line to create and channel radiation (Figure 15).

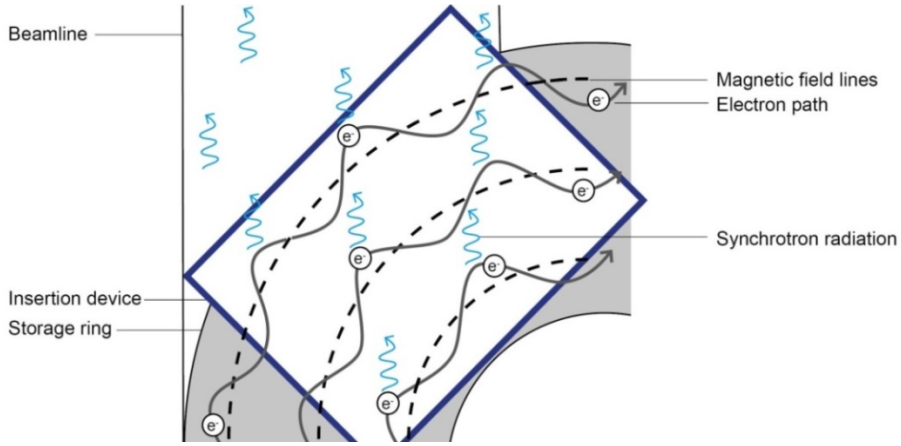

Figure 15. Synchrotron radiation traveling down a beamline after being emitted from bends in the electron path caused by insertion devices (undulators, bending magnets and wigglers) in the storage ring, at the opening to the beamline.

Beamlines usually consist of two hutches (radiation shielding enclosures); the first is the optical hutch which contains focusing mirrors, monochromators, and vacuum tubes to modify the incoming radiation into the required beam. X-ray beams can have a wide range of wavelengths depending on their source. A monochromator enables a beam of a more specific wavelength to be obtained for sample analysis. The second is the experimental hutch which houses the sample stage for mounting and manipulating samples, and the radiation detectors to measure the radiation that has interacted with the sample and has been scattered. Some beamlines have multiple end stations, with more than one experimental hutch, meaning all the optics don't necessarily need to be in the first hutch. For example, the focusing mirrors in the SAXS/WAXS beamline at the Australian Synchrotron are located in the experimental hutch.

SAXS AND WAXS

SAXS and WAXS describe two ranges of angles over which scattered radiation from a sample can be detected (Figure 16).

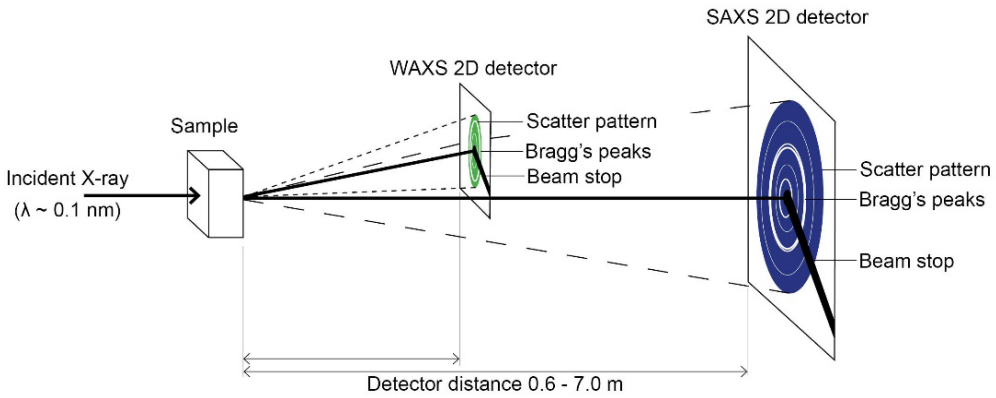

Figure 16. Small angle X-Ray scattering (SAXS) and Wide angle X-Ray scattering (WAXS) synchrotron beamline configurations. 2D detectors are placed to capture scattered rays from a range of angles relative to the incident X-ray (SAXS (0.1 - 10°) and WAXS (5 - 60°)).

THEORY

The 2D radiation detector[99] allows the full 360° scatter pattern from a sample to be collected with background subtraction to remove non-sample related data such as background air scatter, Kapton tape scatter, water scatter and buffer scatter - essentially any scatter unrelated to the sample and sample environment can be removed. SAXS or WAXS beamline setups are achieved by moving the 2D detector further or closer to the sample, respectively. For SAXS, X-rays scattered at low angles relative to the incident X-ray (0.1 - 10° from the incident X-ray) are captured, providing structural information in the 10 - 600 nm range. For WAXS, X-rays scattered at higher angles (5 - 60° from the incident X-ray) are captured, providing structural information in the range of 1 - 60 nm. Measurements across both the SAXS and WAXS range provide detailed insights into the sample's shape and size through its macromolecular structure. Non-scattered X-rays travel directly through the sample and are blocked by the beam stop, which is placed to protect the detector.

Scatter patterns are the result of constructive and destructive interference of the scattered X-rays. Regions of constructive interference are defined as Bragg's peaks according to Bragg's law (Equation 5) which describes the scatter intensity at different scatter angles, giving insights into the samples interatomic structure. At small scatter angles, the Guinier model[100] allows an estimate of particle size through the radius of gyration parameter and the extrapolated intensity at zero angle scatter, a region we are unable to measure due to the beam-stop. The derivation of Bragg's law can be seen when considering two beams with identical wavelengths and phase approaching a crystalline solid (Figure 17). When the beams are scattered by two different atoms in the sample, relative to one another, one beam will traverse an extra length of $2d\ sin(\theta)$, where d is the spacing between planes and θ is the angle between the incident X-ray and the scattering planes. Constructive interference occurs when the length of the scattered rays travelled path is equal to an integer multiple of the wavelength of the incident X-ray, causing the scattered rays to constructively overlap resulting in a greater detected intensity.

$$n\,\lambda = 2\,d\,\sin\theta$$

Equation 5. Bragg's law where n is the peak order, λ is the wavelength of the incident X-ray, d is the interplanar distance and θ is the half angle between the scattering plane and the incident beam.

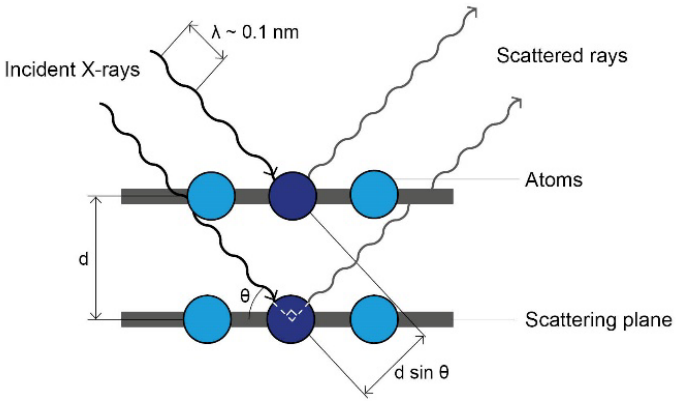

Figure 17. Bragg's law describing the diffraction of X-rays through a lattice where λ the wavelength of the incident X-ray, θ is the half angle between the scattering plane and the incident beam, d is the interplanar distance and d sin θ is half the path length difference between the two waves undergoing interference.

From the radial distribution of intensities on a scatter pattern, we can get an overall idea of the general sample structure. To gather further information from the scatter patterns, radial averaging is used to give a scattering intensity ($I(q)$) as a function of the momentum transfer (q), allowing us to determine structural features when combined with Bragg's law (Equation 6).

$$q = \frac{2\,\pi\,n}{d}$$

Equation 6. Scatter vector q where $\mathbf{q} = \frac{\mathbf{2d\sin\theta}}{\boldsymbol{\lambda}}$ according to Bragg's law, d is the interplanar distance, n is the peak order and q is the corresponding scattering vector.

From the relationship defined above, the scattering vector range (also known as q-range) from SAXS analysis is 0.001 – 0.6 nm^{-1}, providing structural information between 10 and 600 nm, while WAXS analysis has a scattering vector range of 0.01 – 0.1 nm^{-1} providing sample structural information between 1 and 60 nm.

Sources

X-ray sources can be from a laboratory or a synchrotron source (Figure 18), each providing varying wavelengths and flux abilities. Laboratory X-ray generators produce wavelengths in the range of 0.1 - 0.2 nm while synchrotron sources have a broader range of 0.03 - 0.35 nm. Flux is a scalar quantity defined as the surface integral of the component of a vector field perpendicular to the surface at each point. A synchrotron source can achieve an energies between 8 and 12keV (a total photon flux between 2 and 8 x 10^{12} photons/second) from the synchrotron radiation given off in the storage ring. High fluxes allow samples with weak scattering abilities to be analysed under greater intensities, producing good contrast in scatter patterns. Laboratory X-ray sources on the other hand achieve X-ray energies in the range of 1 - 4 keV reducing the intensity range and therefore resolution in scatter patterns. However, greater resolution can be achieved with a laboratory source of X-rays if longer times are used.

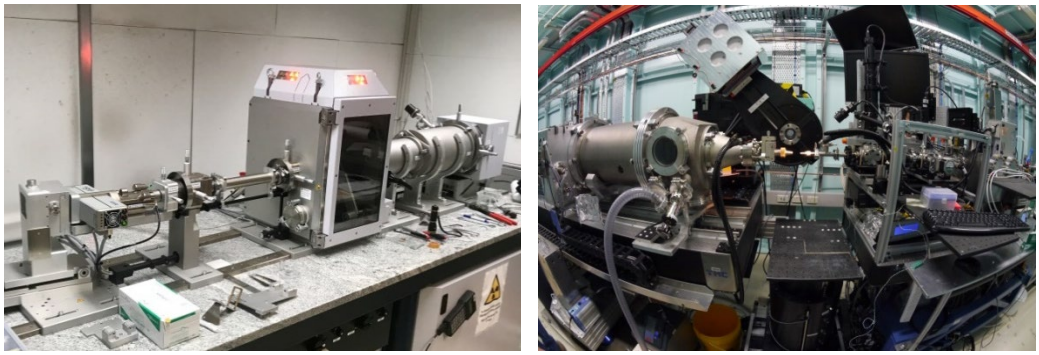

Figure 18. Laboratory source small and wide angle X-ray scattering (SAXS/WAXS) beamline at the Max Planck Institute for Colloids and Interfaces, Germany (*left*) and a synchrotron source SAXS/WAXS beamline at the Australian Synchrotron, Australia (*right*).

Benefits

SAXS/WAXS imaging is an easy method for determining protein structures since it does not require crystallography like other protein imaging techniques, such as macromolecular crystallography. It has the capability of giving structural information between 1 and 600 nm allowing sample volumes to be small with short experimental runs (depending on the X-ray source) and minimal sample preparation.

Considerations

Measuring small scattering angles accurately can be difficult as the diameter of the main beam can be unstable because of divergent beams appearing from the X-ray source. This effect can be lessened if large concave mirrors are used to focus the main beam and in the process minimize these divergent beams. Such mirror adjustments are not possible with laboratory based SAXS/WAXS instruments, which instead use collimation devices for beam focusing. In point-collimation devices, pinholes, are used to focus the X-ray beam while inline-collimation devices, slits, are used for focussing X-ray beams onto samples.

Samples that contain components with random orientations of dissolved or partially ordered molecules need special consideration since a loss of information can result from spatial averaging of the scatter patterns. Such samples are more appropriately examined using crystallography. Sample stage mounting at strategic positions can help to reduce the effects of spatial averaging. Introducing more sophisticated sample chambers, to control environments (ambient temperature or humidity) or to apply mechanical strain during measurements, can provide additional data on samples.

Encasing samples in films, typically Kapton and Quartz, with known scattering characteristics help to isolate samples in a desired environment. However, careful consideration needs to be taken when selecting films so that they do not interfere with the scattered intensities produced by the sample.

Applications for Collagen Materials

SAXS and WAXS scatter patterns from collagen-based materials provide insights into the arrangement and characteristics of fibrils (Figure 19). The position and intensity of the scatter pattern rings result from structural order. The relative peak location provides inter-planar measurements of the fibril diameter[69], D-spacing[88] and intermolecular spacing[14, 94], while the intensity distribution of rings relates to structural order such as fibril orientation[88,70] (Figure 20).

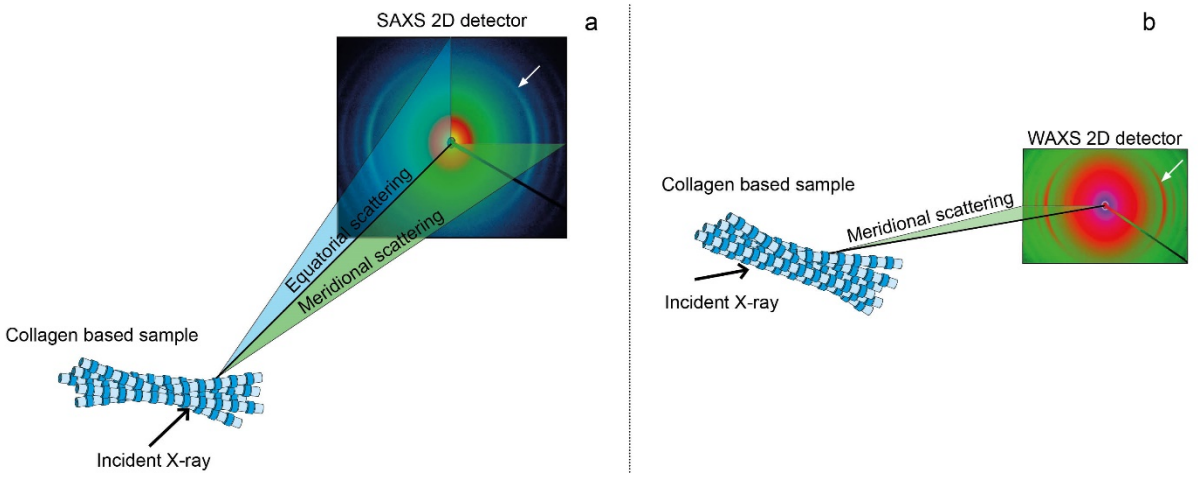

Figure 19. Equatorial and meridional scattering from (a) small angle X-ray scattering (SAXS) and (b) wide angle X-ray scattering (WAXS) used to gather collagen specific information from integrated intensities over the azimuthal q-range (I(q)) from a collagen-based sample. The white arrows indicate the peaks of interest for D-spacing (a) and intermolecular spacing (b) on the scatter patterns.

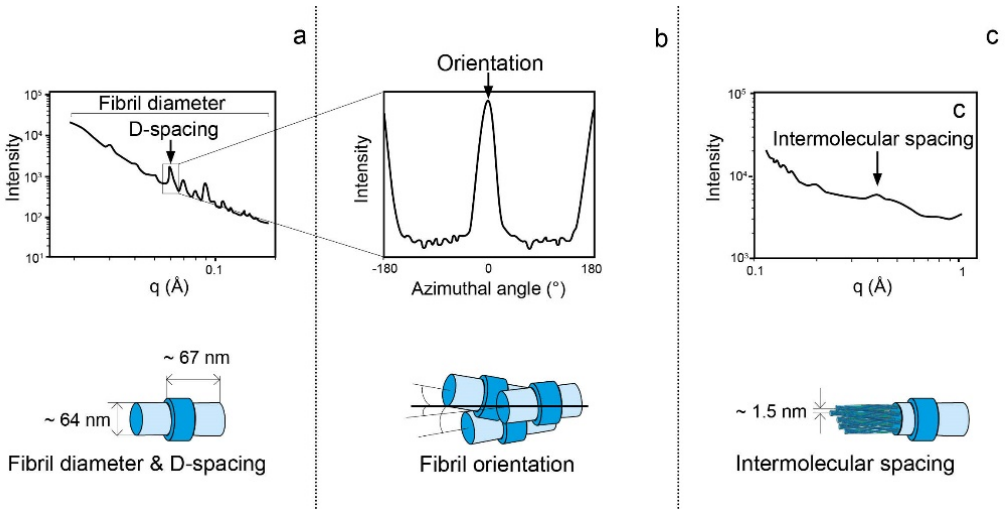

Figure 20. From SAXS integrated intensity profiles (a) fibril diameter and D-spacing are determined in the SAXS q-range with (b) further integration of the 6th order peak over the azimuthal angle to determine the preferred fibril orientation (orientation index, OI). From WAXS integrated profiles the (c) intermolecular spacing can be determined from measurements taken at this higher WAXS q-range which provides smaller structural information.

Fibril diameter

The scattering of X-rays occurs exclusively at the interface of two media with different capacities to scatter radiation, for example, a solid matrix and a pore space containing air. The scatter intensity versus the scattering angle (I(q)) are therefore determined by the geometry of the matrix-pore interface at various length scales derived from the q-range. The area under the I(q) curves can be used to determine fibril diameters in a collagen-based sample.

D-spacing

Collagen's D-spacing arises from the precise arrangement of adjacent tropocollagen molecular chains, which are staggered axially. This leads to distinct and highly regular 'gap' and 'overlap' regions along the macromolecular assembly. The D-spacing reflects an average lateral intermolecular separation within the fibril, and is derived from a broad equatorial peak (Figure 20 (a)), usually the 6th order peak for a I(q) plot on the SAXS q-range. The location of the maximum of the 6th order peak, fitted with a Gaussian curve, is used to calculate the collagen periodicity (D-spacing) using the relationship defined by Bragg's Law (Equation 6).

Fibril Orientation

Plotting the measured intensities over the full azimuthal angle range at the 6th order peak on a SAXS q-range provides information on the fibrils preferred orientation (Figure 20 (b)). The peak intensity relates to the alignment of the collagen fibres, while the peak width relates to the delamination or misalignment of the collagen fibrils. Two methods can be used to numerically define the organization within a fibrous structure, namely orientation index (OI) and Herman's orientation. These have been used to determine the preferred fibril orientation from the intensities collected on SAXS scatter patterns. OI has been used to characterize alignment in leather[88], cornea[18], pericardium[103] and acellular dermal matrix[104] structures while Herman's orientation has been used on a range of fibrous materials including skin[7], bone[105] and various scaffolds[106-108].

Orientation Index

The orientation index (OI) is calculated from the spread in the SAXS scatter intensity over the azimuthal angle of the D-spacing peak in the q-range of 0.045 − 0.055 Å from a SAXS scatter pattern from a fibrous sample. The OI is defined as $\frac{90°-OA}{90°}$, where OA is the minimal azimuthal angle range, centred at 180°, which contains 50% of the micro fibrils[63, 109]. The OI range is from a perfect anisotropic alignment (OI = 1) (Figure 21 (a)) through to isotropy (OI = 0) (Figure 21 (b)).

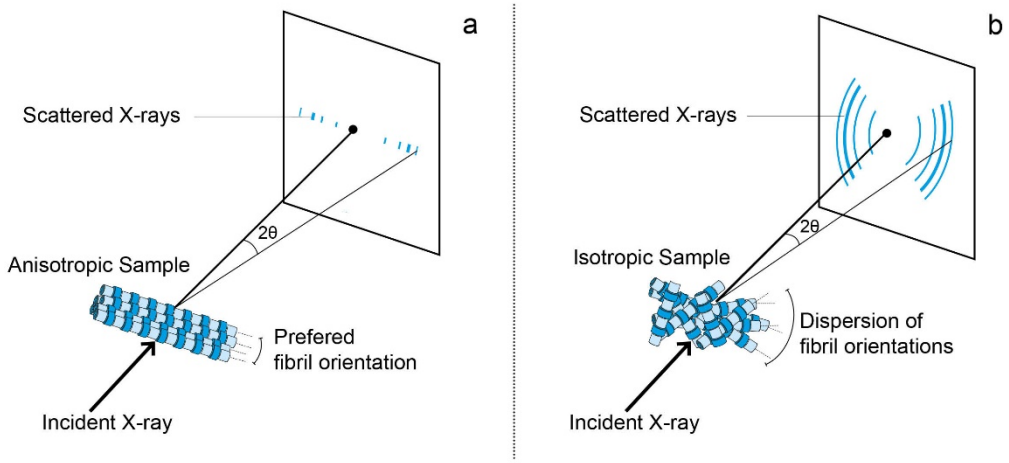

Figure 21. Fibril orientation producing scatter patterns from an (a) anisotropic (highly aligned) sample and an (b) isotropic (randomly aligned) sample where θ is the scattering angle and 2θ is the maximum angle collected by the detector.

2.2.1.5.3.2 Herman's Orientation

Herman's orientation (f) (Equation 7) is used to describe the extent of orientation of fibres relative to an axis of interest[110, 111] from SAXS scatter patterns where complete fibre alignment is represented by f = 1 (Figure 21 (a)), and randomly orientated fibres are represented by f= 0 (Figure 21 (b)).

$$f = 0.5\ \frac{3\sum_0^{\pi} I(Ø)\ sin^2Ø\ cosØ\ d(Ø)}{\sum_0^{\pi} I(Ø)\ cosØ\ d(Ø)} - 1$$

Equation 7. Herman's orientation (f) where Ø is the azimuthal angle made by the fibre axis centred at 180° and I(Ø) is the intensity at a specified azimuthal angle. f is equal to 1 for a perfectly oriented fibrils and is 0 when the fibril orientation is completely random.

Intermolecular spacing

With the detector placed close to the sample (Figure 16) to capture wider scattering angles (WAXS) in the q-range of 0.1 – 1 $Å^{-1}$, small structural detail such as the intermolecular spacing in a collagen-based material can be determined. Using a technical graphing and data analysis package with a peak fitting function (Igor Pro) the peak location in an integrated intensity profile, focused on the 0.35 – 0.45 Å q-range, can be determined. The peak fit function can determine the peak maximums relative to their position on the scattering vector scale (q). Placing the peak location into the relationship derived previously (Equation 6) where n = 1 we can determine the intermolecular spacing (d).

Electron Microscopy

Theory

Electron microscopy utilizes an electron source, commonly a tungsten filament or lanthanum hexaboride source, connected to high voltage (typically 100 - 300 kV) to illuminate samples. With the wavelength of an electron being much shorter than that of light, magnifications of up to x 10^6 can be achieved. Electron microscopy takes two forms, namely scanning electron microscopy (SEM) and transmission electron microscopy (TEM). For SEM, a thin gold or graphite coating is applied to the surface of a sample. The electrons reflected from the coating enable the surface topography of the sample to be examined (Figure 22 (a)). In TEM, samples need to be embedded in a resin to allow for ultrathin sectioning (50 – 100 nm thick). An ultra-thin section of a sample lowers its density and allows electrons to interact with the full sample thickness before reaching the detector (Figure 22 (b)). This creates images with information on the samples internal structure. The image's contrast depends primarily on differences in electron density within the sample, where dark regions in the final image belong to parts of the sample with a high electron density and light areas belong to parts with low electron density. Staining can be used to highlight specific features by increasing the contrast. Staining with heavy metals like osmium tetroxide and lead, which scatter electrons due to their high atomic weight, improves the contrast detected by the microscope.

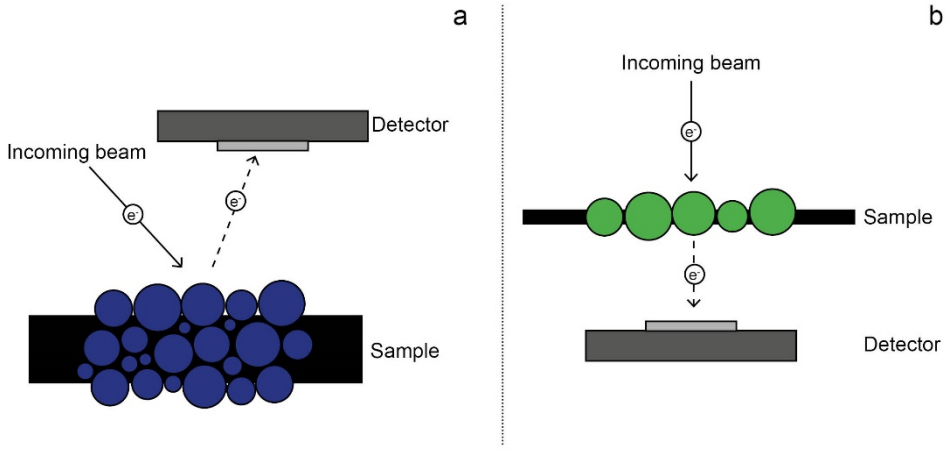

Figure 22. Electron microscopy: (a) scanning electron microscopy (SEM) collecting scattered electrons at the detector and (b) transmission electron microscopy (TEM) collecting transmitted electrons at the detector.

Benefits

TEM and SEM are complementary microscope techniques. SEM views surfaces, while TEM views the interior of extremely thin films. Electron microscopy provides a high resolution image of the structure and the facilities are readily accessible in most research institutions.

Considerations

TEM is used in situations where the interior structure of a sample is to be investigated while SEM is used when the surface of a sample is to be studied. While coating a sample with gold or graphite spray for SEM is relatively simple, for TEM sample preparation is more complex. First, the sample for TEM has to be stabilized, in the case of biological samples with fixatives such as glutaraldehyde, and stained with chemicals that emphasize the capacities of different materials/tissues to conduct electrons. After embedding in resin,

sections of the sample are cut which are thin enough (around 100 µm) to enable the passage of electrons through the material. SEM has lower resolution than TEM, micrometres vs. nanometres.

Applications for Collagen Materials

Measurements of the fibril diameter, D-spacing and inter-fibrillar packing can be made with a good set of TEM images (Figure 23) using an image processing and analysing tool such as ImageJ[18, 112]. TEM images also provide an idea of short order arrangements and structural patterns. SEM can be used to gather information on longer ordered arrangements and surface textures.

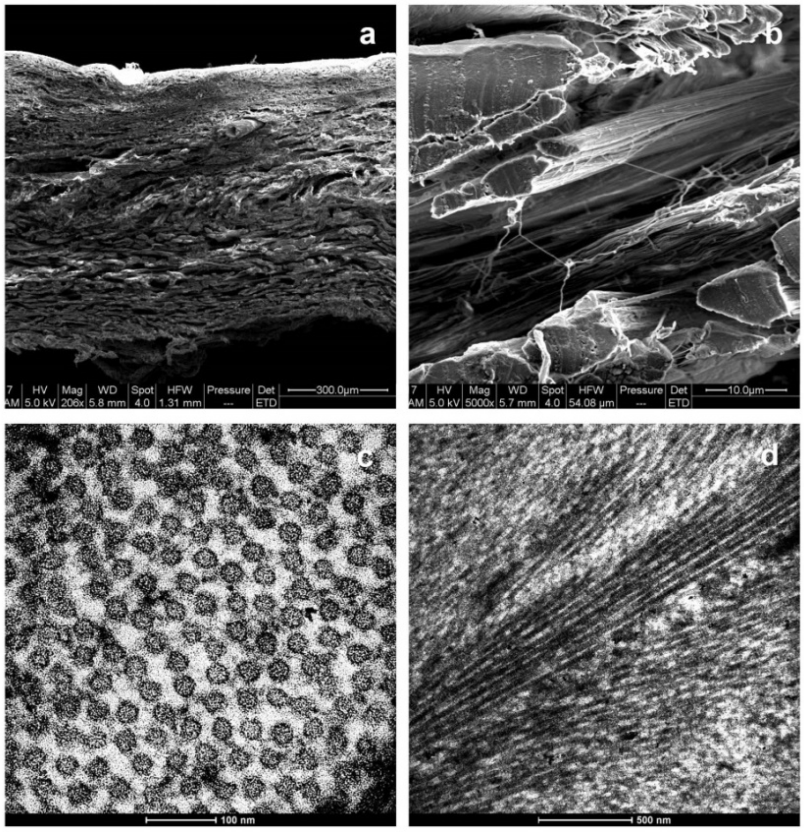

Figure 23. Scanning electron micrscopy of (a) leather cross section showing the two distinct layers and (b) collagen fibers in the corium layer. Transmission electron microscopy of (c) cross-section of corneal collagen and (d) side view of corneal collagen showing characteristic D-spacing. Images were captured at the Manawatū Microscopy Centre, Palmerston North, New Zealand.

Mechanical Testing

Mechanical testing records a material's response to an applied force for quantitative measurements to compare different materials. Quantitative measurements include strength, defined as the maximum force a sample can withstand over a defined surface area and stiffness, defined as a materials ability to resist deformation forces over a defined area in the material's elastic region. Since these measurements are useful for comparing properties of different materials, a range of standardized test methods have been developed to allow comparable measurements to be recorded. Combinations of tests have been determined for leather by the International Organization for Standardization (ISO) to evaluate leather properties. These are discussed in detail below.

Tear Strength Measurements

Tear testing gives a true representation of material strength since the materials failure is the result of a tear propagating from a tear front (puncture), representative of its failure in practice (Figure 24 (b)). The industry defined test (ISO 3377-2:2016) determines the maximum tear load a sample can withstand until failure. The testing criterion requires two sample types to be taken from the leather within a specific location, relative to the tail and backbone of a whole hide, called the official sampling position (OSP) (Figure 24 (a)). At this location one sample (dimensions specified in the standard) is cut parallel to the backbone and the other perpendicular to account for the natural collagen alignment that occurs in hides[15]. The strength of the hide is then determined by the average force required to tear both orientation specific samples, normalized for thickness.

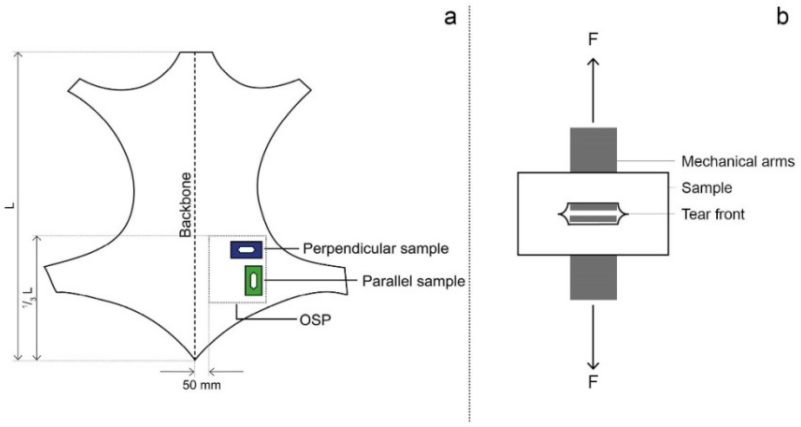

Figure 24. Tear test (a) sampling location and orientation relative to the backbone of a skin/hide where L is the total length of the hide and the OSP is the official sampling position defined by ISO 2418:2017 and (b) the tensile forces F applied to a tear sample with tear fronts defined by the ISO standard.

Tensile Strength Measurements

The industry defined tensile test for leather (ISO 3376:2011) determines the maximum elongation force a sample can withstand before failure. As for the tear test, two sample types (dimensions specified in the standard) are cut relative to the backbone at the OSP, to account for the natural collagen alignment in skins. This method of determining strength is less preferred, because the failure mechanism is less likely to occur in practice (i.e.: application of an even force to a sample cross section until failure) (Figure 25).

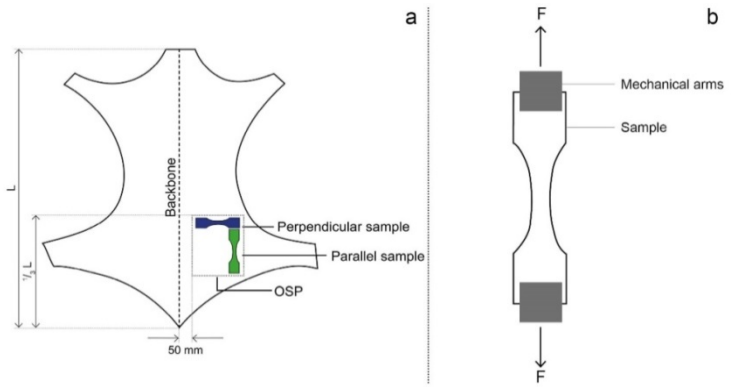

Figure 25. Tensile test (a) sampling location and orientation relative to the backbone of a skin/hide where L is the total length of the hide and the OSP is the official sampling position defined by ISO 3376:2011 and (b) the tensile forces F applied to a tear sample with tear fronts defined by the ISO standard.

Three Point Bend Measurements

The ability of materials to bend (softness in the case of leather) can be determined by the three point bend test (ISO 3377-2:2016) where a force is applied to deflect a sample mounted between two supports, to a specified distance (Figure 26). To determine the material's bend modulus, the resistance of the sample is measured while the force is being applied. While this testing was developed for semi-rigid plastics under defined conditions (ISO 178), it has now been found to be useful for leather where it allows for repeatable quantitative measurement of leather softness[53].

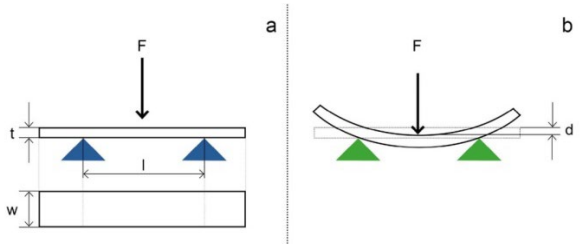

Figure 26. Three point bend test setup (a) (t = 0) where l is the distance between the two supports; T is the sample thickness and w is the sample width. When a force is applied F (b) at t > 0 to deflect the sample to a specified distance d the test is complete.

Isothermal-gravimetric Analysis

Theory

Thermal gravimetric analysis (TGA) is a thermo-analytical technique which measures the variation in sample weight as a function of temperature and time in controlled environments. The changes to the sample weight relative to temperature provide information on the sample's thermal stability and composition. When sample weight loss occurs this suggests that components of the sample are decomposing, evaporating, desorbing or a reducing reaction is taking place. When sample weight is gained, this suggests absorption or oxidation is occurring. Output measurements from a thermo gravimetric analyser include weight, temperature and time where two experimental conditions can be manipulated, namely the heating rate and gas flow. Continuous weight measurements are made from a precision sample pan placed in a temperature-controlled furnace. Temperature profiles can be designed to increase at a constant rate to incur a thermal reaction or kept under isothermal conditions to determine a materials moisture content and absorption/desorption characteristics. For thermal reactions, control of the atmospheric conditions includes adjustments of the gases entering the furnace such as introducing inert gases or oxidizing/reducing gases. For isothermal conditions, the temperature is held constant while the relative humidity of the entering gases is adjusted (Figure 27). Results from the isothermal gravimetric test configuration result in sorption isotherms where the relative humidity can be converted to osmotic pressure to describe the pressure acting on the sample under the various relative humidity conditions[113, 114].

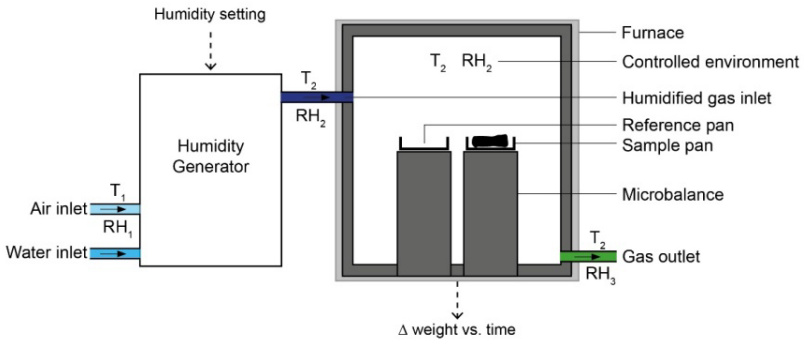

Figure 27. Isothermal-gravimetric analysis connected to a humidity generator for sorption isotherms where T_1 and RH_1 are the inlet air temperature and relative humidity; T_2 and RH_2 are the temperature and relative humidity in the gravimetric analyser and RH_3 is the outlet relative humidity.

Benefits

Since temperature and atmospheric profiles can be programmed into this device, it allows identical environmental conditions to be created for each sample run. Under the isothermal configuration with varying relative humidity conditioning, the absorption and desorption properties of a material can be determined in a controlled environment giving a high degree of certainty in the results.

Considerations

As with most analytical techniques, sample preparation has a significant effect on the quality of data. For good TGA results, it is suggested that the surface area of the sample be maximized in the sample pan to improve resolution and reproducibility of weight measurements. The amount of sample placed in the pan is also important, requiring 10 – 20 mg for most samples and up to 100 mg for samples known to contain a significant amount of volatiles. Baseline drift can be expected in most TGA instruments due to impaired temperature control or unexpected volatiles; ± 0.025 mg is an accepted range of baseline drift (0.25% of a 10 mg sample). Measurement times should be maximized to allow the sample to reach equilibrium with respect to absorption or desorption after each change in the controlled environment's relative humidity.

Applications for Collagen Materials

Water is an important component of collagen-based materials[115]. The ways water interacts with the collagen fibrils and the mechanical properties it imparts have been of interest in a variety of applications from the osmotic pressures induced in tendons[113, 114], to its effect on collagen-based material stiffness[14, 16] and its effect on the collagen structure[13]. The use of relative humidity conditioning provides a means of introducing a known amount of water to a collagen-based material. Coupling this with techniques such as SAXS/WAXS and mechanical testing, one can investigate the changes water introduces into the structure and the effects on its mechanical performance[16].

Chapter 3. Mapping Tear Strength and Collagen Fibril Orientation in Bovine, Ovine and Cervine Hides and Skins

Kelly S. J., R. L. Edmonds, S. Cooper, K. H. Sizeland, H. C. Wells, T. Ryan, N. M. Kirby, S. Mudie and R. G. Haverkamp, Mapping Tear Strength and Collagen Fibril Orientation in Bovine, Ovine and Cervine Hides and Skins. *Journal of the American Leather Chemists Association* 113 (1):1-11 (2018).

Abstract

Leather is a natural and variable material. The variation in strength has previously been shown to be due in part to the collagen fibril orientation. However, the extent of variation in strength and orientation over a skin/hide is not well established. Synchrotron small angle X-ray scattering is used to measure collagen fibril orientation (O) and orientation index (OI). Tear strength is measured in two orthogonal directions across ovine and cervine skins and bovine hides. Average normalized strengths varied between species with cervine leather having the greatest overall strength followed by bovine then ovine leather. Ovine had the greatest variability in strength across the skin. There were no obvious regions of generally stronger or weaker skin within individual skins or hides. Collagen fibril orientation in leather made from of ovine, bovine and cervine skins have been analysed quantitatively and in detail. The predominant collagen fibril direction was perpendicular to the backbone of all species, with the greatest perpendicular alignment in ovine followed by cervine. Findings suggest an unpredictable variability in collagen arrangements within each species but a notable difference in strength between species.

INTRODUCTION

Collagen is a major constituent of skin and is responsible for many of its functional properties such as strength and flexibility[116]. It accounts for 75% of the dry weight of skin, the mechanical properties of which are mostly dependent on the structural arrangements of the fibres that make up collagen[117, 118]. The structural arrangement of the fibres in collagen most influences its mechanical properties. The collagen fibres are anisotropic and are strongest in the direction of their component fibres[70, 119] and weakest in the direction perpendicular to the fibres[120, 121].

Slight variations in the collagen fibre arrangement can alter the mechanical properties of skin significantly, for example increasing its flexibility over joints to facilitate movement and increasing its strength in areas of high friction, such as the soles of the feet, for protection[122]. The orientation of collagen fibres in the skin varies from area to area to provide a local architecture creating the required mobility, flexibility and rigidity[123] by the forces operating at these sites[124, 125]. This variability in skin's properties around the body was recognized in the late 1800's, when studies were performed on people to determine the optimal direction for surgical incisions. Langer lines[126], Kraissl lines[127] and Borges lines[128] were developed to show the natural collagen orientation and maximum skin tension in human skin as a topological map of the body which are still used by surgeons today[129, 130]. This idea has been extended further to dogs where collagen orientation mapping has also been performed, resulting in a set of canine tension lines to assist with surgical incisions[131].

A series of studies have been performed to determine the mechanical properties of skin[117, 132, 133] and more specifically the application of biaxial loading where its effects on collagen orientation were observed[7, 132, 134, 135]. In unloaded skin the collagen fibres are largely unaligned; when tensile loading is applied the fibres become more aligned. The classical theory behind this change in alignment suggests that the overall strength of the collagen becomes dependent on the mechanical properties of the fibres themselves[7, 51, 134, 136], with fibres initially orienting in the direction of the applied strain. Then, once aligned, the individual fibres themselves bear the strain. However, another theory suggests that a more plastic response is observed due to inner sliding within each fibre, contributing a given stress to the global response. The mechanical response, on the other hand, is primarily due to the structural effect of the fibres network[51, 135].

Information on the collagen fibre alignment and its influence on the mechanical properties of animal skins could have important implications for the tanning and leather industries. In particular, information is needed on how the natural collagen arrangement varies in skin around the body and how this influences the mechanical properties of the skin from different areas. To date there are only limited studies in animals. The collagen fibril orientation has been measured over a bovine hide, using the angular dependence of transmitted microwave intensity. Findings alluded to a correlation between the fibril orientation and the forces that would have occurred in the live animal[137-139]. A small angle x-ray scattering (SAXS) and tear testing study on ovine hides demonstrated that tear strength was distributed with decreasing strength when moving from the backbone down to the flanks[12]. The relationship between tear strength and collagen alignment in a selection of mammals including horse, goat, sheep, water buffalo and cattle[47] showed a significant correlation between

the edge-on collagen fibril alignment and tear strength, where a trend of greater collagen alignment resulted in greater tear strength.

In this work the variation in and relationship between collagen orientation, orientation index and tear strength is mapped using tear testing and SAXS imaging, measured normal to the grain surface, for standard beamhouse tanned ovine and cervine skins and bovine hides. This has only previously been studied at the official sampling position (OSP) of selected mammals[47] and at two other locations (back and belly) of ovine leather[12].

Methods

Leather. The leather used in the study had been processed to crust according to standard beamhouse methods. Bovine leather were obtained from a co-operating leather tannery. The leather was made using conventional processes which included: lime-sulphide liming, sulphuric acid pickling and chrome tanning. Cervine leather were also obtained from a co-operating deer skin tannery using conventional processes which included: painting with lime-sulphide paint, depilation, liming, pickling with sulphuric acid and conventional chrome tanning. In addition, ovine leather were produced in-house for this study from Romney cross animals of the same age according to the following procedure. After rehydrating the skins, the adhering fat and flesh were removed mechanically with a conventional fast acting (<4 hours) lime sulphide paint (200g/L commercial flake sodium sulphide, 45g/L sodium hydroxide, 50g/L hydrated lime and 23g/L pre-gelled starch thickener) applied to the flesh (inner) side of the raw skins at a rate of 400g/m². The painted skins were incubated at 10-15°C for 3 hours. The wool was manually removed and the skins washed to remove the lime. Ammonium sulphite (2% (w/v)) was added to lower the pH to 8 followed by the addition of a commercial bate enzyme (Tanzyme (0.1% w/v)). After incubation at 35 °C for 75 min the treated skins were washed and pickled in 20% w/v sodium chloride and 2% w/v sulphuric acid. The pickled pelts were degreased in a drum with degreasing solution (10% common salt, 8% non-ionic surfactant and 4% Oxazolidine A (Zoldine ZA-78 from Angus)) for 30 minutes at 35°C. Sodium bicarbonate was added to neutralize the skins to be tanned (4.5% (based on pickled weight) of 33% basicity, 25% chromium content chromium sulphate powder (Chromosal B from Lanxess, Germany)). The wet blue pelts were then neutralised for 1 hour in 1% sodium formate and 0.15% sodium bicarbonate solution followed by water washes then retannage (2% synthetic retanning agent (Tanicor PW, Clarient, Germany), 3% vegetan (mimosa, Tanac, Brazil)). Finally, fatliquors were added (a total of 6% mixed fatliquors) and the temperature rose to 50°C for 45 minutes. The addition of 0.5% formic acid fixed the crust leather for 30 minutes was followed by draining. The tanned pelts were then washed with water before being dried, conditioned and staked.

Test samples. Samples for testing were taken from a grid (Figure 28) placed on one half of two ovine skins, two bovine hides processed to upholstery grade and two cervine skins; all were halved from neck to tail. The sampling grid was adjusted to accommodate the species differences in skin/hide size with the grids for the ovine skins being 80 x 80 mm, the smallest size enabling two tear tests and SAXS measurements (see below); the grids for the bovine hides and cervine skins were 200 x 200 mm to limit the total number of samples (Table 3). From each sampling grid square, two samples (35 x 20 mm) were removed for tear tests and one (8 x 8 mm)

for SAXS measurements (solid grey square in Figure 28 (a)). To establish if SAXS measurements taken in the central 8 x 8 mm sample for each grid square was representative of the skin or hide in the rest of the grid square, extra samples were taken from the OSP (solid grey squares in Figure 28 (b)). 8 x 8 mm samples were taken from the centre as well as the corners of the grid square at the OSP for comparison. These additional samples were 40 mm apart in the ovine skin samples and 100 mm apart in the bovine and cervine skin samples.

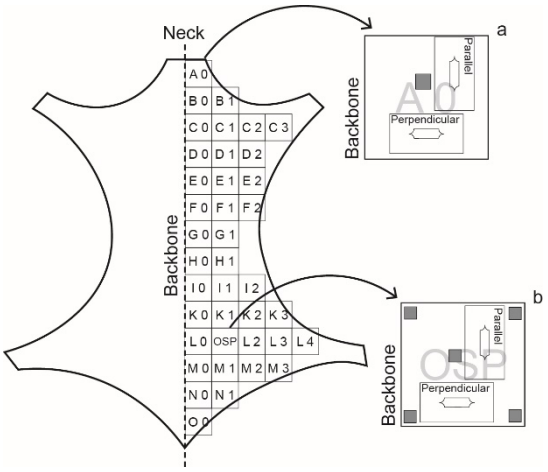

Figure 28. Grid pattern used for sampling hides showing the locations of the samples taken for tear testing and small angle X-ray scattering (SAXS) measurements (solid grey squares) at (a) general locations and at (b) the official sampling position (OSP).

Table 3. List of skins and hides with size and number of samples taken from each for analysis using industry standard tear testing (ISO 3377-2:2002) and small angle x-ray scattering (SAXS) measurements.

Sample	Size of halved hide (m^2)	Sample spacing m)	Number of samples for tear strength measurements	Number of samples for SAXS measurements*
Ovine skin halved (neck to tail) – skin I	0.20	0.08 0.04 at OSP	31 parallel; 31 perpendicular	35
Ovine skin halved (neck to tail) – skin II	0.22	0.08 0.04 at OSP	35 parallel; 35 perpendicular	39
Bovine hide halved (neck to tail) – skin I	1.52	0.2 0.1 at OSP	38 parallel; 38 perpendicular	44
Bovine hide halved (neck to tail) – skin II	1.64	0.2 0.1 at OSP	41 parallel; 41 perpendicular	45
Cervine skin halved (neck to tail) – skin I	1.80	0.2 0.1 at OSP	45 parallel; 45 perpendicular	49
Cervine skin halved (neck to tail) – skin II	2.08	0.2 0.1 at OSP	52 parallel; 52 perpendicular	56

*Five areas were analysed in the official sampling position (OSP) samples and one area in each of the other samples. Nine SAXS measurements (3 x 3 grid in the centre of the sample with 0.5 mm spacing between measurement points) were made on each sample and used to calculate the orientation (O) and orientation index (OI) which were then averaged.

Tear strength. Measurements of tear strength were performed according to standard methods (ISO 3377-2:2002) and normalized for thickness so strengths are comparable between samples. Two samples (at right-angles or parallel to the backbone) were cut from each sample grid position and conditioned at a constant temperature (20 °C) and relative humidity (65%) for 24 hours before tear testing with an Instron 4467.

Small Angle X-ray Scattering (SAXS). The Australian Synchrotron SAXS/WAXS beamline was used to establish the SAXS diffraction patterns in each sample. SAXS has proven useful in analysing collagen structures in a range of materials, such as cornea[140], bones[141] and leather[88]. A total of nine SAXS measurements were taken from the centre of each sample in a 3 x 3 pattern with 0.5 mm spacing between the measurement points (Figure 28). To determine the representativeness of a single SAXS measurement in the middle of the sample, at the OSP, additional SAXS measurements were taken in the corners of the sample (Figure 28b).

For each of the above measurements a high-intensity undulator source was used with an energy resolution of 10^{-4} from a cryo-cooled Si(111) double-crystal monochromator. The beam size (full width half maximum (FWHM) focused at the sample) was 250 x 80 µm with a total photon flux of about 2 x 10^{12} photons s^{-1}. All diffraction patterns were recorded with an X-ray energy of 8 keV using a Pilatus 1M detector with an active area of 170 x 170 mm and a sample to detector distance of 3371 mm. The exposure time for diffraction patterns was in the range of 1- 5 s, and data processing was carried out using the Scatterbrain software[142]. Intensities were displayed as absolute detector counts.

Orientation and Orientation Index. The Orientation (O) and the Orientation Index (OI) were calculated from each of the nine SAXS measurements taken for each sample and the average value taken to represent the O and the OI for the grid square. The OI was defined as (90°−OA)/90°, where OA is the minimal azimuthal angle range, centred at 180°, that contains 50% of the micro-fibrils [88, 109]. The OI varies between 0 and 1 with 0 describing an isotropic, random arrangement and 1 describing fibrils all oriented in the same direction. The OI was calculated from the spread in the azimuthal angle of the D-spacing peak at 0.059 − 0.060 $Å^{-1}$. The O was taken as the centre of the Gaussian curve fitted to azimuthal angle – intensity plot. The O is determined as the point on the x-axis corresponding to the greatest measured intensity where the x-axis has a horizontal angle measured clockwise from 0° at the graph origin (**Figure 3.5**). The average O was determined by turning vectors with direction O and magnitude OI into Cartesian form by taking the arctan of the sum of cos(O*OI) and sin(O*OI) to get the average angle.

Samples. The selection of samples used in this study is listed in Table 3. The bovine hides and cervine skins are much larger than the ovine, so the sampling points are more widely spaced.

Results

Tear Strength. The average tear strength normalized for thickness varied between species with ovine skins having the least strength which was approximately 50% that of the bovine hides and cervine skins (Table 4). The cervine skins had the greatest strength which was approximately 20% higher than those of the bovine hides.

Table 4. Average tear strength, collagen fibril orientation (O) and orientation index (OI) of the ovine and cervine skins and bovine hides studied. An O angle of 0° is along the backbone.

Species	Perpendicular Tear Strength (N/mm)	Parallel Tear Strength (N/mm)	O (°)	OI
Ovine	20	22	51	0.44
Bovine	42	43	48	0.38
Cervine	54	51	44	0.24

When tear strengths in individual animals were compared (Table 5), there was a similar trend with the individual ovine skins having lower average tear strengths than the individual bovine hides; these in turn had lower strengths than the individual cervine skins. There were significant differences between the individuals in each species, in particular in the ovine, where Ovine 1 had tear strength values more than double that of Ovine 2. The difference between the individual bovine hides was not as marked, and the difference between the individual cervine skins was the least. Ovine skins are known in the industry to be more variable than bovine hides or cervine skins, even within the same breed and age.

Table 5. Average tear strengths, collagen fibril orientation (O) and orientation index (OI) of the individual ovine, bovine and cervine half hides studied. An orientation angle of 0° is parallel to the backbone. P-values are for a t-test of whether the means are different (where P, 0.05 indicates the means are significantly different).

Sample	Perpendicular Tear Strength (N/mm) Average (St.Dev)	Parallel Tear Strength (N/mm) Average (St.Dev)	O (°) Average (St.Dev)	OI Average (St.Dev)
Ovine 1	12 (8)	13 (8)	77 (24)	0.47 (0.15)
Ovine 2	27 (11)	30 (8)	24 (9)	0.40 (0.11)
P-value Ovine 1 and Ovine 2	0.121	0.156	**< 0.001**	**0.030**
Bovine 1	33 (11)	39 (17)	30 (10)	0.29 (0.17)
Bovine 2	50 (14)	47 (12)	66 (2)	0.25 (0.11)
P-value Bovine 1 and Bovine 2	**<0.001**	**<0.001**	**< 0.001**	**0.031**
Cervine 1	50 (13)	45 (12)	44 (23)	0.22 (0.15)
Cervine 2	58 (10)	56 (10)	44 (2)	0.26 (0.11)
P-value Cervine 1 and Cervine 2	**0.002**	**<0.001**	0.196	**0.039**

There were only small differences between the tear strengths measured parallel and perpendicular to the backbone at each individual sample point (data not shown) and for each species (Table 5). However, the average perpendicular tear strength varied considerably between individuals and between species which was also the case for parallel tear strengths (Table 6). The tear strengths at the different measuring points varied between individuals of each species and between the species. There was no apparent pattern to the distribution of perpendicular or parallel tear strengths at the various measuring points in the different individuals and species (Figure 29), rather the tear strengths at each position varied widely between individuals of a species and between the species. Although there were considerable differences between

individuals within a species, there were only insignificant differences between the average tear strengths measured perpendicular and parallel to the backbone between species (Table 4).

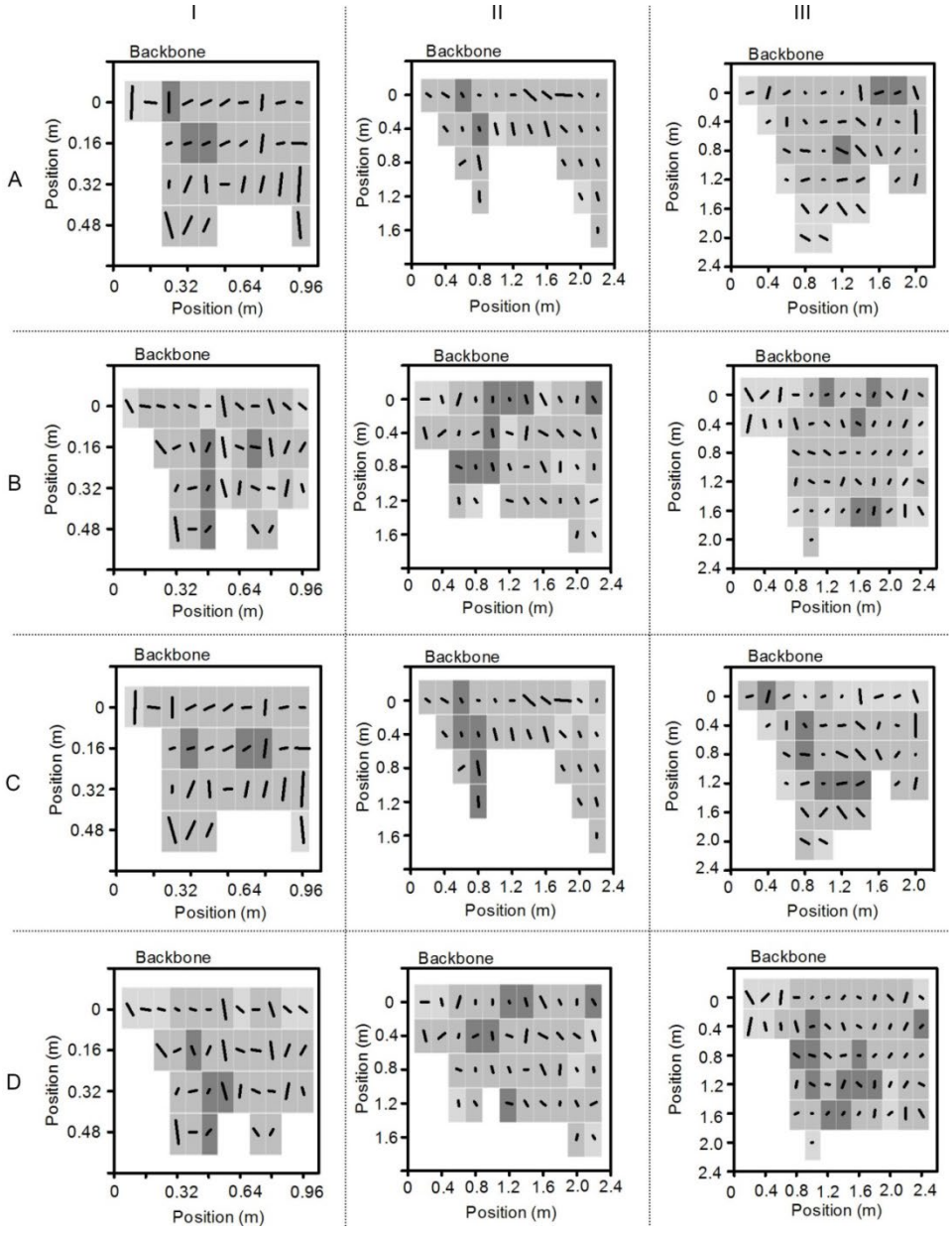

Figure 29. Ovine skin (I), Bovine hide (II) and Cervine hide (III) collagen orientation, orientation index and directional tear strength map. Data is for two ovine halved skins from two animals (a, c) and (b, d) with the neck on the left. (a, b) displays the perpendicular tear strength. (c, d) displays the parallel tear strength relative to the backbone. Vector direction indicates the collagen fibril orientation; vector magnitude indicates the OI; shading indicates tear strength relative to the backbone as detailed in the key: middle column (grey) average for the half hide +/- one standard deviation; left column (light grey) average – one standard deviation; right column (dark grey) average + one standard deviation.

Figure	Key (N/mm)		
I A	< 4	4– 19	> 19
I B	< 4	4– 21	> 21
I C	< 16	16– 38	> 38
I D	< 22	22– 39	> 39
II A	< 21	21– 44	> 44
II B	< 37	37– 65	> 65
II C	< 13	13 - 48	> 48
II D	< 36	36 - 60	> 60
III A	< 35	35– 57	> 57
III B	< 50	50– 66	> 66
III C	< 38	38– 66	> 66
III D	< 53	53– 69	> 69

SAXS Measurements. Small angle X-ray scattering produced clear scattering patterns with pronounced diffraction rings due to the collagen D-spacing (Figure 30). From these the azimuthal angle intensity variation was plotted and the well-defined distributions were used to obtain the average fibril orientation and orientation index at the 6th order diffraction peak. Most of the samples showed a well-defined unimodal fibril orientation.

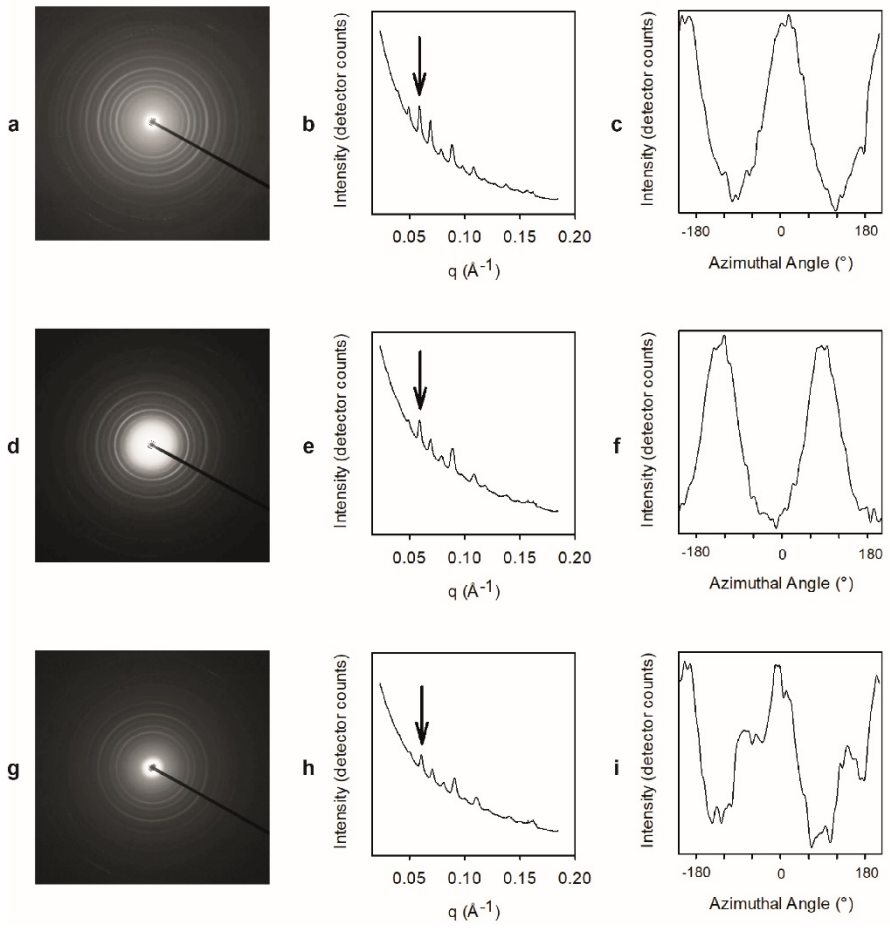

Figure 30. Small angle X-ray scattering (SAXS) of leather from the official sampling position (OSP) of hides halved from neck to tail. (a, d and g) SAXS scattering patterns for (a) ovine; (d) bovine and (g) cervine species; (b, e and h) equatorial intensity profile where the selected 6th order D-period diffraction peak is indicated by the arrow; (c, f and i) azimuthal intensity profile of the selected 6th order D-period diffraction peak.

Variation of O in the OSP grid square sample. There was little variation between the O values calculated for each of the nine measuring points separated by 0.5 mm in the 3 x 3 grids studied (Figure 31b, d and f). There was also little variation between SAXS measurements taken in the centre of the OSP sample as compared to those taken in the corners of the OSP samples (Figure 31a, c and e) indicating central sampling for O gave representative data for the entire grid sample area on the skins and hides in this study. The OSP is known to be the most consistent in regards to physical testing (such as tear), and hence it was important to confirm the idea in the content of these SAXS measurements.

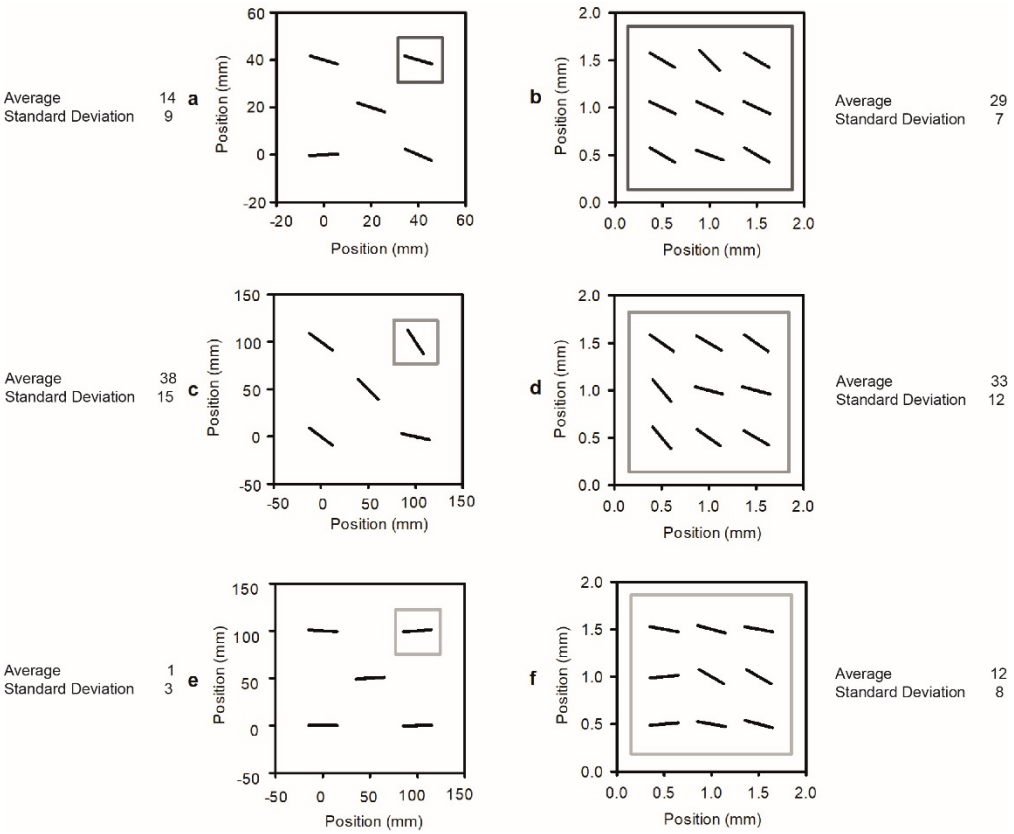

Figure 31. Collagen orientation (O) represented by the vector direction at different small angle x-ray scattering (SAXS) measuring positions in samples from the official sampling position (OSP) of (a, b) an ovine skin; (c, d) a bovine hide; and (e, f) a cervine skin. For (a, c, e) the values are for the 5 SAXS measuring points made at the OSP sample grid square. For (b, d, f) the values are for the 3 x 3 sampling grid for the grey box, highlighted on the left figures, where the average O across the nine points creates this vector. An angle of 0° represents alignment from head to tail, along the backbone. Averages and standard deviations are calculated across all the vectors shown on the graph.

Orientation Index. The average OI varied between species with cervine skins having the least aligned collagen fibres and ovine hides having the most aligned fibres (Table 5).

Orientation. The average collagen alignment was predominately perpendicular to the backbone in all species (average = 48°; SD ± 3°) (Table 6). Despite this trend the O varied considerably between measurement points (Figure 28) and between species (Table 4).

Table 6. A comparison of averaged tear strength parallel and perpendicular to the backbone, orientation (O) and orientation index (OI) between species. P-values are for a t-test of whether the means are different (where $P < 0.05$ indicates the means are significantly different).

Comparison	Parallel Tear Strength (N/mm)	Perpendicular Tear Strength (N/mm)	O (°)	OI
P-value (Ovine and Bovine)	0.314	0.192	0.143	0.115
P-value (Ovine and Cervine)	0.103	0.056	0.172	0.140
P-value (Bovine and Cervine)	**0.036**	**0.032**	0.095	**<0.001**

Correlation between O and Tear Strength. When the O and tear strength at each measurement site were compared (Figure 32), there was no significant correlation between the direction of the collagen fibres and the tear strength. Tear strength perpendicular to the backbone was not correlated with a low orientation angle, and the tear strength parallel to the backbone was not correlated with a high orientation angle.

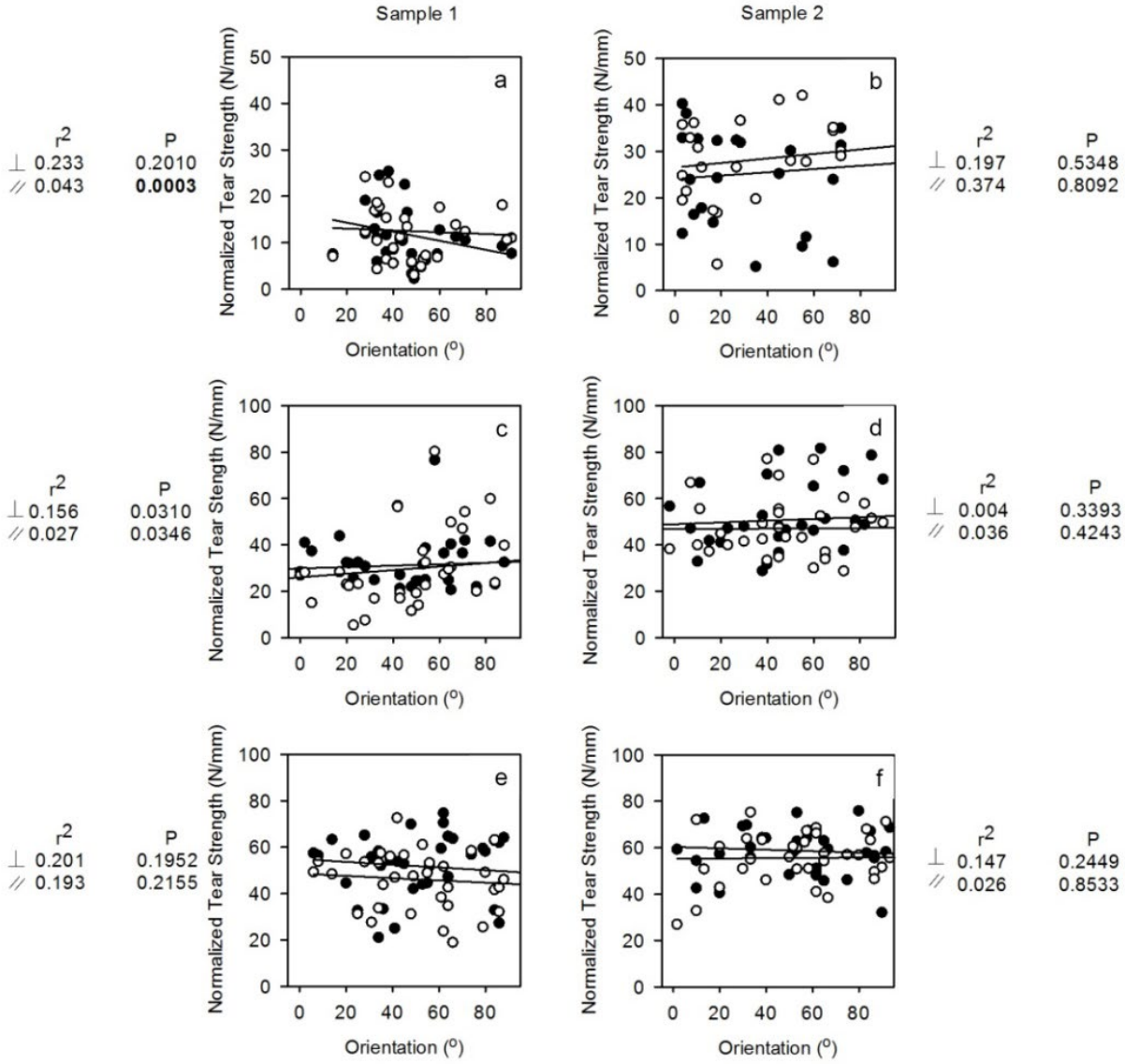

Figure 32. Relationship between orientation (O) and tear strength measured perpendicular (filled circles) and parallel (hollow circles) to the backbone for (a, b) ovine (c, d) bovine and (e, f) cervine half skins/hides at all measurement sites. r^2 and P-values reflect best linear fit parameters where ⊥ represents perpendicular to the backbone measurements and // represents parallel to the backbone measurements. An orientation of 0° represents alignment from head to tail, along the backbone, while 90° is perfectly perpendicular to the backbone.

Difference between Belly and Back. The individual values of OI and tear strength for each of two regions, the back area and the belly, of the skins and hides have been selected as a basis for comparison between species (Figure 33). These locations are likely to have similar structure-property relationships and may provide better measurements for comparison between species than averages for whole skins/hides. With this comparison we see the correlation between OI and tear strength in both tear directions is stronger in the backbone region of the bovine hides and cervine skins. In ovine skins the correlation is weak at both locations and tear directions (Table 7). These finding are consistent with what has been tentatively proposed previously[47].

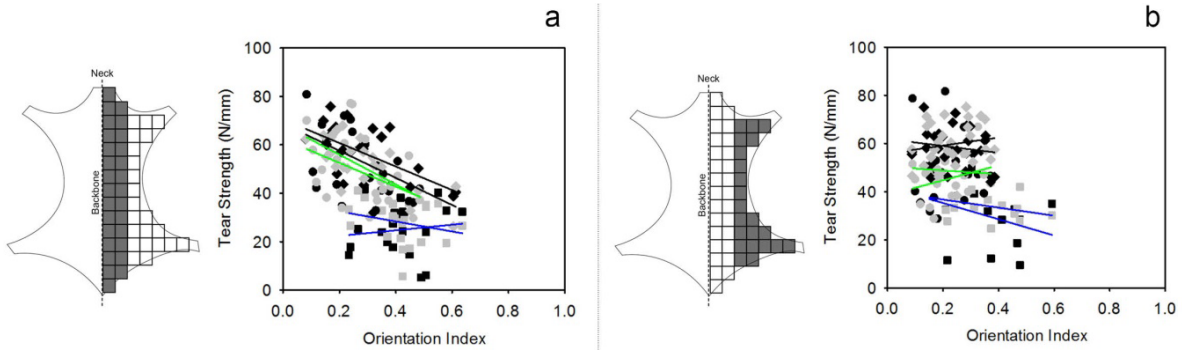

Figure 33. Relationship between tear strength measured perpendicular (black) and parallel (grey) with the orientation index (OI) along the (a) backbone and (b) belly for ovine (square), bovine (circle) and cervine (diamond). Linear interpolation r^2 values are shown in Table 7.

Table 7. Linear interpolation r^2 values for directional tear strength and Orientation Index (OI) in Figure 33.

Species	Trend line colour	r^2 backbone (perpendicular)	r^2 backbone (parallel)	r^2 belly (perpendicular)	r^2 belly (parallel)
Ovine	Blue	0.12	0.25	0.33	0.33
Bovine	Green	0.54	0.42	0.05	0.30
Cervine	Black	0.55	0.74	0.15	0.15

Discussion

This study has shown that tear strength varies considerably over the skins of ovine and cervine and hides of bovine leather, and that there is no predictable pattern in an individual. However, there are limitations in this study with the sample size of just two animals per species.

Overall it was found that cervine skins and bovine hides had the greatest strength and ovine skins the least; in none of the species could a part of the skin/hide be identified to have a consistently higher strength than another. The variation in leather strength in different species has been observed before[47], where it is primarily thought to be due to the collagen alignment, viewed edge-on, with stronger leather having a greater in plane alignment with little cross over between layers[5] or high angle of weave. We see different trends here with SAXS measurements made normal to the grain surface showing us the collagen alignment viewed flat-on. Fibril diameters have also been found to weakly correlate with leather strength in bovine leather, but not in ovine leather[69].

Previous work on a calf hide and ovine skin found a preferred collagen alignment parallel to the backbone and limbs[12, 137]. In contrast, the averaged results presented here found the preferred arrangement was perpendicular to the backbone across all species which may be attributed to the larger number of sampling points taken at the limbs, where the alignment tended to be more perpendicular to the backbone. Alignment parallel to the backbone is consistent with the idea that the collagen lies perpendicular to the maximum stretch direction needed for animal movement. A variety of studies have been performed on humans to determine surface movement errors in biomechanics resulting from markers placed on the skin when trying to

determine bone movement during exercise[59, 143]. Significant surface movement difference relative to bone movement is observed over joints[144], suggesting skin has significant movement during motion. This supports the idea that forces applied to the skin resulting from animal movement could influence collagen alignment and that this movement could result in collagen aligning in the direction of strain[7, 118]. In cases where aligned collagen fibres experience repetitive strain, below their failure limit, the collagens helix substructure has been shown to recover when the load is removed[145]. However, these forces are not acting in isolation. The downward force acting on skin from gravity is constant and can become larger when the weight is increased due to dense hair coverage. In the case of the ovine skins an additional 4-9 kg/animal of clean fleece weight[146] (with an additional 15-80% when grease and dirt is present[147]) is loaded onto the skin. If this persistent force is contributing to the strain applied on the skin this could provide an explanation for why the ovine skins we observed here tended to have the collagen fibrils most aligned in the direction of gravity for a standing animal.

Conclusions

Normalized tear strength measured across ovine and cervine skins and bovine hides showed cervine leather had the greatest overall strength followed by bovine then ovine leather. Ovine had the greatest variability in strength across the skin. There were no obvious regions of generally stronger or weaker skin within individual skins or hides. The predominant collagen fibril direction was perpendicular to the backbone of all species, with the greatest alignment found in ovine followed by cervine then bovine. These findings have important implications for manufacturers of leather products. They show there is no relationship between flat-on orientation measurements over the whole skin and with tear strength. The orientation maps presented here suggest it is the selection of the species that should be considered first if strength is a priority rather than the location within a skin/hide.

Chapter 4. Artificially modified collagen Fibril Orientation Affects Leather Tear Strength

Kelly S. J., Wells H. C., Sizeland K. H., Kirby N., Edmonds R. L., Ryan T., Hawley A., Mudie S. and Haverkamp R. G., Artificially modified collagen fibril orientation affects leather tear strength. *Journal of the Science of Food and Agriculture* 98(9):3524-3531.

Abstract

Ovine leather has around half the tear strength of bovine leather and is therefore not suitable for high value applications such as shoes. Tear strength has been correlated with the natural collagen fibril alignment (orientation index, OI). It is hypothesized that it could be possible to artificially increase the OI of the collagen fibrils and that an artificial increase in OI could increase tear strength. Ovine skins, after the pickling and bating, were strained bi-axially during chrome tanning. The strain ranged from 2% to 15% of the initial sample length, either uniformly in both directions by 10% or with 3% in one direction and 15% in the other. Once tanned the leather tear strengths were measured and the collagen fibril orientation measured using synchrotron based small angle X-ray scattering. The OI increased as a result of strain during tanning, from 0.48 to 0.79 ($P = 0.001$), measured edge-on and the thickness normalized tear strength increased from 27 N/mm to 43 N/mm ($P < 0.001$) after leather was strained 10% in two orthogonal directions. This is evidence to support a causal relationship between high OI (measured edge-on) and tear strength. It also provides a method to produce stronger leather.

INTRODUCTION

Skins possess a sophisticated stretch mechanism in which collagen fibres glide and align in the direction of strain resulting in the individual fibres equally absorbing the forces[7, 118]. Collagen is a major component of skins and its structural arrangement greatly influences the strength of leather products[2]. Increased collagen fibre alignment has been found to be associated with increased tear strength in leather produced from a variety of animals and a linear relationship has been demonstrated between tear strength and the degree of collagen fibril alignment[47]. It has been proposed that an important contribution to the greater tear strength of bovine leather compared to ovine leather is the greater collagen fibril orientation index (greater fibril alignment) in the plane of the leather[5]. This lower strength of ovine leather means that it is not suitable for high value applications such as shoes and upholstery. Tear strength is also related to collagen fibril diameter to a small extent although there is species variation with a weak correlation between fibril diameter and tear strength for bovine leather but not ovine leather[69].

Mechanical methods have been used to influence alignment of component fibres in the production of a variety of materials to enhance strength. Laminated dough (or puff pastry) utilizes rolling to align gluten fibres to create sheets[148] and re-enforced concrete has strategically embedded steel fibres, placed in the direction of tensile stresses to enhance the tensile strength of concrete[149]. In biological materials fibre arrangements are also mechanically influenced. Collagen is the most abundant fibrous protein in the body and it is the arrangement of these fibres that has the greatest influence on the mechanical performance of connective tissue like tendons[150] and skin[7, 126] where fibres lie in the direction of major stress.

The tanning process affects the alignment of collagen in skins[151] and has an impact on strength.. Drying of bovine leather under strain has been shown to increase the tensile strength of bovine leather[152]. Tensile testing gives the ultimate material strength however having a large force distributed evenly over a segment of material is not common in practice. Tear testing, on the other hand, matches the mode of failure in practice where a puncture to the material experiences straining which then propagates into a tear[7] and is therefore a better measure of the performance of the material. Coupling these measurements with small angle X-ray scattering (SAXS) analysis provides further insights into the structural arrangements of the collagen fibrils and how these relate to the material strength of the material[12].

Stretching leather while in the drying stage of manufacture has been used to increase surface area[152-154] with a noted effect on the leather's stiffness and strength. Biaxial stretching on wet partially processed bovine hides found that there was a significant increase in the tensile modulus of leather and this was correlated to the collagen orientation perpendicular to the surface, as measured by wide angle X-ray diffraction[155]. The fibre planes that lay parallel to the surface were less affected by the biaxial stretching. Thickness and hydration state affects the collagen orientation during stages of the processing of ovine pelts to leather. An increase in thickness and hydration state increased alignment during the tanning stages while the application of mechanical stresses during the final staking stage increased the collagen fibre alignment [151].

Although tear strength has been correlated with the natural collagen fibril alignment (orientation index, OI) in leather[5, 47] and other materials[42, 156] it has not been shown either that this is a causal relationship (more than

just a correlation), neither has it been shown that it is possible to increase strength by artificially increasing the orientation index. Here we investigate the hypothesis that a causal relationship exists between orientation and tear strength and to use this concept to create stronger materials.

Methods

Leather preparation. Leather was prepared from ovine pelts which were expected to yield typical strength leather using conventional beamhouse and tanning processes. The ovine pelts were from 8 to 10 month old New Zealand Romney sheep**.** After rehydrating the skins, adhering fat and flesh was removed mechanically and conventional lime sulfide paint (140 g/L sodium sulphide, 50 g/L hydrated lime and 23 g/L pregelled starch thickener) was applied to the flesh side of the skin at a rate of 400 g/m^2. Following incubation at 20 °C for 16 hours keratinaceous materials were removed and the skins washed in water to remove the lime. Following the last wash ammonium sulphate was titrated into the water to lower the pH to 8 and a commercial bate enzyme, Tanzyme (0.1% (w/v)), was added before the skins were incubated at 35 °C for 75 min. Following further washing in water the skins were pickled in 20% (w/v) sodium chloride and 2% (w/v) sulphuric acid.

Control and test samples (each 200 x 200 mm) were obtained from the rehydrated and unhaired pelts at the official sampling positions with the orientation to the backbone noted for all samples.

The test squares were mounted in a biaxial stretching device which applied and maintained strain (2% and 7%; 3% and 15%; 10% and 10%) during the beamhouse and tanning process which was carried out in a bath that contained the stretching apparatus. This choice of strain was determined by: a) for the 10%, 10% stretch the maximum equal biaxial stretch possible determined by the strength of the operator; b) for the 3 and 15% strain, the maximum possible by the strength of the operator in the easier to stretch direction, perpendicular to the backbone, 15% followed by the maximum possible in the direction normal to this after the first strain is applied 3%; c) approximately half of the strain in the unequal biaxial strain. The control samples were processed as normal (Figure 34).

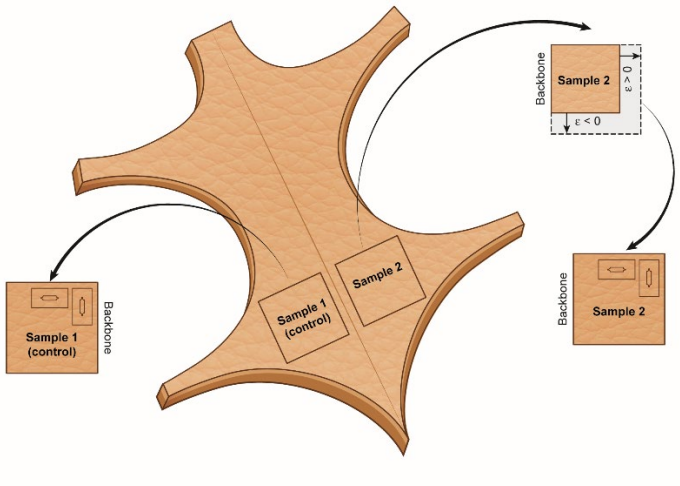

Figure 34. Sampling positions for stretching and tearing from the official sample position (OSP) on the Ovine skin.

Following pickling the control and test samples were degreased in 4% non-ionic surfactant (Tetrapol LTN, Shamrock, New Zealand) for 90 min and then washed. After being neutralized in a 1% disodium phthalate solution (Feliderm DP, Clariant, U.K) for 30 min. The samples were processed overnight at 25 °C in a 5% chrome sulphate solution (Chromosal B, Lanxess, Germany). The following day the samples were neutralized in 1% sodium formate and 0.15% sodium bicarbonate solution for 1 hour, washed in water, and retanned with 2% synthetic retanning agent (Tanicor PW, Clariant, Germany) and 3% vegetable tanning (mimosa) (Tanac, Montenegro, Brazil). Finally the skins were treated with a 6% fatliquor solution and fixed with 0.5% formic acid for 30 min. After a final wash in cold water the stretched samples were removed from the biaxial stretching devices and left to dry with the control samples.

Tear strength. Tear strengths were measured according to standard methods (ISO 3377-2:2002) and normalized for thickness. Samples were cut from the official sampling position and treated at constant environment conditions (20 °C and 65% relative humidity) for 24 hours before tear strengths were recorded on an Instron 4467 instrument.

SAXS analysis. For SAXS analysis two types of samples were taken from both the stretched and control leather samples (Figure 35). Circles (4 mm diameter) were punched from the leather to perform measurements with the X-rays perpendicular to the surface, flat on. Nine diffraction patterns were recorded on each sample using a three by three grid with 0.25 mm spacing between points. Samples were measured at ambient humidity.

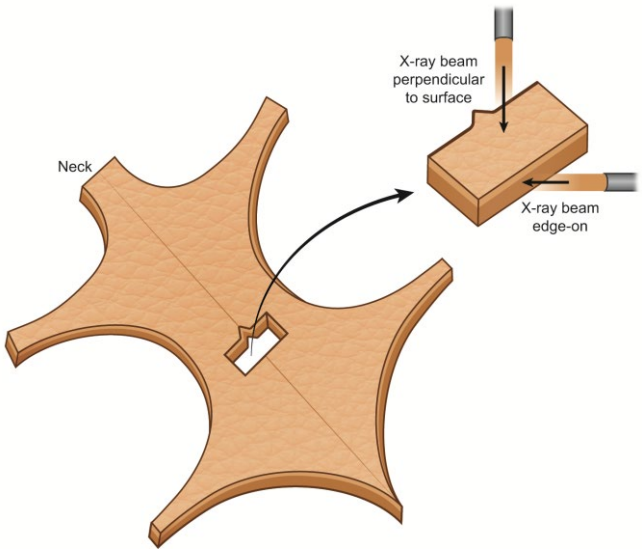

Figure 35. Orientation of sample relative to the X-ray beam to produce edge-on measurements.

The second sample type, for edge-on analysis, consisted of thin strips of leather (1 x 5 mm) that were placed with the cross section (the cut edge) facing the X-ray beam. Measurements were made with 0.25 mm spacing between points in a vertical line down the cross section from the grain to the corium.

The diffraction patterns were recorded on the Australian Synchrotron SAXS/WAXS beamline. A high-intensity undulator source was utilized with an energy resolution of 10^{-4} from a cryo-cooled Si(111) double-crystal monochromator. The beam size (FWHM focused at the sample) was 250 x 80 µm with a total photon flux of about 2 x 10^{12} photons s^{-1}. All diffraction patterns were recorded with X-ray energy of 8 keV using a Pilatus 1M detector with an active area of 170 x 170 mm and a sample to detector distance of 3371 mm. The exposure time for diffraction patterns was in the range of 1–5 seconds, and data processing was carried out using the Scatterbrain software. Intensities displayed are all absolute detector counts (one X-ray detected one detector count), except where stated otherwise.

The collagen orientation was determined from the azimuthal angle for the maximum intensity of the D-spacing diffraction peaks. The orientation index (OI) was the primary measure used where OI is defined as (90°−OA)/90°, where OA, the orientation angle, is the minimal azimuthal angle range, centred at 180°,that contains 50% of the micro fibrils [11, 109]. The OI range takes us from perfect anisotropic alignment which is represented by an OI of 1, through to an OI of 0 which represents isotropy. The OI was calculated from the spread in the azimuthal angle of the D-spacing peak at 0.059 − 0.060 $Å^{-1}$. Each OI value presented here represents the average of 14 − 36 measurements of one sample.

Results

Stretch-tanned leather. Three leather samples were prepared with biaxial stretching during tanning, each with a non-stretched counterpart which was cut from the same skin to act as the control.

Measured as a percentage of length gain relative to their original length, the following strains were used in the preparation of the tanned leather: 2% parallel to the backbone and 7% perpendicular to the backbone; 3% parallel to the backbone and 15% perpendicular to the backbone; 10% parallel to the backbone and 10% perpendicular to the backbone.

It required less force to stretch the skins in the direction perpendicular to the backbone than parallel to the backbone. The resulting tanned leather did not shrink after strain was removed and had an area gain of 9%, 18% and 21% respectively.

SAXS. The leather samples gave scattering patterns with well-defined diffraction peaks (Figures 3 a, b). Choosing the fifth order D-period diffraction peak, and plotting the variation in the intensity of this peak with azimuthal angle, it is seen that there is a simple unimodal collagen fibril orientation distribution when measured edge-on (Figure 36).

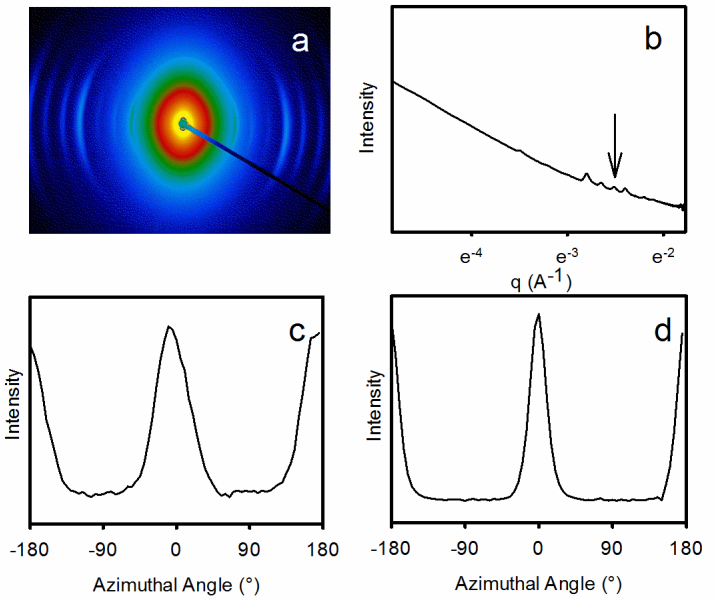

Figure 36. An example of the SAXS pattern (a) and its corresponding intensity profile (b) for a stretched leather sample. Integrated intensity plots (I(q)) at the 5th diffraction peak for non-stretched (c) and stretched (d) leather samples measured edge-on to X-ray beam.

Collagen fibril re-orientation. A change in orientation and a change in the orientation index are observed as a result of the strain during tanning (Figure 37 and Table 8). The fibrils change orientation towards the direction of the applied strain, measured both edge-on and flat on, with the largest change occurring edge-on (ΔOI = 0.31, P= 0.001) . The fibrils become more oriented (the OI increases) with strain for orientation measured edge-on. However, for the OI measured flat-on the relationship between OI and strain is not simple. When the dominant strain is perpendicular to the direction of the initial preferred orientation of the fibrils (this initial direction is parallel to the backbone), the OI goes down with strain. When the strain is applied equally in two directions the OI doesn't change significantly (ΔOI = 0.02, P = 0.78).

Table 8. Stretched samples and their orientation index measured flat-on and edge-on and fibre orientation where OL is the original length, OI is the orientation index, SD is the standard deviation, the fibril orientation is relative to 0° which is perpendicular to the backbone and P-values are relative to the control, non-stretch tanned leather.

Stretch parallel to backbone (% OL)	Stretch perpendicular to backbone (% OL)	OI (flat-on ± SD)	OI (edge-on ± SD)	Fibril Orientation (°)	P values (flat on, edge on)
2	7	0.37 ± 0.07	0.66 ± 0.26	-1	0.48, <0.001
3	15	0.32 ± 0.14	0.79 ± 0.04	-3	0.06, 0.001
10	10	0.42 ± 0.09	0.65 ± 0.11	-17	0.78, 0.001
0	0	0.40 ± 0.08	0.48 ± 0.01	-10	n/a

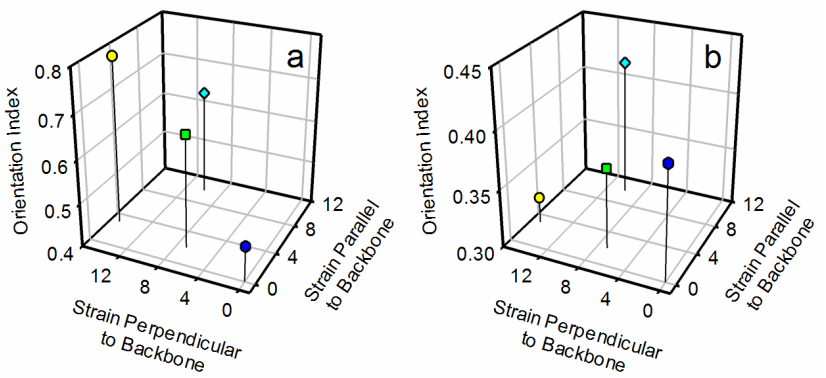

Figure 37. Bi-axial stretching and its effect on the edge-on (a) and flat-on (b) orientation index.

Model of OI change with thickness. If the collagen fibrils are not lying flat then as the thickness of the leather decreases on stretching the angle of these fibrils to the plane of leather will decrease. This will cause an increase in OI. Previously a model was developed for the change in OI with thickness changes[151] and the details are repeated here.

The range of fibre angles in a sample is given by the orientation angle, OA, which is defined as the subtended angle that contains half the fibrils, i.e. it satisfies Equation 8**;**

$$0.5 = \frac{\int_{\emptyset=-\frac{OA}{2}}^{\emptyset=\frac{OA}{2}} \theta\, N(d\emptyset)}{\int_{\emptyset=-90^\circ}^{\emptyset=90^\circ} \theta\, N(d\emptyset)}$$

Equation 8. The orientation angle (OA) defined as the subtended angles (Ø) which contain half the fibrils in a sample.

Where N is the number of fibrils, and Ø is the fiber angle (relative to the plane of the leather). In practice this is determined from the SAXS diffraction pattern by the integrated intensity verses azimuthal angle for one of the D-spacing diffraction peaks, Equation 9:

$$0.5 = \frac{\int_{\emptyset=-\frac{OA}{2}}^{\emptyset=\frac{OA}{2}} \emptyset\, I(d\emptyset)}{\int_{\emptyset=-90^\circ}^{\emptyset=90^\circ} \emptyset\, I(d\emptyset)}$$

Equation 9. The orientation angle (OA) relative to an integrated intensity (I(dØ)) over an azimuthal angle (Ø).

Where I is diffraction intensity of a selected D-spacing diffraction peak above a fitted background and $\boldsymbol{\theta}$ is the azimuthal angle of the diffracted X-rays. OI is derived from OA by Equation 10.

$$OI = \frac{90^\circ - OA}{90^\circ}$$

Equation 10. Orientation Index (OI) relative to the orientation angle (OA) centred at 90°.

Therefore, for perfect alignment in the reference direction OI = 1 and for a completely isotropic arrangement of fibrils OI = 0.

If a sample of leather containing a fibre shrinks in thickness uniformly, and the fibre is at an angle θ_1 from the base, then the new angle of the fiber, θ_2, depends on the change in thickness by Equation 11.

$$\frac{T_2}{T_1} = \frac{tan\ \theta_2}{tan\ \theta_1}$$

Equation 11. Changes to the relative fibre angle (θ) from a uniform change in thickness (T).

Where T_1 is the original thickness, and T_2 is the new thickness.

Rearranging Equation 11 for θ_2 gives the new angle of the fiber after the leather has decreased in thickness:

$$\theta_2 = tan^{-1}\left(\frac{T_2}{T_1}\ tan\theta_1\right)$$

Equation 12. Fibre angle after a decrease in thickness.

It is then possible to calculate a transformed OA after stretching. It is only necessary to calculate the transformation by Equation 12 of the angle that is the OA to calculate the new OA that represents the new fibre distribution.

The change in the thickness in the leather produced as a result of stretching while tanning (compared with the unstretched material) can then be used to calculate the change in OI due to this affine transformation. It is found that the change in OI can be explained solely by the change in thickness (Table 9).

Table 9. Tear force for tanned leather parallel and perpendicular to the backbone where OL is the original length, NTF is the normalized tear force and P-values are relative to the control, non-stretch tanned leather.

Stretch perpendicular to backbone (% OL)	Stretch parallel to backbone (% OL)	Parallel NTF (N/mm ± SD)	Perpendicular NTF (N/mm ± SD)	P values (parallel, perpendicular)
2	7	34 ± 3.33	38 ± 3.23	0.084, <0.001
3	15	38 ± 1.19	43 ± 4.24	0.083, 0.005
10	10	43 ± 2.37	38 ± 0.80	<0.001, <0.001
0	0	27 ± 0.36	29 ± 3.60	n/a

Strength changes from stretching during tanning. The absolute tear strength of the leather was less for leather tanned while stretching (Table 4.3). However, as a result of the thickness change with stretching, the tear strength normalized for thickness increased as a result of tanning under strain (Table 9). In leather processed without strain (the control samples) the tear strength when torn parallel (27 ± 0.4 N/mm) or perpendicular (29 ± 3.6 N/mm) to the backbone were not statistically different (P = 0.73). For the leather prepared by tanning under strain, the normalized tear strength increases in both directions (Figure 38), showing that tanning under strain does cause a change in thickness normalized strength of the material as hypothesized. However, the relationship between strain and tear strength also depends on the relative directions of the applied strain and the measured direction of the tear strength. When the tear strength is

measured in the same direction (where the "direction" means the direction of the initiated fracture, which is at right angles to the direction of the movement of the jaws used for tearing) as the strain had been applied during tanning, the maximum strength is achieved with the maximum strain in that direction (42.8± 4.2 N/mm for both of these parallel to the backbone, and 42.8 ± 2.4 N/mm for both of these perpendicular to the backbone). However, when the tear strength is measured perpendicular to the direction the strain had been applied during tanning the relationship is not as simple, with the tear strength increasing with greater strain when the strain is in the direction parallel to the backbone but staying relatively constant for increasing strain perpendicular to the backbone.

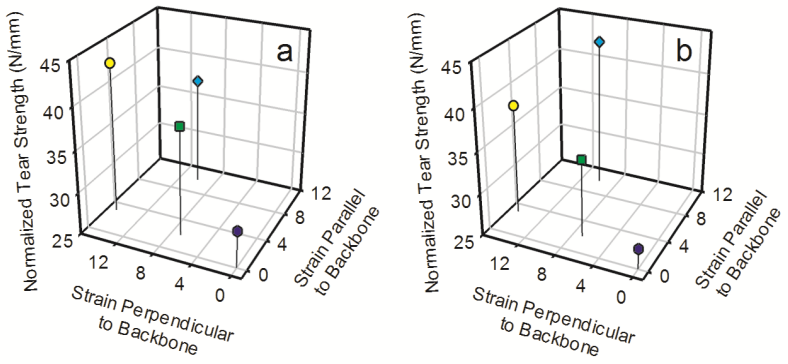

Figure 38. Bi-axial stretching and its effect on normalized tear strength parallel to the backbone (a) and perpendicular (b).

Structure – strength relationship. A relationship can be seen between OI and tear strength (Figure 39). A greater in-plane OI produces greater tear strength in both the parallel and perpendicular tear directions. There is a strong linear correlation between strength and collagen fibre orientation measured edge-on (R^2 0.65 and 0.86 respectively for a least squares linear fit).

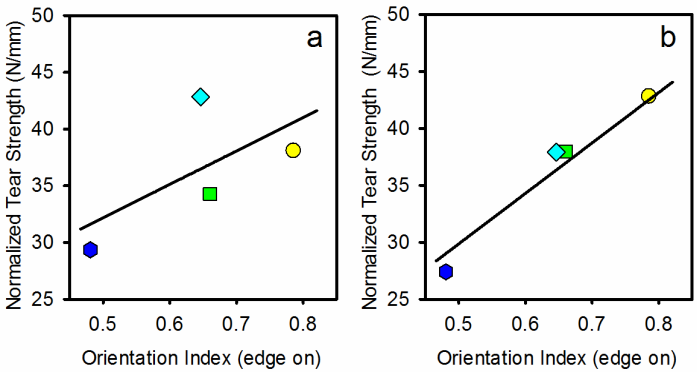

Figure 39. Edge-on orientation index and normalized tear strength torn parallel (a) and perpendicular (b) to the backbone: (green square) strain applied at 2% parallel to the backbone and 7% perpendicular to the backbone; (yellow circle) strain applied 3% parallel to the backbone and 15% perpendicular to the backbone; (blue diamond) strain applied 10% parallel to the backbone and 10% perpendicular to the backbone; (deep blue hexagon) control with no strain applied.

Discussion

Collagen fibril structural changes. It is apparent that it is possible to modify the structural arrangement of collagen fibrils in leather by modification to the tanning process. The OI increases both as measured edge-on (so that the layered structure of collagen fibrils is enhanced) and as measured flat-on (Table 8). The increase in OI measured edge-on is approximately proportional to strain during tanning, in the range of strain used in these experiments. With an increase in fibre alignment edge-on there is a decrease in the OI measured flat-on (Figure 40). The hides required less stress to strain them in the direction perpendicular to the natural fibril orientation. The reason for this is that the fibrils are strong along their length [70, 119] but the connections between fibrils are weak [121] so that it is much easier to pull the fibrils apart than to stretch them.

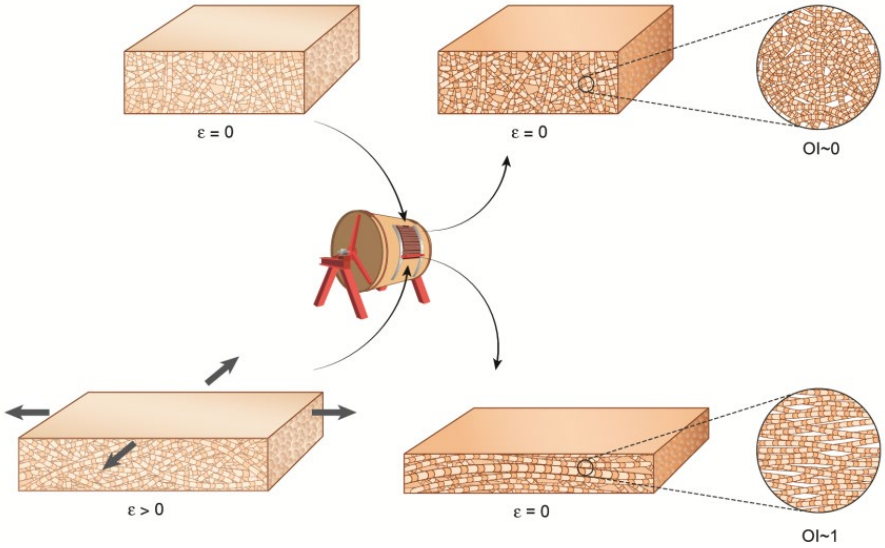

Figure 40. Tanning under strain (ε) and its effect on fibril alignment.

The strain possible in this work was limited by the force available with the apparatus, but it may be possible to strain the leather more and therefore increase the OI further.

Structure affects strength. Overlaying the orientation information with the tear strength has provided a basis to develop an understanding of the relationship between process-modified collagen fibril orientation and strength. Previously it had been seen that there is a correlation between the native OI and tear strength in leather made from the hides of different animals of the same species[5] and between animals of different species[47] and this suggested the concept of developing a structure with an artificially high OI to generate extra strength. This would achieve two purposes: firstly to support the concept that there is a causal relationship between OI and tear strength and secondly as a method to produce a manufactured material with modified or improved properties.

Utilizing this natural property of strong skin, here it has been shown to be a cause and effect relationship between collagen alignment and mechanical function by artificially creating a high OI material which resulted in a material with greater tear strength. It was found that the OI could be increased very substantially in-plane from 0.48 to 0.79. The edge-on OI is most influenced by the stretch forces applied perpendicular to the backbone.

Tear strength is affected by the collagen fibre orientation where a tear propagates more easily between the fibrils than across the fibrils (Figure 41). Therefore changing the orientation affects the ease of tear differently in different directions. In cases where the fibres are aligned perpendicular to the movement of the jaws for the tear test (Figure 41 (a)) the tear direction is along the path of least resistance which is perpendicular to the movement of the jaws. However, when fibres are aligned perpendicular to the direction of the movement of the jaws for the tear test (Figure 41 (b)) the tear propagates in this same direction as the applied force, along the path of least resistance between the collagen fibrils. When fibrils are more highly aligned they display their greatest tear strength to forces applied perpendicular to the fibril direction.

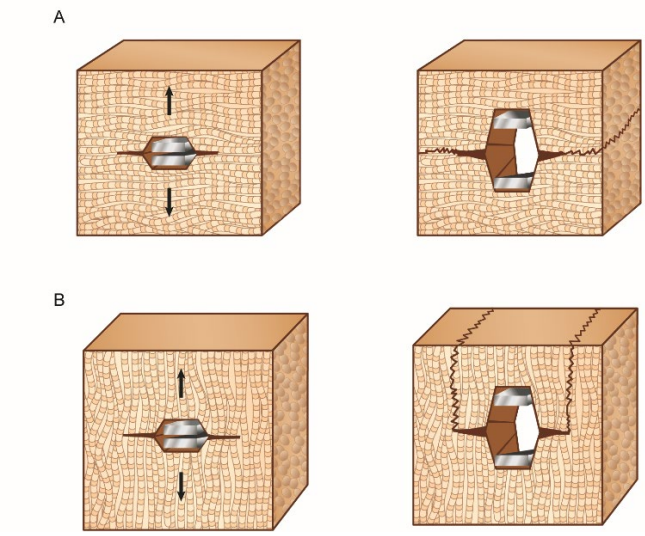

Figure 41. Tear propagates more (a) readily along the direction of the collagen fibrils when parallel to the movement of the jaws for the tear test. Tear propagation is (b) resisted by collagen when arranged perpendicular to the movement of the jaws for the tear test. The arrows represent the direction of movement of the jaws of the tear test apparatus.

Material application considerations. The ability to manipulate the collagen structures in skins to produce leather with customized characteristics could prove valuable for industry applications when producing skins with specialized mechanical properties. Understanding how the application of strain can change the collagen alignment, which ultimately determines a significant portion of the tear strength properties of the leather, allows manufacturers to introduce processing steps to align the collagen fibrils to tailor the leather to the properties they desire. This concept could be implemented to allow ovine leather to be used for a wider range of applications and thus offer a significant increase in value and it may also be possible to increase the tear strength of other leather (such as bovine) that is naturally stronger than ovine. Once stretched the tanned skins don't return to their original size allowing for a gain in surface area as well as stronger leather. A surface area gain of up to 21% was achieved here. Leather is sold by surface area so the increase in surface area increases revenue. The thickness of the leather is important for each application and leather is split of shaved to achieve the desired thickness. Therefore the thickness normalized strength is the primary tear strength consideration, rather than the absolute tear strength of leather prior to splitting. Although the absolute tear strength decreased on stretching during tanning, the strength for any given thickness of leather produced by this method will be stronger than for a corresponding leather made without stretching during tanning. A further understanding of the natural collagen fibre alignments found in skins would provide a useful basis for more strategic stretching to produce certain properties in the leather.

Conclusions

Evidence has been provided to support a causal relationship between a high edge-on collagen fibril OI and tear strength. A relationship is found between the amount of strain applied during tanning and resultant thickness normalized tear strength. The tear strength depends on the relative directions of strain applied during tanning and the measured direction of tear strength. A greater in-plane OI produces greater tear strength in both the parallel and perpendicular tear directions to give a strong linear correlation between strength and collagen fibre orientation measured edge-on. Previously this relationship had been seen in a range of natural collagen materials but in this instance a material has been manufactured with improved properties demonstrating both the causal relationship and the ability to use this modify natural materials. This concept could be implemented to allow ovine leather to be used for a wider range of applications and thus offer a significant increase in value.

Chapter 5. Effect of moisture content on collagen packing and stiffness in stretch-tanned leather

Kelly S. J., Weinkamer R., Bertinetti L., Edmonds R. L., Sizeland K. H., Wells H. C., Fratzl P. and Haverkamp R. G., Effect of collagen packing and moisture content on leather stiffness, *Journal of the Mechanical Behavior of Biomedical Materials,* **90**:1-10 (2019).

Abstract

Applications for skin derived collagen materials, such as leather and acellular dermal matrices, usually require both strength and flexibility. In general, both the tensile modulus (which has an impact on flexibility) and strength are known to increase with fibre alignment, in the tensile direction, for practically all collagen-based tissues. The structural basis for flexibility in leather was investigated and the moisture content was varied. Small angle X-ray scattering was used to determine collagen fibril orientation, elongation and lateral intermolecular spacing in leather conditioned by different controlled humidity environments. Flexibility was measured by a three point bending test. Leather was prepared by tanning under biaxial loading to create leather with increased fibril alignment and thus strength, but this treatment also increased the stiffness. As collagen aligns, it not only strengthens the material but it also stiffens because tensile loading is then applied along the covalent chain of the collagen molecules, rather than at an angle to it. Here it has been shown that with higher moisture content, greater flexibility of the material develops as water absorption inside collagen fibrils produces a larger lateral spacing between collagen molecules. It is suggested that water provides a lubricating effect in collagen fibrils, enabling greater freedom of movement and therefore greater flexibility. When collagen molecules align in the strain direction during tanning, leather stiffens not only by the fibre alignment itself but also because collagen molecules pack closer together, reducing the ability of the molecules to move relative to each other.

INTRODUCTION

Leather is a fibrous type I collagen material prepared from animal skins. It is the strength and flexibility of leather that are the primary characteristics that make it a useful product. Other aspects such as being a natural product, the appearance and smell also contribute to the demand for leather. For clothing, soft and supple leather is particularly important, and for shoes, the main high value use for leather, it must be strong but not too stiff. Bending or tensile stiffness depend on the inherent properties (Young's modulus) of the skins or hides[157], which are affected by treatment processes such as fatliquoring[158], and the moisture content of the leather[159]. Leather can be considered to have a two layer structure, composed of the outer grain and the inner corium where the size and packing of collagen fibres differentiates the layers. In the corium, fibres are at their largest with diameters of approximately 0.1 mm. The fibres become finer as they approach the grain surface where the diameters are approximately 0.001 mm[35]. The variation in diameter allows for fine interweaving of the smaller fibres in the grain layer, creating a smooth aesthetically pleasing surface, while the larger fibres in the corium interweave more loosely allowing fibril movement for stretching and resistance to tear propagation[160].

Leather properties are not only attributed to fibre size, but also the arrangement of the collagen fibril bundles that make up the fibres. The arrangement of fibrils has been shown to have a large effect on the mechanical properties of leather and other similar materials. When the fibrils are arranged in parallel layers the material is stronger than when there is an isotropic arrangement[5, 47]. The fibril arrangement varies from one animal species to another[47] and with the age of the animal[3, 161]. The fibril arrangement and therefore strength can also be altered by processing conditions through mechanical applications or by different chemical treatments[151, 162, 163].

Beside structural aspects, the chemical composition influences the mechanical performance of leather. During the tanning process, cross linking agents such as chromium sulphate or vegetable tannins, fats and oils are introduced into the animal skin to increase the integrity of the collagen matrix. Water is also an important component of leather where the moisture content affects both its flexibility and strength. Dry leather is stiff and brittle compared to hydrated leather, where the strongest leather typically have moisture contents over 50%[164]. The treatment process of leather and its water content cannot be considered independently from one another. Increases in moisture content have been observed with increasing fatliquor treatment where fatliquor content has been correlated with leather strength[165] and flexibility, in part by retaining moisture[13], and also by preventing fibres sticking together[166]. Fatliquoring is the last of the wet processing stages in the production of leather. Adding emulsions to a regulated environment helps to achieve an even fat distribution within the leather, improving its strength and mechanical properties[167]. There are many formulations of fatliquors, but the property they have in common is that they contain amphoteric compounds that assist to retain water in the collagen structure.

The structure of collagen is linked to its moisture content. When collagen is hydrated, the length of the collagen fibril slightly increases which can be measured by the increase in D-spacing, the regular banding on

each collagen fibril[168, 169]. Dehydrating collagen leads to strong tensile forces being generated as fibrils attempt to shorten[114, 170].

The structural factors that lead to stiffness in collagen materials have not been fully elucidated. However, there is evidence from studies with 2-propanol treated collagen scaffolds that a decrease in intermolecular spacing (not necessarily accompanied by water loss) increases stiffness[171] and that it is the fibril-to-fibril contact which influences the mechanical properties of the material rather than the fibril core[172].

Collagen structural features at the nanometre scale, which may be affected by water content, are best quantified by techniques that do not require substantial chemical treatment or dehydration. Small angle X-ray scattering (SAXS) has been shown to be a powerful technique for determining a range of structural features of collagenous materials including D-spacing, fibril diameter, fibril orientation and intermolecular spacing[88, 173]. These parameters have been recorded at various hydration states to observe how water interacts with collagen structures in the cornea[81] and in rat tail tendon, turkey leg tendon and bone[81] with notable effects on internal stresses due to osmotic pressure[113, 114].

In the current study the influence of two factors and their interplay with leather structure and function are investigated: first, the presence or absence of a tensional strain during the tanning process and, second, the moisture content of the leather. The aim of this study is to clarify the influence of these two factors on the size and arrangement of the collagen fibrils, and to connect these structural changes to the measured mechanical properties of the leather. For the investigations SAXS, scanning electron microscopy and three point bending tests are employed. The two-layer composition of leather implies that structural information is collected in the grain and the corium layer separately.

Methods

Leather preparation. Conventional beamhouse and bath tanning processes were used to process ovine pelts into leather. The ovine pelts were from 8 to 10 month old New Zealand Romney sheep. After rehydrating the skins, adhering fat and flesh was removed mechanically and conventional lime sulphide paint (140 g L^{-1} sodium sulphite, 50 g L^{-1} hydrated lime and 23 g L^{-1} pregelled starch thickener) was applied to the flesh side of the skin at a rate of 400 g m^{-2}. Following incubation at 20 °C for 16 hours keratinaceous materials were removed and the skins processed and then washed in water to remove the lime. Following the last wash, ammonium sulphate was added into the water to lower the pH to 8 and a commercial bate enzyme, Tanzyme (0.1% (w v^{-1})), was added before the skins were incubated at 35 °C for 75 min. Following further washing in water the skins were pickled in 20% (w v^{-1}) sodium chloride and 2% (w v^{-1}) sulphuric acid. 200 x 200 mm^2 samples were cut from each pelt from either side of the backbone with the backbone's location marked on each sample. At this point, during the tanning procedure, applications of stretching forces are applied to samples by placing them on a biaxial stretching device. The remainder of the tanning procedure was carried out under stretched conditions (details below) or, in the case of the control samples, the skins tanned left to tan normally under no strain. Following pickling the pelt samples were degreased in 4% non-ionic surfactant (Tetrapol LTN, SHAMROCK, Auckland, New Zealand) for 90 min and then washed. After being pretanned with 2% Oxizolidine (Zoldine ZE, Angus Chemical Company, Chicago, USA) solution and neutralized to a pH of 7.0 using 1% sodium

format end 3% sodium bicarbonate, the skins were washed and then a 1% disodium phthalate solution (Feliderm DP, CLARIANT, Leeds, U.K) was added for 30 min. the samples were processed overnight at 25 °C in a 5% chrome sulphate solution (Chromosal B, LANXESS, Köln, Germany). The following day the samples were neutralized in 1% sodium formate and 0.15% sodium bicarbonate solution for 1 hour, washed in water, and retanned with 2% synthetic retanning agent (Tanicor PW, CLARIANT, Leeds, U.K) and 3% vegetable tanning (mimosa) (TANAC, Montenegro, Brazil). Finally the skins were treated with a 6% fatliquor solution and fixed with 0.5% formic acid for 30 min. After a final wash in cold water the stretch tanned samples were removed from the biaxial stretching devices and left to dry with the control samples. Both samples were dried under tension and not subsequently rewetted and dried without tension.

Stretch tanned leather. From the 200 x 200 mm^2 samples, three were selected for biaxial stretching to be applied by a custom made device for the second part of the tanning process, after the skins were pickled. The pickled pelts were mounted in the biaxial stretching device which applied and maintained stretch during the beamhouse and bath tanning process. The strain applied was 3% perpendicular to the backbone and 15% parallel to the backbone. Uneven stretch directions were selected due to the natural ease of stretching the skins parallel to the backbone rather than perpendicular.

Conditioning Method 1: Relative humidity pre-conditioning. For conditioning method 1 the leather samples were pre-conditioned by equilibration in various humidity environments using saturated salt solutions to achieve specific relative humidities. The leather samples were placed into sealed containers containing one of the following saturated salt solutions: potassium carbonate, sodium bromide and sodium chloride which yielded 43.2%, 57.6% and 75.3% relative humidities, respectively. The samples were allowed to equilibrate at these humidities for up to 48 hours. When ready for testing, the samples were sealed in Kapton tape prior to small angle x-ray scattering (SAXS) analysis at the SAXS/WAXS beamline at the Australian Synchrotron to ensure they remained as close as possible to their humidity- equilibrium state, or were quickly placed in the three point bend test setup where testing was fast enough to not allow samples to equilibrate with the ambient environment.

Conditioning Method 2: Relative humidity *in-situ* conditioning. For conditioning method 2 the samples were humidity conditioned *in-situ* using a custom-built humidity chamber connected to a humidity generating device. An interface on the humidity generator device allowed the humidity to be set and monitored during the experiment through a humidity sensor in the sample chamber. Relative humidity setting included 0%, 40%, 60%, 80% and 100% where the 0% relative humidity was achieved by placing the sample directly into the vacuum sample chamber on the bench top SAXS (the Nanostar) while 100% was achieved by placing the samples in water for 24 hours followed by the humidity chamber in the sample area of the Nanostar with the air-lines blocked. The other humidities were set on the humidity generator, with the air lines open, and monitored for the duration of the experiment. Air flow was set at 10 L min^{-1} and de-ionized water was used for water vapour generation. Water vapour lines to the humidity chamber were insulated to prevent condensation. A quartz window (SPI SUPPLIES, West Chester, PA, USA) was used for short camera to detector measurements while a Kapton film window was used for the long camera to detector measurements to prevent scattering at peaks of interest.

Small angle X-ray scattering (SAXS) synchrotron analysis. For SAXS analysis samples were taken from both the stretched and control leather samples. Thin 2 mm strips were cut from the leather to perform measurements with the X-rays flat on to the grain surface. Measurements were made with 0.5 mm spacing between points in a three by three grid on the grain surface. The diffraction patterns were recorded on the Australian Synchrotron SAXS/WAXS beamline. A high-intensity undulator source was utilized with an energy resolution of 200 nm from a cryo-cooled Si(111) double-crystal monochromator. The beam size (FWHM focused at the sample) was 250 x 80 µm with a total photon flux of approximately 2 x 10^{12} photons s^{-1}. SAXS diffraction patterns were recorded using X-ray energy of 18keV and a sample to detector distance of 3.30 m for measurements in the low Q-range (Fig. 1(b)) and for the high Q-range, an X-ray energy of 18 keV was used with a sample to detector distance of 0.56 m (Figure 43 (a)). Measurements were made using a Pilatus 1M detector with an active area of 170 x 170 mm. The exposure time for diffraction patterns was in the range of 1–5 seconds in gapless mode, where each recorded pattern is taken as an average of consecutive patterns, and data processing was carried out using the Scatterbrain software. Intensities displayed are all absolute detector counts (one X-ray photon detected = one detector count), except where stated otherwise.

SAXS bench-top analysis. Leather samples were taken from both the stretched and control leather samples. Thin 0.5 mm strips were cut from the leather to perform the measurements with X-rays edge-on for measurements of both the grain and corium layers in plane. Two measurement points were made in each leather layer with 200 µm spacing between points and a beam diameter of 115 µm. The diffraction patterns were recorded on the SAXS II Nanostar in the scanning-SAXS configuration with rotating anode X-ray generator, crossed Göbel mirrors and HiStar area detector (Bruker AXS) under vacuum. Setup configurations included a short sample to detector distance of wide angle x-ray scattering (0.05 m) and a long sample to detector distance for small angle x-ray scattering measurements (1.10 m). Data was processing using the DPDAK software package [174].

D-spacing. Fitted with Gaussian curves, the maxima of the 6th order peaks positions from the integrated intensity profiles (Figure 43 (c, e)) are determine from each sample to calculate the D-spacing according to (Equation 13) derived as follows;

$$Q = \frac{4\pi\ sin\theta}{\lambda}$$

Equation 13. D-spacing is determined from the fundamental principles of SAXS that state the intensity of the scattered X-rays are a function of momentum transfer (Q) which is related to the scattering angle (θ) from the wavelength of radiation used (λ).

Combining (Equation 13) with Bragg's law we can quantify structural detail at an interplanar distance (L) relative to the order of the Bragg peak (n) for a selected Q-range (Equation 14).

$$L = \frac{2\pi n}{Q}$$

Equation 14. Interplanar distance ($\boldsymbol{L}$) relative to the order of the Bragg peak ($\boldsymbol{n}$) for a selected Q-range.

Lateral intermolecular spacing. From a short sample to detector configuration (Figure 43 (d, f)) at the beamline the intermolecular packing could be determined from SAXS data captured in the Q-range of 0.3 – 0.5 $Å^{-1}$. Peaks were fitted using the 'Peak Fitting' function in Igor Pro to determine the primary peak location within the Q-range. This was used in the relationship defined above (Equation 14) to determine the lateral intermolecular spacing. This is the distance between the collagen molecules that make up a collagen fibril.

Orientation index. Orientation Index (OI) is defined as (90°−OA)/90°, where OA is the minimal azimuthal angle range, centred at 180°, which contains 50% of the micro fibrils[109, 175]. The OI range takes us from perfect anisotropic alignment which is represented by an OI of 1, through to an OI of 0 which represents isotropy. The OI was calculated from the spread in the azimuthal angle of the D-spacing peak between 0.055 − 0.065 $Å^{-1}$. Each OI value presented here represents the average of 14 − 36 measurements of one sample.

Isothermal thermogravimetric analysis. Moisture contents were determined from isothermal thermogravimetric analysis (Q500, TA Instruments Co.). Ten milligrams of leather sample were held at room temperature (approximately 28 °C) from 0% to 90% relative humidity in 10% increments (10 mg s^{-1} ramp rate) with 3 hour hold times after each increase under a nitrogen atmosphere. At 0% relative humidity a moisture content of 0.018 mg mg^{-1} was seen in the control leather and 0.038 mg mg^{-1} in the stretch tanned leather. These values were used as the reference points for the other relative humidity environments.

Three point bending test. The bending properties of the leather samples were determined by loading leather samples to a 10 mm deflection in a three-point bending configuration with a 20 mm support span. The loading rate was 0.4 mm s^{-1}. Leather was pre-conditioned in controlled humidity environments according to conditioning method 1 (created by saturated salt solutions) for 24 hours prior to testing. The Young's modulus of leather samples was determined based on the load vs. deflection curve using the beam flexure theory as described in ISO 178:2010. Measurements were made on an Instron 4467 instrument (ITW, Massachusetts, USA). Samples were cut parallel or perpendicular to the backbone and placed in the three point bend test setup. Force deflection curves were recorder for the sample with the grain side facing both up and down.

Effective Young's modulus. From the force deflection curves, created by the three point bend tests, the *effective* Young's modulus (E_{eff}) was determined to provide the relative bending stiffness of the material normalized for the sample dimensions and the length of the support span during the three point bend test (Equation 15),

$$\frac{dF}{dx} = \frac{4\,E_{eff}\,a^3 b}{L^3}$$

Equation 15. Effective Young's Modulus where $\frac{dF}{dx}$ is the average slope from the force vs. deflection curve, a is the thickness of the sample, L is the length between the supports in the bending test and b is the width of the sample.

It should be noted that the term effective Young's Modulus is used because the measured samples are not isotropic and not perfectly elastic. Additionally, there are variations in structure through the thickness of the material which do not behave in the same way under tension and compression.

Apparent Density. Sample volumes and weights were measured in triplicate for each of the control and stretch tanned leather to determine their apparent densities. Rectangular samples were taken from each leather type and measured using callipers to calculate the sample volume. The samples were then left to equilibrate at ambient conditions for 24 hours before their weights were recorded.

Scanning electron microscopy. Samples were taken from the stretch tanned and control leather for microscopy according to standard procedures. Sample surfaces were coated with a thin conductive layer and the accelerating voltage was kept low during imaging under a field emission environmental scanning electron microscope (FE-ESEM) (EOL, JSM-7001F).

RESULTS

Moisture content of leather samples. The measured moisture content of the leather increases after conditioning at higher relative humidity, as would be expected (Figure 50). The equilibrium constant for the water uptake of the control and stretch tanned leather were 3.2 µg mg^{-1} and 2.6 µg mg^{-1}, respectively. The stretch tanned leather has a consistently lower uptake of moisture compared with the control.

Leather thickness and density. Cross-sectioned scanning electron microscopy images of the leather were used to determine the overall and layer thickness of each leather type (Figure 42). A notable reduction in overall leather thickness is seen in the stretched leather compared with the control (2.24 mm vs. 0.94 mm) (Table 10). The applied strain during the tanning procedure to produce the stretch tanned leather appeared to affect the corium more than the grain layer with a significant difference in thickness compared to the control (0.43 mm vs. 1.41 mm, respectively). This is also reflected in the grain to corium ratio where the control leather ratio is half that of the stretch tanned leather (0.6 vs. 1.2, Table 10). As a result, the apparent density of the stretch tanned leather was greater than the control under ambient conditions (343 kg/m^3 vs. 215 kg/m^3) (Table 11).

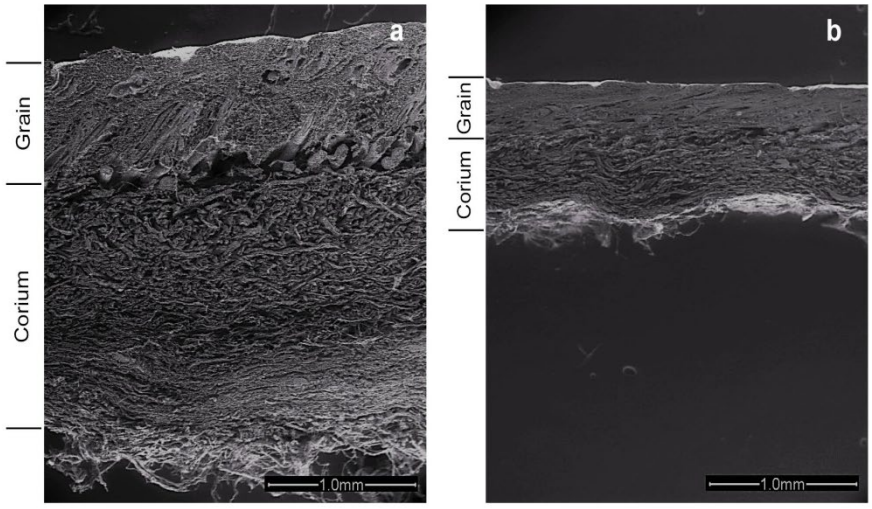

Figure 42. Scanning electron microscopy images of the (a) control, non-stretch tanned leather and (b) stretch tanned leather cross-sections showing the grain (*top*) and corium layers with a comparable scale.

SAXS. The intensity rings on the scattering pattern that correspond to peaks on the integrate profiles used to measure the D-spacing and lateral intermolecular spacing were clearly visible in all samples (Figure 43). Small angle X-ray scattering intensity (over the long sample to detector distance for the low Q-range (Figure 44 (a, c)) and the short sample to detector distance for the high Q-range (Figure 44 (b, d)) show a peak shift under varying relative humidity for the control and stretched leather (Figure 44 (a, b) and (c, d) respectively).

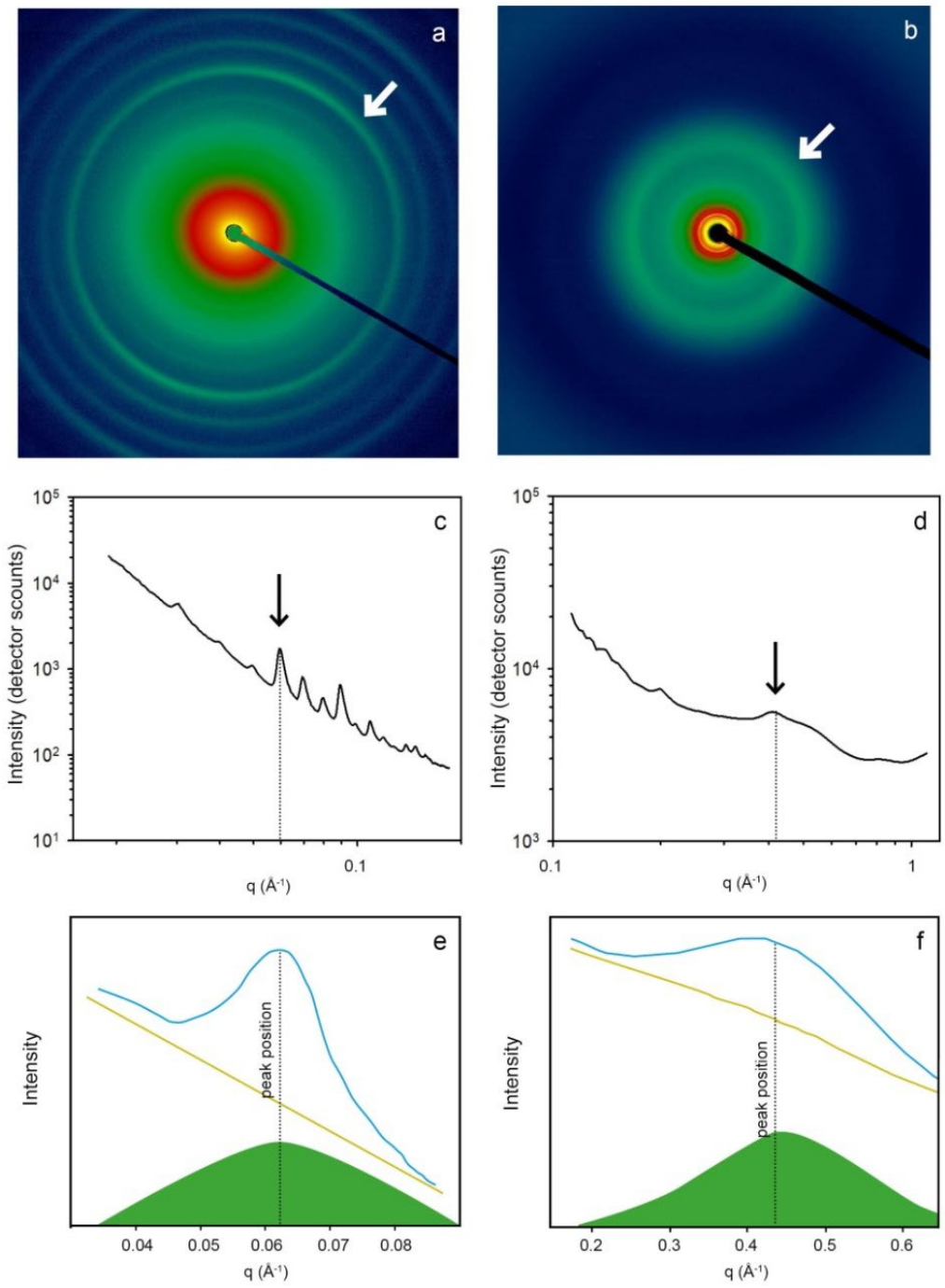

Figure 43. 2D Scattering patterns from (a) long sample to detector configuration (3.30 m) for Small Angle X-ray Scattering (SAXS) measurements over a low Q-range (0.01 – 0.15 $Å^{-1}$) and (b) short sample to detector (0.56 m) for SAXS measurements over a high Q-range (0.10 – 1.00 $Å^{-1}$) where the azimuthal angle is measured anticlockwise from the horizontal and Q is calculated from the scattering angle where $Q = \frac{4\pi \, sin\theta}{\lambda}$ (defined above in Equation 13). Measurements were made at the Australian Synchrotron. The arrows point to the peak of interest. The respective integrated intensity profiles (c, d) show the peaks of interest which were used to determine (e) D-spacing and (f) lateral intermolecular spacing from the peak location according to (Equation 14 above).

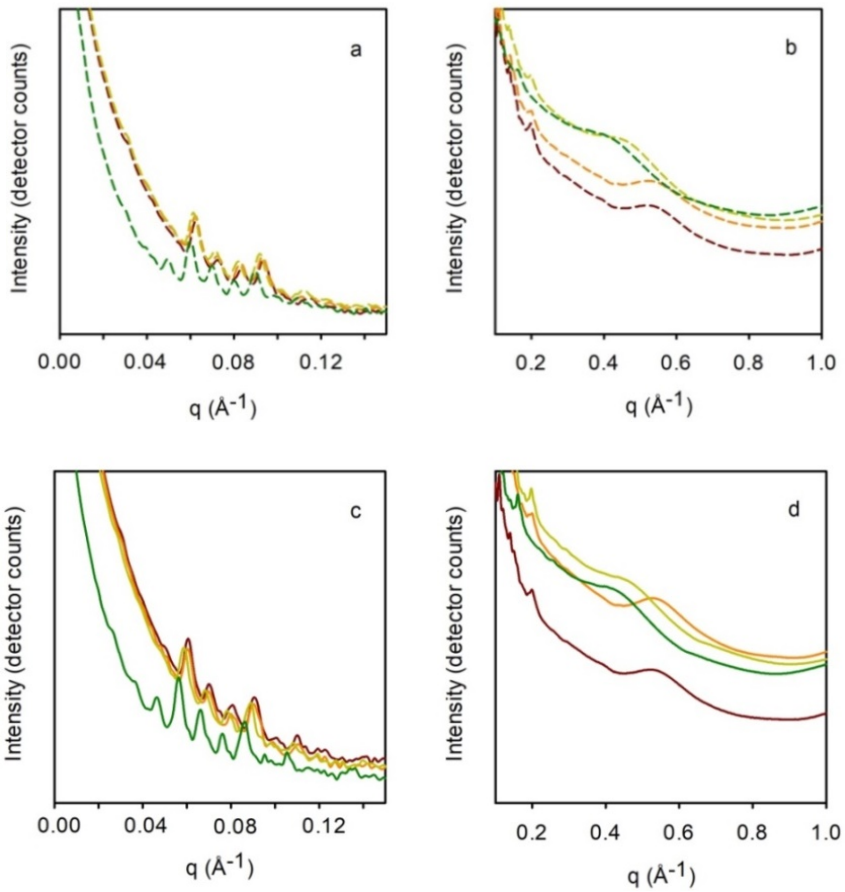

Figure 44. Small Angle X-ray scattering intensity spectrums for the (a, b) control and (c, d) stretched leather under the long camera to detector configuration (a, c) and the short camera to detector configuration (b, d) after relative humidity pre-conditioning (Conditioning Method 1) where red represents condition at 40% relative humidity, orange represents condition at 60% relative humidity, yellow represents condition at 80% relative humidity and green represents condition at 100% relative humidity.

D-spacing. A roughly linear increase in the collagen fibril D-spacing is seen with moisture content across both leather samples when viewed flat-on (normal to the grain surface) and edge-on (Figure 51 & Figure 45 respectively), showing both the grain and corium leather layers. The D-spacing in the stretched leather is greater than that found in the control, most likely due to residual strain in the fibres after the stretching strain was applied during tanning. D-spacing in the grain tended to be higher than that found in the corium in all cases (Figure 45) although three out of ten differences were not considered statistically different according to a t-test for un-equal variance (Table 12). The variation in D-spacing between samples of different moisture contents is similar.

The average change in D-spacing from dry to hydrated is similar in both leather types, a 2.8% change (1.39 ± 0.33 nm) in the control leather and a 2.3% change (1.35 ± 0.36 nm) in the stretched leather from edge-on SAXS measurements.

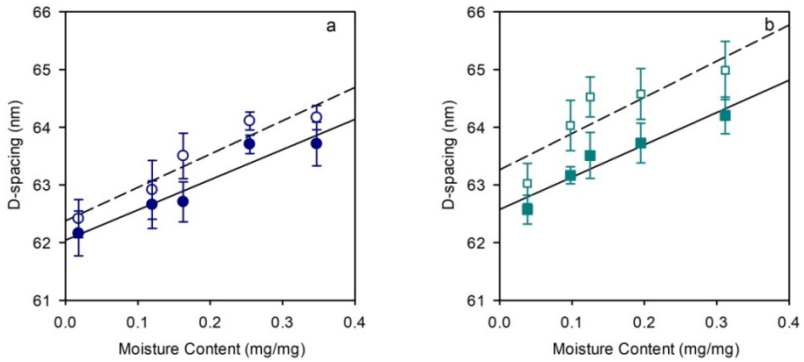

Figure 45. Variations in D-spacing from edge-on measurements with moisture content on (a) control, non-stretch tanned leather and (b) stretch tanned leather where hollow shapes represent the D-spacing in the grain layer and filled shapes represent the D-spacing in the corium layer (slope = (a) 5.79 ± 0.96 nm/(mg/mg), (a) 5.24 ± 0.94 nm/ (mg/mg)), (b) 6.27 ± 2.03 nm/ (mg/mg), (b) 5.60 ± 0.96 nm/ (mg/mg); r^2 = (a) 0.92, (a) 0.92, (b) 0.76, (b) 0.92 for the grain (dashed line) and corium (solid line) of the control and stretch tanned leather respectively).

Lateral intermolecular spacing. Using a short sample to detector configuration information was gathered on the lateral intermolecular spacing between the tropocollagen molecules, which make up the fibrils. With increasing moisture content we find a roughly linear correlation with the lateral intermolecular spacing in both edge-on and flat-on sample orientations (Figure 46 & Figure 52, respectively). From dry to hydrated an increase of 3.82 ± 0.12 Å (63.3%) is seen in the control compared with 3.12 ± 0.07 Å (59.1%) in the stretched leather from edge-on SAXS measurements (Figure 46). Lateral intermolecular spacing in the grain layer compared with corium was not statistically different (Table 13).

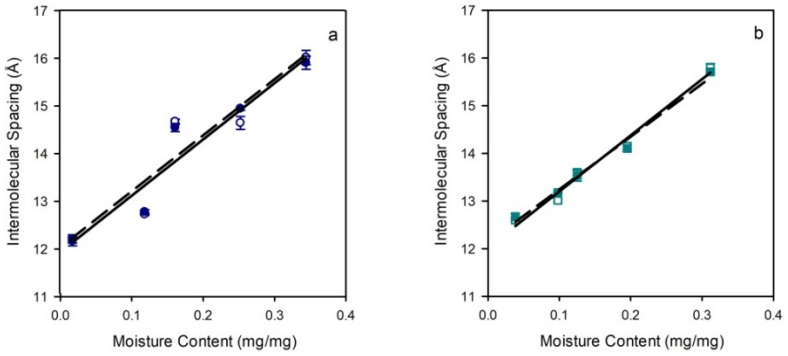

Figure 46. Variations in lateral intermolecular spacing from edge-on measurements with moisture contents from relative humidity *in-situ* conditioning on (a) control, non-stretch tanned leather and (b) stretch tanned leather where hollow shapes represent the lateral intermolecular spacing in the grain layer and filled shapes represent the lateral intermolecular spacing in the corium layer (slope = (a) 11.89 ± 2.47 Å/(mg/mg), (a) 11.89 ± 2.47 Å/(mg/mg), (b) 11.79 ± 0.84 Å/(mg/mg), (b) 11.09 ± 0.71 Å/(mg/mg); r^2 = (a) 0.90, (a) 0.93, (b) 0.84, (b) 0.86 in the grain (solid line) and corium (dashed line) of the control and stretch tanned leather respectively). Note the error bars on some points are not visible since the variation within the sample repeats was < 0.05.

Orientation index. The collagen fibrils relative alignment (orientation index, OI) is determined from the edge-on SAXS measurements. The stretch tanned leather generally has a higher OI than the control, non-stretch tanned leather (Figure 47). However, this could be attributed to the smaller cross sectional sample thickness. The fibrils relative alignment increases with moisture content in both sample types with a greater change seen in the stretch tanned leather.

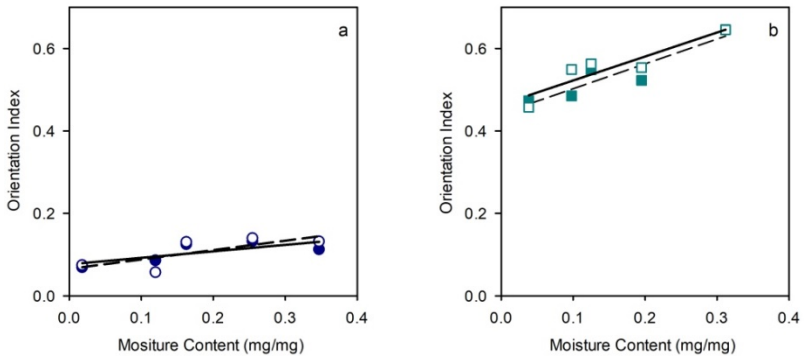

Figure 47. Variations in the orientation index from edge-on SAXS measurement with moisture contents from relative humidity *in-situ* conditioning on (a) control, non-stretch tanned leather and (b) stretch tanned leather where hollow shapes represent the orientation index in the grain layer and filled shapes represent the orientation index in the corium layer. (slope = (a) 0.16 ± 0.08 1/(mg/mg), (a) 0.23 ± 0.11 1/(mg/mg), (b) 0.58 ± 0.15 1/(mg/mg), (b) 0.60 ± 0.15 1/(mg/mg); r^2 = (a) 0.55, (a) 0.84, (b) 0.57, (b) 0.85 in the grain (solid line) and corium (dashed line) of the control and stretch tanned leather respectively).

Leather stiffness. The mechanical bend test compresses one side of the sample while loading the other side with tension (stretching) forces. Since leather has a variation in structure through the thickness of the material, the force-deflection curves are different when samples are placed with the grain side up vs. corium side up (Figure 53). The Young's moduli for the stretch tanned leather is almost double that of the control, in all instances (Figure 48). As we increase the moisture content through relative humidity conditioning we notice a uniform reduction in the Young's modulus. The decrease in Young's modulus is more pronounced in the case where the corium is at the bottom and, therefore, loaded under tension.

With a preferred collagen alignment parallel to the backbone, in natural (control leather) and more so in artificially enhanced leather (stretch tanned), the Young's modulus is greater when sampled parallel to the backbone compared to perpendicular (Figure 48 (a, b) vs. (c, d)).

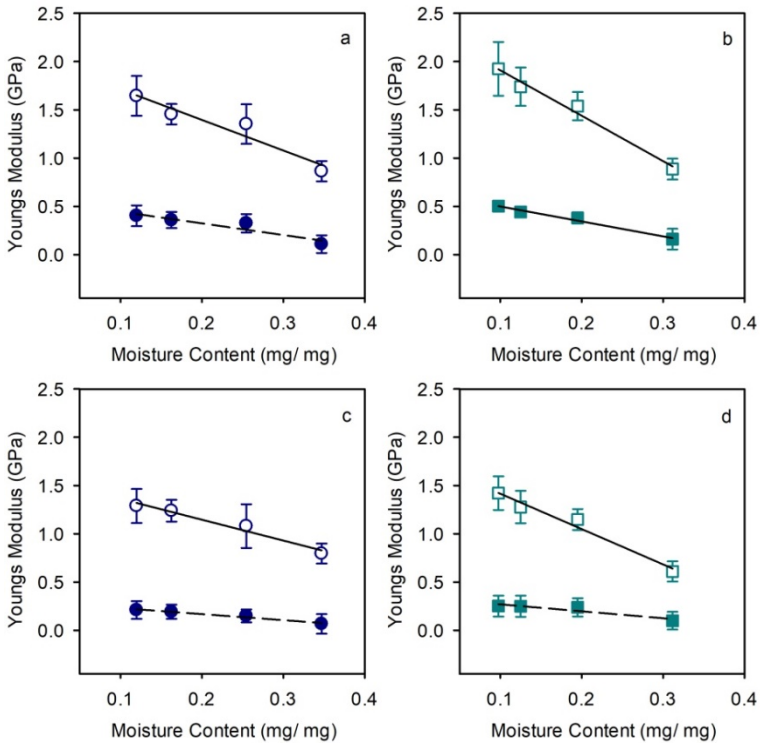

Figure 48. Variations in Young's Modulus with moisture contents from relative humidity pre-conditioning on samples cut perpendicular to the backbone (a, b) (r^2 for the control grain and corium (0.92, 0.88) and slope = -3.17 ± 0.64 GPa/(mg/mg), -1.21 ± 0.32 GPa/(mg/mg); r^2 for the stretch tanned leather grain and corium (0.98, 0.98)) and slope = -4.70 ± 0.41 GPa/(mg/mg), -1.54 ± 0.15 GPa/(mg/mg) and those cut parallel to the backbone (c, d) (r^2 for the control grain and corium (0.96, 0.97) and slope = -2.16 ± 0.28 GPa/(mg/mg), -0.62 ± 0.08 GPa/(mg/mg); r^2 for the stretch tanned leather grain and corium (0.97, 0.87)) and slope = -3.66 ± 0.42 GPa/(mg/mg), -0.72 ± 0.20 GPa/(mg/mg) for the control (dark blue circles) and stretch tanned leather (light blue squares), grain side up (hollow shapes, solid line) and corium side up (filled shapes, dashed line).

Correlations between structure and mechanics. Increasing lateral intermolecular spacing is correlated with reducing material stiffness (Young's modulus) (Figure 49. The lateral intermolecular spacing increases similarly in the two layers. The material stiffness appears to decrease with increasing moisture content, albeit each layer was not measured independent of another.

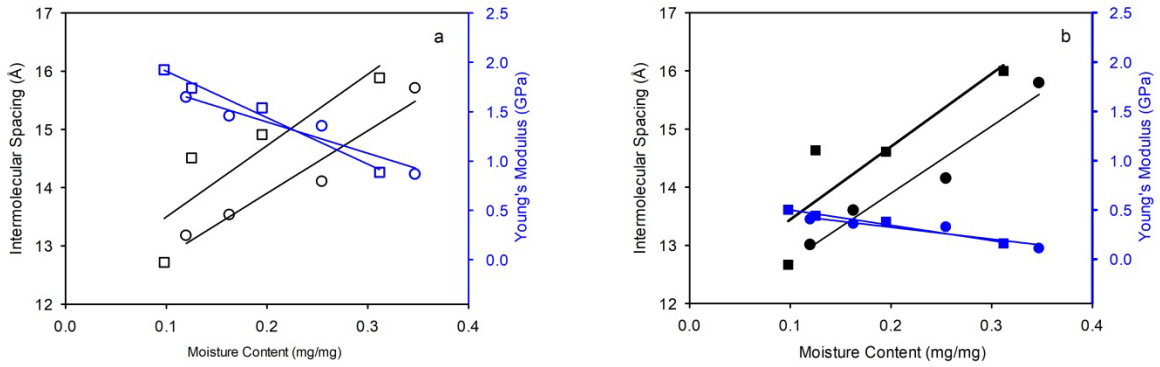

Figure 49. Effect of moisture content in the (a) grain (hollow shapes) and (b) corium (filled shapes) of control, non-stretch tanned leather (circles) and stretch tanned leather (squares) on the lateral intermolecular spacing (black) and Young's modulus (blue).

Discussion

It is known that the material properties of leather can be altered by the chemical and mechanical processing. Properties such as strength and stiffness are important for most practical applications of the material. For high value applications such as shoes, the ability to customize strength and stiffness properties would be invaluable in creating fit for purpose materials. From the findings presented here we show how moisture contents can be used to manipulate collagen structures which affect mechanical properties. Controlling the moisture content can tune the material stiffness, meaning we can create both strong and flexible leather.

The two layer structure in leather results from the skin of which it was derived. Each of the layers provides different mechanical properties, defined by the collagen fibre size. The grain layer is more rigid with smaller fibres allowing for a dense and highly interwoven structure while the corium, consisting of large more loosely interwoven fibres, has a greater ability to respond to strain providing leather with high strength and flexibility. During stretch tanning the fibres in each layer rearrange longitudinally in the direction of the applied strain, while packing closer together. The effect of closer packing is seen to a greater extent in the corium layer by a significant reduction in cross-sectional thickness when compared to the control, non-stretch tanned leather.

Tanning under strain results in leather that is approximately half as thick as when it is tanned without strain (.94 mm vs. 22.4 mm). The reduction in thickness and increase in density suggests that the void spaces in the fibre matrix have been reduced, primarily in the corium layer where the greatest reduction in thickness was seen. The D-spacing is larger in the grain compared with the corium and this difference is enhanced by the application of strain during tanning. However, the effects of strain appear to have less of an effect on the lateral intermolecular spacing in each of the layers with both showing a similar reduction under stretching. Assuming that the relative change of D-spacing under stretch is similar to the relative change in fibril length (i.e. the strain is roughly homogeneous), the measurements show that the collagen fibrils have a reduced fibril volume under strain, and, as such, can pack closer together[104] creating a more dense structure. Applied strain during tanning appears to be correlated with an increase in the fibril's orientation index however there is more than one contribution to this behaviour. Fibre realignment does occur with the application of straining forces during tanning; however there is a significant increase in the OI just from the reduction in the sample's cross-section thickness[39]. In soft tissues such as tendon and pericardium, there is also a curvilinear microstructure, known as crimp[176], which is straightened at low strain[118, 121] and is important for the mechanical properties of these tissues. This is an entropic process also observed for free tropocollagen molecules[50] and what change in curvature does exist could instead be attributed to a reorientation of fibres toward the direction of applied stress[7, 70].

Tanning introduces cross-links between collagen fibrils. These cross links are formed by both the chromium and vegetable tannins. It is believed that cross-linking agents restrict the sliding of fibrils relative to each other[166] and they have been seen to change the fibril arrangement[121]. The early processing stages of leather making prior to tanning removing what are considered natural cross links in the form of glycosaminoglycans, which are generally considered to provide rigid structures resistant to sliding, although this has been questioned by recent experimental work[103]. Here we have not varied any of these factors, but have varied the

water content. Water can be controlled by varying the humidity conditions (as done here) or by changes to components such as fatliquor which is normally added to leather[151]

At 40% relative humidity, which was regarded as being close to ambient moisture conditions, stretch tanned leather is much stiffer than leather tanned without strain (33.5 kPa vs. 15.3 kPa). Leather is primarily composed of type I collagen from the skin. Since skin is a natural material, suited to purpose on the live animal, it is anticipated that there are structural and functional differences in samples depending on the anatomical location that they are taken. Natural collagen alignment is greatest along the backbone of an animal, becoming less oriented in the skin at the limbs[15]. This is speculated to be suited to providing strength and flexibility in different regions of the live animal. Mechanical testing at orthogonal orientations provides insights into the different stiffness's within a piece of leather. Here we compared samples cut perpendicular and parallel to the backbone (Figure 48). An applied load during tanning results in an increased packing density of fibrils and a realignment of fibrils along the direction of the applied force, which in this case was parallel to the backbone.

The stretch tanned leather has thinner and more tightly packed fibrils that are in greater contact with one another, compared with the control, non-stretch tanned leather. A greater fibril-to-fibril contact restricts fibril movement requiring a greater deformation force to overcome a large internal friction, making the overall leather stiff. When no strain is applied to the fibres during tanning, the fibril's relative alignment is low. This leaves the fibrils in less contact with one another with no residual strain on the fibres themselves and more void spaces in the fibre matrix. The void spaces in the matrix allow for another degree of freedom for fibre movement in response to an applied strain, thus requiring a lower deformation force seen here as a low Young's modulus.

At equilibrium, the moisture content of leather is linearly proportional to the moisture in the environment. The stiff, stretch tanned leather absorbs less water than the control, non-stretch tanned leather, with the respective equilibrium constants for water sorption: 2.6 $\mu g\ mg^{-1}$ and 3.2 $\mu g\ mg^{-1}$. The denser and tighter packing of collagen fibrils in the stretch tanned leather may restrict how water is incorporated into its structure.

With increases in humidity, we introduce more water into the leather structure and notice an increase in the D-spacing due to the hydrophilic nature of the collagen molecules. The rate of change in D-spacing with moisture content appears to be a less prominent mechanism for water uptake compared to the changes seen in the lateral intermolecular spacing. Tropocollagen molecules, that align and bundle together to comprise the fibril, are coated in a hydration cylinder[81, 177] which allows for water mediated hydrogen bonding between the molecules while also separating molecules by more than one water molecule [178]. As the humidity increases, water molecules are added to the tropocollagen hydration shell, progressively increasing the lateral intermolecular spacing (59.1% and 63.3% increase between the dry and the wet state for the stretch tanned leather and the control leather respectively (Table 14)). This suggests that the majority of the absorbed water is incorporated laterally, around the collagen fibrils, rather than longitudinally, along the collagen fibrils, from the lower increases in D-spacing with moisture content (2.3% and 2.8% increase for the stretch tanned leather and the control leather respectively (Table 14)).

The applied strain during tanning, which is seen to induce a change in structure thought to have an effect on water uptake, could also be chemically based. Changes to the collagen structure may also affect the efficacy of chemical uptake during the tanning process which may influence the hydrophobicity of the fibres. As such this could also contribute to the observed changes in the collagen structure after conditioning at the various relative humidity environments, where the stretch tanned leather has a lower water uptake compared with the control, non-stretch tanned leather.

Dehydrated collagen is known to be stiffer than wet collagen[14, 179] where the increase in stiffness seen in dry collagen has been attributed to restricted fibril movement and an inability to re-arrange in response to deformation forces[7, 180]. High lateral intermolecular spacing reflects a higher level of hydration in the tropocollagen molecules which can be linked to improved mechanical properties, such as a reduction in stiffness. This is shown here by the excellent correlation between moisture content and Young's Modulus Figure 48) suggesting that the stiffness gained from stretch tanning is lost as the water content is increased.

Conclusions

The influence of stretch tanning and varying moisture contents were investigated in regards to their interplay with leather structure and function. Firstly the effect of strain during the leather making process has some noted effects on the collagen structure. The stretch tanned leather has more aligned slender fibrils with a more densely packed structure, seen as a reduction in sample thickness and an increase in D-spacing. With this structure the leather has a significantly greater Young's modulus, compared to leather processed normally, thought to be attributed to an overall densification and realignment of the fibrillar structure causing greater fibril-to-fibril contact. Secondly the effect of moisture content on the leather structures and mechanical performance was determined. The lateral intermolecular spacing and D-spacing both increase with increasing moisture content in both leather types. The more predominate increases were seen in the lateral intermolecular spacing suggesting more water is incorporated laterally rather than longitudinally. Less remarkable effects were seen in changes to the fibril alignment as the moisture content varied. The moisture content does however offer some mediating effects to the material stiffness by providing a lubricating effect from a thicker water layer which helps to reduce the internal friction between the fibrils.

The dominant feature of material stiffness is fibril alignment and packing density which work in a synergistic manner to increase the material stiffness. The primary swelling of the fibrils is in the lateral direction where the close packing of the fibrils doesn't appear to limit the lubricating effect the greater hydration shell appears to offer fibrils that are less well aligned. As such, the fully hydrated stretched leather is less stiff than fully hydrated non-stretched leather.

Chapter 6. Data on collagen structures in leather with varying moisture contents from small angle X-ray scattering and three point bend testing

S. J. Kelly, R. Weinkamer, L. Bertinetti, R. L. Edmonds, H. C. Wells, K. H. Sizeland, P. Fratzl and R.G. Haverkamp. Data on collagen structures in leather with varying moisture contents from small angle X-ray scattering and three point bend testing, *Data in Brief*, **21**:1220-1226 (2018).

Abstract

Artificial collagen alignment was experimentally introduced into ovine leather through biaxial strain during tanning. Leather samples produced normally, non-stretch tanned leather, along with those produced by stretch tanning, were conditioned in various relative humidity environments followed by small angle X-ray scattering analysis and three point bend testing. The collagen D-spacing, lateral intermolecular spacing and flexural properties (Young's modulus) were analysed under varying moisture contents. The data presented is associated with the research article entitled Effects of collagen packing and moisture content on leather stiffness (Kelly et al., 2018)[16].

Value of the Data

- Characterization of the effect of moisture content on the Young's modulus of stretch tanned leather.
- The presented data demonstrate the structural and mechanical effect of water being incorporated into the collagen structure in leather.
- Stretch tanning is shown to have an effect on the collagen structure and flexibility of leather.
- Structural data (collagen D-spacing and lateral intermolecular spacing) show how the change in water content is reflected in the collagen structure.
- Flexibility data (Young's modulus) show how water provides a lubricating effect on leather stiffness.

Data

The data presented here offers additional measurements at different sample orientations to that presented in Kelly et al., 2018[16]. Here we present results from SAXS measured flat on to leather surface for samples tanned normally (control) and those tanned under biaxial strain (stretch tanned leather). The data sets are divided into three parts.

- Part 1 characterizes the thickness (Table 10), apparent density (Table 11) and moisture contents achieved from the various relative humidity environments (Figure 50) for the two leather types.
- Part 2 contains the collagen structural information (D-spacing (Figure 51 and Table 12) and lateral intermolecular spacing (Figure 52 and Table 13) of the two leather types at varying moisture Kelly et al., 2018.
- Part-3 shows the force-deflection curve (Figure 53) of the two leather types, where we see the increased stiffness of the stretch tanned leather.

Part 1. Characteristics of the two leather types (non-stretch tanned (control) and stretch tanned leather).

Table 10. Thicknesses of control, non-stretch tanned leather and stretch tanned leather grain and corium layers. Data are presented as the average (standard deviation). P-values are from a t-test assuming unequal variance between the grain and corium layers of the control and stretch tanned leather and the grain to corium ratio of each leather type. These correspond to Figure 42 in Kelly et al., 2018[16].

Sample	Grain thickness (mm)	Grain: Corium Ratio
Control leather (Grain, corium)	0.83 (0.04), 1.41 (0.11)	0.6 (0.1)
Stretch-tanned leather (Grain, corium)	0.51 (0.08), 0.43 (0.05)	1.2 (0.1)
P-value (Grain, corium)	*<< 0.05, << 0.05*	*<< 0.05*

Table 11. Apparent density of each leather type at ambient conditions.

Sample	Length (m)	Width (m)	Thickness (m)	Volume (m^3)	Weight (kg)	Density (kg/m^3)
Control leather 1	0.01309	0.00991	0.00212	2.75E-07	0.000057	208.7
Control leather 2	0.01338	0.0099	0.00202	2.67E-07	0.000059	220.5
Control leather 3	0.01369	0.00976	0.00205	2.73E-07	0.000059	217.2
Stretch tanned leather 1	0.01175	0.00955	0.00093	1.04E-07	0.000036	345.3
Stretch tanned leather 2	0.01126	0.00977	0.00094	1.04E-07	0.000034	325.7
Stretch tanned leather 3	0.01018	0.00964	0.00092	8.99E-08	0.000031	340.2

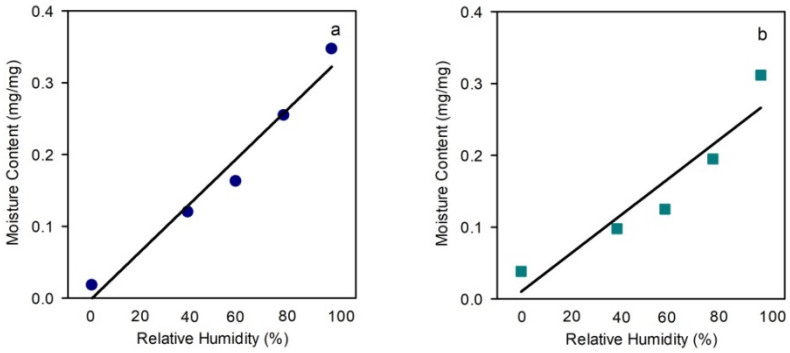

Figure 50. Isothermal gravimetric analysis at various relative humidity environments to determine leather moisture content. Dark blue points are (a) the control leather (slope = 3.2 ± 0.3 µg/mg, r^2 = 0.97); and (b) the stretch tanned leather (slope 2.6 ± 0.5µg/mg, r^2 = 0.89).

Part 2. Structural collagen information determined by small angle X-ray scattering (SAXS) under varying moisture contents.

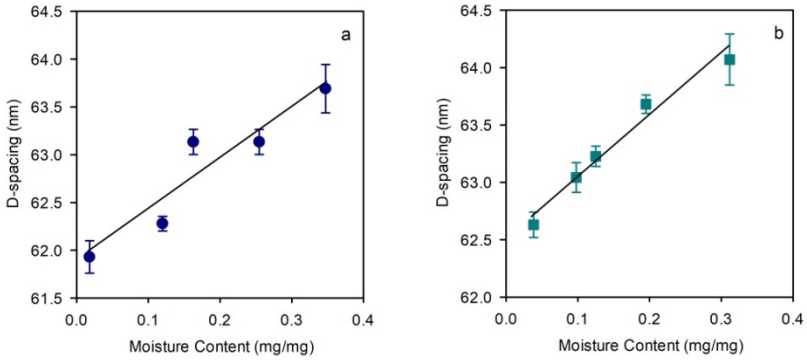

Figure 51. Variations in D-spacing from flat on measurements with moisture content in (a) control leather and (b) stretch tanned leather (slope = 5.11 ± 1.88 r^2 = 0.79, slope = 4.78 ± 0.60 r^2 = 0.97 respectively).

Table 12. D-spacing values for each leather type after relative humidity conditioning with small angle x-ray scattering measurements [13] made edge on to leather samples using bench top SAXS (*top,* Figure 45 presented in Kelly et al., 2018[16]) and those made flat on to leather surface using synchrotron based SAXS (*bottom,* Figure 51). Data are presented as the average (standard deviation). P-values are from a t-test assuming unequal variances in the D-spacing in the grain vs. corium from edge on measurements, and between the control and stretch tanned leather in the flat on measurements.

Sample	**D-spacing after relative humidity conditioning (nm)**				
	0%	**40%**	**60%**	**80%**	**100%**
	Edge on measurements				
Control (Grain, corium)	62.41 (0.33), 62.16 (0.39)	62.92 (0.51), 62.66 (0.41)	63.50 (0.40), 62.71 (0.35)	64.11 (0.16), 63.71 (0.16)	64.17 (0.21), 63.71 (0.38)
P-value (Grain vs. corium)	*0.17*	*<< 0.05*	*<< 0.05*	*<< 0.05*	*<< 0.05*
Stretch-tanned leather (Grain, corium)	63.03 (0.35), 62.58 (0.25)	64.03 (0.44), 63.17 (0.15)	64.99 (0.34), 63.52 (0.40)	64.58 (0.44), 63. 73 (0.35)	64.50 (0.50), 64.21 (0.32)
P-value (Grain vs. corium)	*0.08*	*<< 0.05*	*<< 0.05*	*<< 0.05*	*0.13*
	Flat on measurement				
Control	61.93 (0.17)	63.04 (0.13)	63.23 (0.09)	63.68 (0.08)	64.07 (0.22)
Stretch-tanned leather	62.63 (0.11)	62.28 (0.08)	63.13 (0.13)	63.13 (0.13)	63.69 (0.25)
P-value(Control vs. stretched)	*<< 0.05*	*<< 0.05*	0.23	*<< 0.05*	0.31

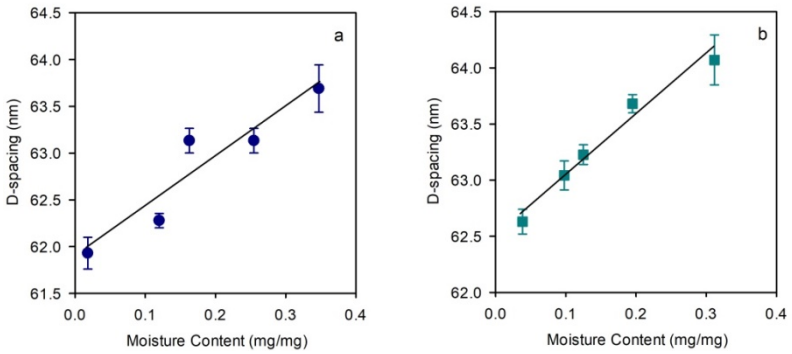

Figure 52. Variations in lateral intermolecular spacing from flat on measurements with moisture content on (a) control leather and (b) stretch tanned leather (slope = 1.60 ± 0.13, 1.35 ± 0.08; r^2 = 0.81, 0.90 respectively). Note the error bars are not visible on some points since the variation within sample repeats was < 0.05.

Table 13. Lateral intermolecular spacing[14] values for each leather type after relative conditioning for measurements made edge on to the leather samples using bench top SAXS (*top,* Figure 46 presented in Kelly et al., 2018 [16]) and those made flat on to the leather surface using synchrotron based SAXS (*bottom,* Figure 52). Data are presented as the average (standard deviation). P-values are from a t-test assuming unequal variances in the lateral intermolecular spacing of the grain vs. corium from edge on measurements. P-values are from a t-test assuming unequal variances in the lateral intermolecular spacing in the grain vs. corium from edge on measurements and between the control and stretch tanned leather in the flat on measurements.

Sample	Lateral intermolecular spacing after relative humidity conditioning (Å)				
	0%	**40%**	**60%**	**80%**	**100%**
	Edge on measurements				
Control leather *(Grain, corium)*	12.10 (0.10), 12.15 (0.09)	12.67 (0.03), 12.72 (0.05)	14.64 (0.05), 14.51 (0.09)	14.61 (0.14), 14.91 (0.04)	16.00 (0.15), 15.89 (0.14)
P-value	*0.56*	*0.44*	*0.35*	*0.16*	*0.65*
Stretch tanned leather *(Grain, corium)*	12.60 (0.04), 12.67 (0.07)	13.01 (0.03), 13.18 (0.01)	13.60 (0.06), 13.53 (0.11)	14.15 (0.07), 14.10 (0.07)	15.79 (0.09), 15.71 (0.06)
P-value	*0.65*	*0.14*	*0.65*	*0.67*	*0.52*
	Flat on measurement				
Control leather	9.68 (0.26)	11.57 (0.03)	11.61 (0.02)	13.76 (0.24)	15.34 (0.05)
Stretch tanned leather	9.70 (0.26)	11.64 (0.02)	11.64 (0.03)	15.40 (0.10)	15.71 (0.59)
P-value	*0.90*	*<< 0.05*	*<< 0.05*	*<< 0.05*	*0.12*

Table 14. Collagen fibril structural parameters characterize the collagen fibril structure when dry and wet, with rate of change in structure as water is added to the structure for measurements made edge on to the leather surface using bench top SAXS (*top*), and with measurements made flat on to the leather surface using synchrotron based SAXS (*bottom*). Data are presented as the average (standard deviation).

Sample	Parameter	Dry*	Wet**	Rate of change	Δ (dry to wet)
	Edge on measurements				
Control *(Grain)*	D-spacing (nm)	62.38 (0.21)	64.17 (0.21)	5.79 (0.96)	2.9%
	Intermol. spacing (Å)	11.86 (0.53)	16.00 (0.15)	11.89 (2.47)	34.9%
Control *(Corium)*	D-spacing (nm)	62.04 (0.20)	63.71 (0.38)	5.24 (0.94)	2.7%
	Intermol. spacing (Å)	11.86 (0.53)	15.89 (0.14)	11.89 (2.47)	34.0%
Stretch *(Grain)*	D-spacing (nm)	63.27 (0.37)	64.99 (0.50)	6.27 (2.03)	2.7%
	Intermol. spacing (Å)	12.02 (0.15)	15.79 (0.09)	11.79 (0.84)	31.4%
Stretch *(Corium)*	D-spacing (nm)	62.58 (0.17)	64.21 (0.32)	5.60 (0.96)	2.6%
	Intermol. spacing (Å)	12.14 (0.13)	15.71 (0.06)	11.10 (0.71)	29.4%
	Flat on measurements				
Control	D-spacing (nm)	61.93 (0.17)	63.69 (0.25)	5.11 (1.89)	2.8%
	Intermol. spacing (Å)	9.68 (0.26)	15.69 (0.15)	1.60 (0.13)	63.3%
Stretch	D-spacing (nm)	62.63 (0.11)	64.07 (0.22)	4.78 (0.60)	2.3%
	Intermol. spacing (Å)	9.70 (0.26)	15.43 (0.02)	1.35 (0.08)	59.1%

* Dry represents measurement at 0% relative humidity measurements (under vacuum).
** Wet represents measurement at 100% relative humidity measurements (soaked in water). Dry measurements from the Synchrotron flat on measurements were interpolated from measurements at 40, 60, 80 and 100% relative humidity points.

Part 3. Force deflection curves determined by three point bend tests for the tow leather types, showing the increased stiffness of the stretch tanned leather.

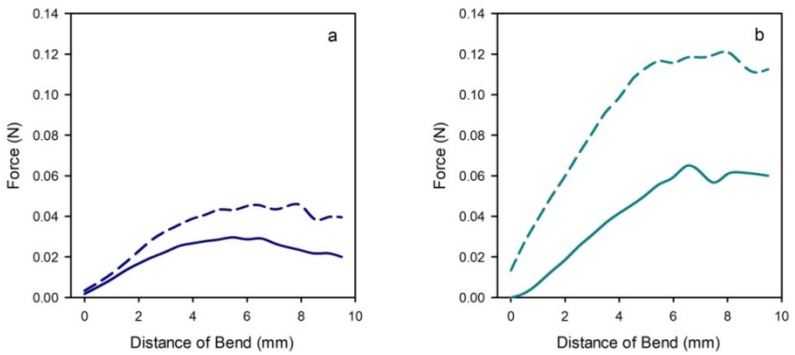

Figure 53. Force deflection curves for (a) control leather and (b) stretch tanned leather where the corium side under tension is represented by the dashed line and the grain side under tension is represented by the solid line.

Experimental Design, Materials, and Methods

The details of the experimental work and materials are provided in Kelly et al., 2018[16].

Chapter 7. A small angle X-ray scattering study of the changes caused by preservation on corneal collagen structures

Kelly S. J., L. du Plessis, J. Soley, K. H. Sizeland, R. G. Haverkamp and P. J. Kelly. A small angle X-ray scattering study of the changes caused by preservatives on corneal collagen structures. *Manuscript in preparation.*

Abstract

Small angle X-ray scattering (SAXS) and electron microscopy are complementary techniques allowing structural measurements and imaging of biological tissue where collagen is the main structural component. Fixation is often required for the preservation and sectioning of tissue before it is analysed and is known to have an effect on collagen structures. We used clinically normal sheep corneas (N = 9) to determine the effects of common preservatives on measurements of collagen made using small angle X-ray scattering (SAXS) analysis and transmission electron microscopy (TEM). Compared to the control cornea there was a significant increase in the fibril diameter of collagen in corneas stored for 5 days in all the preservatives studied (5% glutaraldehyde (37.08 nm), 10% formalin (36.44 nm), Triton X (38.27 nm) and 0.9% phosphate buffered saline (PBS) (36.68 nm) versus frozen (35.52 nm)). D-spacing increased significantly in corneas placed in Triton X (65.58 nm versus 65.42 nm (frozen)) but decreased significantly in those in 5% glutaraldehyde and 10% formalin (64.96 nm, 65.15 nm respectively). Collagen fibrils in corneas in 5% glutaraldehyde and 10% formalin had significantly greater orthogonal alignment (decreased orientation index) (0.15 and 0.22 respectively). Overall, storage in 0.9% phosphate buffered saline resulted in the least changes in collagen parameters measured by SAXS. Storage in Triton and PBS reduced transparency. The preservation media used in this study have a notable effect on collagen D-spacing, fibril diameters and relative arrangement. If tissue is analysed after preservation, understanding the effect the preservative has on the tissue structure is important to obtain comparable data from studies using SAXS.

Introduction

Collagen is the most abundant fibrous protein in animals where it provides strength and structure to a variety of soft and hard tissues. The basic unit of collagen is a repeating series of three amino acids that form alpha chains and coil together in a triple helix, the basic collagen molecule. The long collagen molecules pack together in a staggered side-by-side fashion to form collagen fibrils that are characterized by areas of higher and lower collagen molecule overlap, termed D-spacing. Collagen fibrils can be arranged in a mainly parallel fashion, which is a high orientation index, to give strength to the tissue, as seen in tendon for example. They can also be largely random (orthogonal) and form a mesh like structure which provides resistance to tear propagation and flexibility as in the skin[7].

Small angle X-ray scattering (SAXS) is an analytical method used to determine the nanostructure of materials. When X-rays are passed through a sample they are diffracted by its components and mathematical analysis of the resulting scatter patterns provides information on the shape and size of the components. Typically, SAXS analysis provides structural information on objects between 10 and 100 nm in size and has the advantages of being non-destructive and requiring minimal sample preparation[93]. The technique has been used for the analysis of a wide range of substances including biological materials where it has been particularly useful in studies of collagen in leather[6, 15, 69, 181], tendon[173, 182], and the cornea[81, 183-188].

The ultrastructure of collagen can also be determined by microscopy, but to produce the thin tissue sections that are studied, tissues must first undergo chemical fixation. This prevents degradation of tissues by autolysis and putrefaction, stabilizes the ultrastructure, and introduces structural rigidity which facilitates sectioning. Fixation, however, also brings about changes in the size and shape of tissue components and these have been described for collagen when examined by high resolution transmission electron microscopy (TEM).[46] Knowing how fixation changes the ultrastructure is important and the processing needs to be chosen carefully to preserve features of interest in the studied tissue. Although SAXS analysis can be carried out on unprocessed tissue, often only fixed samples are available. There is only minimal data on the effects of fixation of collagen on the parameters that can be measured by SAXS. Fullwood and Meek (1993)[189] found the interfibrillar spacing in bovine corneas fixed in 2.5% glutaraldehyde in 0.1 M phosphate buffered saline was not significantly greater than in fresh corneas (63.8 nm ± 2.8 vs. 63.4 nm ± 2.7; $P > 0.2$). However, the D-spacing, the gap between the overlapping parallel collagen molecules in fibrils, was significantly decreased (64.99 ± 0.17 vs. 64.49 ± 0.23; $P < 0.001$). Using rat Achilles tendon, Turunen et al., (2017)[190] found formalin generally preserves collagen organization with no difference in D-spacing of samples left in an unspecified formalin formulation for 48 hours and a reference sample stored in phosphate buffered saline (PBS). Kayed et al., (2015)[103] found an increased relative alignment of collagen fibrils (orientation index) in pericardium stored in Triton X compared to that in 0.6% glutaraldehyde (0.192 (0.021) vs. 0.117 (0.021). Freezing of human corneas had no effect on X-ray scattering patterns (Fratzl and Daxter (1993)[81].

To provide further information on the effects of commonly used preservatives on collagen parameters determined by SAXS analysis, we studied sheep corneas collected into a range of commonly used formulations. Furthermore, we performed TEM on all samples to complement the SAXS data.

Methods

Preservatives. *Karnovsky's fixative* consisting of 2.0 g of paraformaldehyde, 5.0 mL of 50% glutaraldehyde, 20.0 mL of 0.2M cacodylate buffer, and 1 M sodium hydroxide to establish a pH of 7.4. *Formalin* (10%) consisting of 100mL of 37-40% formaldehyde, 900 mL of distilled water, monosodium phosphate (4.0 g) and disodium phosphate anhydrous (6.5 g). *Triton X* consisting of 20 mM of trisaminomethane with 1 nM of Ethylenediaminetetraacetic (EDTA) acid, 1.25 mL of 10% Triton X and 1.25 mL of sodium deoxycholate (DOC). P*hosphate buffered saline (PBS)* was formulated by dissolving 4.5 g of sodium chloride in 500 mL of deionized water before heat sterilization.

Samples. Clinically normal corneas were collected from adult female sheep immediately after slaughter at an abattoir in Fielding, New Zealand. The corneas were divided to provide duplicates for SAXS and TEM. The halves of one cornea were immediately wrapped in cling wrap and frozen at -80°C to act as a control. The halves of the remaining 8 corneas were submerged in 2 mL of preservative, either 5% glutaraldehyde, 10% formalin, Triton X or 0.9% PBS. After 5 days, one half of each cornea was analysed by SAXS and the other half placed into Karnovsky's fixative for TEM imaging.

Small Angle X-ray Scattering (SAXS). The SAXS/WAXS beamline at the Australian Synchrotron in Melbourne, Australia was used to examine the collagen structure in the sheep corneas treated with various fixatives. The samples were mounted flat on to the X-ray beam (along their optical axis from anterior to posterior) to perform surface diffraction measurements where nine diffraction patterns were recorded using a three by three grid with 0.25 mm spacing between points. A high-intensity undulator source was utilized with an energy resolution of 10^{-4} from a cryo-cooled Si (111) double-crystal monochrometer. The beam size full width half maximum (FWHM) focused at the sample was 250 x 80 µm with a total photon flux of approximately 2 x 10^{12} photons s^{-1}. All diffraction patterns were recorded with an X-ray energy of 12 keV using a Pilatus 1M detector with an active area of 170 x 170 mm and a sample detector distance of 3337 mm. The exposure time for diffraction patterns was in the range of 1 – 5 seconds. Data processing was carried out using the ScatterBrain software. *D-spacing.* Gaussian approximations were used to determine the peak position of the maxima of the fifth order diffraction peak from the intensity versus q plot (Figure 55) where q is defined as the scattering vector. The D-spacing was calculated according to fundamental SAXS principals and Bragg's law. *Orientation Index.* The relative alignment of the collagen fibrils, the orientation index (OI), is defined as (90° - OA)/90°, where OA is the minimal azimuthal angle range, centred at 180° that contains 50% of the micro fibrils.[109] The OI range is from perfect alignment, represented by an OI of one, through to isotropy where the OI is zero. The OI was calculated from the spread in the azimuthal angle of the D-spacing peak at 0.045 – 0.055 $Å^{-1}$ (Figure 55). Each OI value represents an average of 9 measurements per sample. *Fibril Diameter*. Smoothing the sharp D-peaks from the intensity versus q plot over the full q-range (0.01 $Å^{-1}$ - 0.1 $Å^{-1}$) (Figure 55), we determined the fibril diameters by expressing the scattered intensities in terms of volume fraction distribution of scatters. Applying the total non-negative least squares model and the 'cylinder AR' model using "Irena"[101] (a macro developed for analysing SAXS data and more specifically particle size distributions in SAXS data running in Igor Pro, a data analysis tool (Wavemetrics, Lake Oswego, OR, USA)), the fibril diameters from the scatter intensity patterns could be determined under the assumption that fibrils have a cylindrical shape.

Transparency test. The effect of the preservatives on corneal transparency was evaluated subjectively by observing a 4 x 4 mm (1 point black line) cross through the corneas (Figure 54).

Transmission Electron Microscopy. After fixation for 48 hours the corneal samples were dehydrated in graded ethanol washes (from 25% to 100% in increments of 25), embedded in resin (Procure 812, ProSciTech, Australia) before ultra-thin sections of 60 to 70 nm were cut with an ultra-microtome (Leica EM UC7, Leica, Germany) and mounted on a copper grid. Following negative staining with ammonium molybdate, the sections were examined by transmission electron microscopy (Tecnai G2 Biotwin, FEI Company, USA).

Results

Transparency test. The printed cross below the sample was clearly visible through the control cornea (Figure 54) and those preserved in 5% glutaraldehyde and 10% formalin. It was less clearly visible through the cornea in PBS (S) and not visible through the cornea stored in Triton X (T).

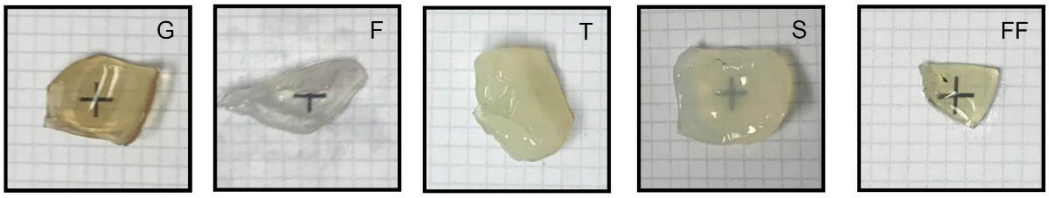

Figure 54. Transparency of sheep corneas preserved in 5% glutaraldehyde (G), 10% formalin (F), Triton X (T), phosphate buffered saline (S) and a frozen and thawed untreated control (FF).

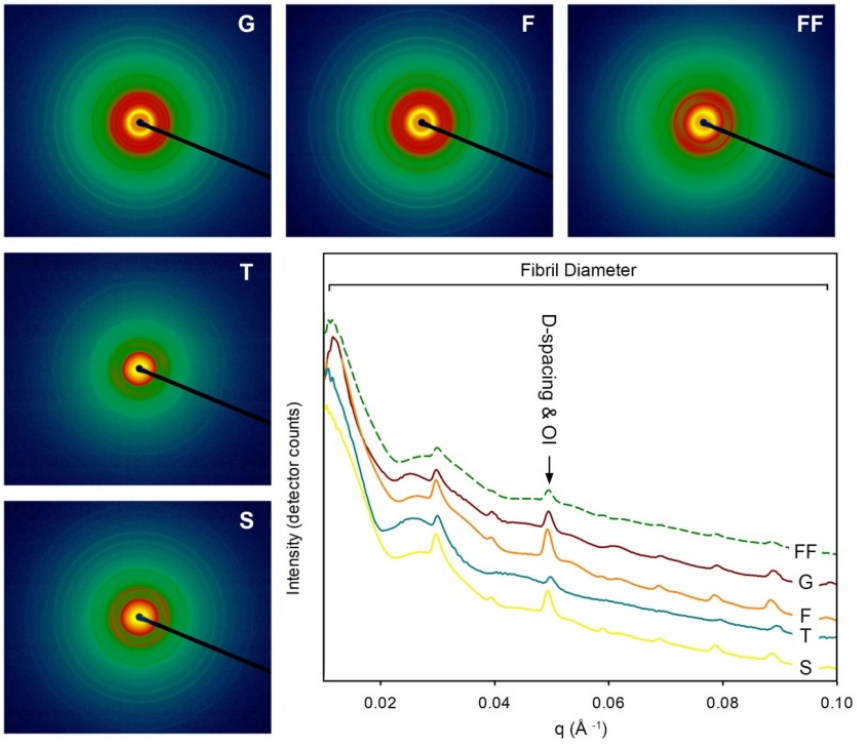

Figure 55. Photo images of 2D small angle X-ray scattering patterns produced by frozen and thawed control sheep corneas (FF) and corneas preserved in 5% glutaraldehyde (G), 10% formalin (F), Triton X (T), and phosphate buffered saline (S). Graph showing intensity profiles over the measured q-range for 5% glutaraldehyde (G, dark red), 10% formalin (F, orange), Triton X (T, teal), phosphate buffered saline (S, yellow) and frozen/thawed (FF, green) sheep cornea samples. The arrow indicates peak (0.045 – 0.055 $Å^{-1}$) used to determine D-spacing and orientation index (OI).

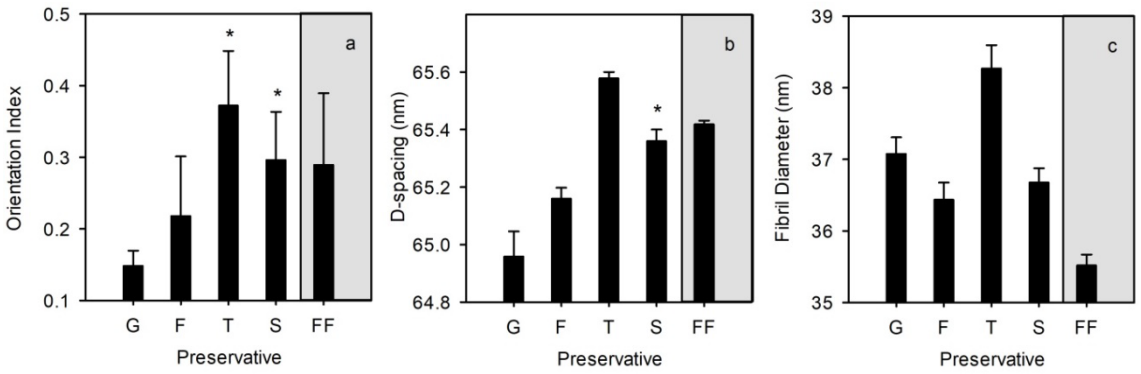

Figure 56. Means and standard deviations of (a) orientation indices, (b) D-spacings and (c) fibril diameters of collagen in frozen and thawed control sheep corneas (FF, highlighted in grey) and those preserved in 5% glutaraldehyde (G), 10% formalin (F), Triton X (T), and phosphate buffered saline (S) as determined by small angle X-ray scattering (SAXS). An * indicates values that were not significantly different from the control.

Table 15. Results of small angle x-ray scattering analysis to determine average (standard deviation) orientation index, D-spacing and fibril diameter of sheep corneas treated with 5% glutaraldehyde (G), 10% formalin (F), Triton X (T), and 0.9 % phosphate buffered saline (S). P-values relate to the control untreated cornea sample values (FF).

Species	**Collagen Properties**	**Preservative**				**Control**
		G	**F**	**T**	***S***	***FF***
Sheep	Orientation Index	0.15 (0.02)	0.22 (0.08)	0.37 (0.08)	0.30 (0.07)	0.29 (0.06)
	P-value	*P < 0.05*	*P < 0.05*	***0.19***	***0.87***	-
	D-spacing (nm)	64.96 (0.09)	65.16 (0.08)	65.58 (0.02)	65.36 (0.04)	65.42 (0.01)
	P-value	*P < 0.05*	*P < 0.05*	*P < 0.05*	***0.57***	-
	Fibril Diameter (nm)	37.08 (0.23)	36.44 (0.24)	38.27 (0.32)	36.68 (0.20)	35.52 (0.15)
	P-value	*P < 0.05*	*P < 0.05*	*P < 0.05*	*P < 0.05*	-

SAXS. Results of SAXS analysis are presented in Figure 55, 56 and Table 15.

Glutaraldehyde. The corneas stored in 5% glutaraldehyde had significantly lower OI and D-spacing values than the control ($P < 0.05$). Fibril diameters, however, were significantly higher ($P < 0.05$).

Formalin. Similar to the glutaraldehyde treated samples, the corneas treated with formalin had OI and D-spacing values significantly lower than in the control ($P < 0.05$). The fibril diameters were also significantly higher.

Triton X. The OI did not change significantly in the corneas stored in Triton X ($P = 0.19$) but fibril diameters and D-spacing were significantly greater ($P < 0.05$) and the largest recorded in the experiments.

Phosphate buffered saline. No significant differences were seen between the OI and D-spacing values of the control and the corneas preserved in PBS ($P = 0.87$ and $P = 0.57$, respectively) but fibril diameters were significantly higher ($P < 0.05$) than in the control.

TEM. To enable samples to be viewed by TEM, all the duplicates of the samples used for SAXS were processed using the same protocol, mainly fixation in Karnovsky's fixative, dehydration in ethanol, and embedding in polyester resin before sectioning. Each of these steps affect the morphology of collagen[189] and it was not therefore possible to perform quantitative comparisons of results obtained by SAXS analysis and TEM. Rather,

the TEM provided qualitative visual support for the SAXS analysis findings in all the samples studied (Figure 57). The collagen fibrils in the stroma of the sheep corneas preserved in 10% formalin, and particularly those preserved in 5% glutaraldehyde, appeared to be of similar diameter with relatively small interfibrillar spaces showing a short range order. The epithelial cells appeared normal. TEM of the Triton X preserved corneas indicated larger diameter fibrils with large variations in interfibrillar spacing, very irregular packing and poor short range order. The epithelial cells were no longer present. There was a similarly disordered array of the collagen fibrils in the corneas preserved in 0.9% PBS but fibril diameters appeared smaller than those in the Triton X preserved samples.

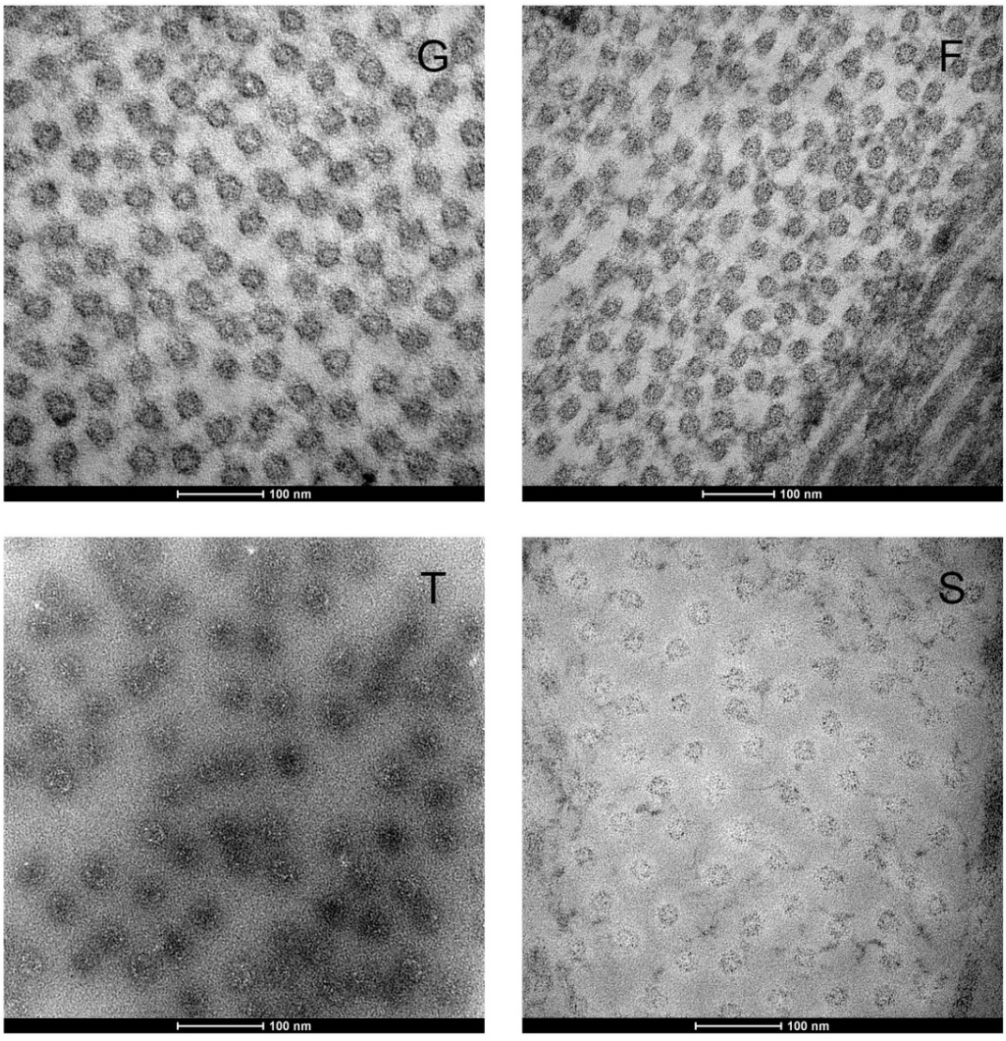

Figure 57. Transmission electron microscopy images of collagen fibril cross-sections in the stroma of sheep corneas treated with 5% glutaraldehyde (G), 10% formalin (F), Triton X (T) and phosphate buffered saline (S).

Discussion

While sophisticated modern techniques enable more detailed analysis of the nanostructure of materials, the processing required before analysis often leads to significant changes being introduced in the shapes and sizes of the different tissue components. For example, tissues prepared for TEM are changed during fixation and then again during the dehydration step required before embedding. Following that, there are a variety of resins available for embedding, each of which alters the nanostructure of tissue components in different ways[189]. Although there are reasonable data on the changes brought about in tissues by processing for TEM[44, 46, 189, 191], there is little and only fragmented data on the effects of tissue processing for SAXS analysis.

Our study has shown commonly used fixatives and preservatives introduce significant changes in the ultrastructure of corneal collagen. Formalin and glutaraldehyde resulted in significantly increased collagen fibril diameter, greater orthogonal alignment (decreased orientation index), and decreased D-spacing. Both formalin and glutaraldehyde are relatively small and can penetrate between collagen molecules and form cross linkages that bind collagen molecules together and stabilize their structural arrangement. Before such cross links can form, however, it has been suggested that the hypotonic fixative solution moves into the fibrils and causes them to swell[189]. The swollen fibrils would be expected to be larger and longer leading to increased fibril diameter and D-spacing measurements that is consistent with our findings on samples stored in formalin and glutaraldehyde. It is not clear how the more extensive and stronger cross linkages induced by formalin and glutaraldehyde molecules between collagen fibrils might have been responsible for the more random arrangement of the fibrils found in our study.

Under TEM the fibrils in our 5% glutaraldehyde and 10% formalin samples appeared to have uniform diameters with short-range order interfibrillar spacing. This has been shown to be essential for the optical transparency [4, 17] we noted for these samples in our transparency testing. Further, the epithelial and endothelial cells in the 5% glutaraldehyde and 10% formalin samples appeared normal, which is also a requirement for corneal transparency. The presence of specialized water-soluble structural proteins (crystalline proteins) and high levels of enzymes such as aldehyde dehydrogenase and transketolase in the cytoplasm of the epithelial cells[192] results in refractive indices of the cytoplasm and cell organelles that are within a range that does not produce scattering of light.

Triton X is a non-ionic detergent used in tissue engineering to produce implantable acellular matrix scaffolds from heart valves[193], tendons[194] and ligaments[195]. In removing proteoglycans and the intercellular matrix between collagen fibrils, the Triton X likely facilitated the entry of its PBS diluent into fibrils causing them to swell and increase the fibril diameter and D-spacing as seen in our SAXS analyses of the samples. By TEM the fibrils also appeared larger and there was considerable variation in interfibrillar spacing, very irregular packing and poor short range order, all consistent with the marked lack of transparency we noted in our transparency testing.

Storage in PBS only resulted in a significant increase in collagen fibril diameter. This most likely was because the cornea is normally maintained in a slightly dehydrated state by the endothelial cells on its inner surface[83, 84]. The 0.9% PBS we used in the study would thus be relatively hypotonic to the cornea and water would have moved into the corneal samples increasing the hydration status of the fibrils and causing them to swell[173, 196]. The resultant mild corneal oedema (an abnormal accumulation of fluid in tissue) would also have interfered with the optimal spacing of the fibrils which is essential for transparency[197, 198] and explain the loss of clarity of the cross we noted in our transparency test.

Conclusions

In conclusion, our study has shown that commonly used preservatives bring about significant changes in collagen parameters (relative alignment (OI), D-spacing and fibril diameter) measured by SAXS. It is important these changes are recognized so that comparable data can be obtained from studies using SAXS analysis on tissues processed in different ways.

Chapter 8. Tropical Keratopathy (Florida Spots) in Cats

Bolfa P., **Kelly S. J.**, Wells H. C., Sizeland K. H., Scott E. M., Kirby N., Mudie S., Armien A. G., Haverkamp R. G., and Kelly P. J., Tropical keratopathy (Florida Spots) in Cats. Journal of Veterinary Pathology DOI: 10.1177/0300985818789483.

Abstract

The authors used microscopy and synchrotron-based small-angle X-ray scattering analysis (SAXS) to describe lesions macroscopically typical of Tropical Keratopathy ("Florida spots") from 6 cats on St Kitts. Microscopically, there were varying degrees of epithelial hyperplasia and thinning of the cornea (by 4% to 18%) due to loss of corneal stroma associated with dense accumulations of collagen in the superficial stroma. The collagen fibrils in lesions were wider and had more variable diameters (39.5+ 5.0 nm, mean +SD) than in normal corneas (25.9+3.6 nm; $P < .01$). There were occasional vacuoles (<1 mm) in the corneal epithelium basement membrane but no evidence of inflammation, oedema, stromal neovascularization, fibrosis, acid-fast organisms, or structures suggestive of a fungal organism. SAXS analysis showed collagen fibril diameters and variation in size were greater in stroma containing the lesions compared to normal corneas (48.8+ 4.5 nm vs 35.5+ 2.6; $P < .05$). The d-spacing of collagen in the stroma of lesions and normal corneas was the same, but the average orientation index of collagen in lesions was greater (0.428+ 0.08 vs 0.285 + 0.03; $P < .05$). A survey revealed Florida spots lesions were static over time and became less obvious in only 1 of 6 affected cats adopted on St Kitts and taken to areas in the US where lesions are not reported. An anterior stromal collagen disorder with various degrees of epithelial hyperplasia is the pathologic hallmark of lesions clinically identical to Florida spots in cats from St Kitts.

Introduction

Corneal lesions in cats and dogs termed Florida spots, Florida fungus, Florida Keratopathy, mycotic Keratopathy, acid-fast spots, Tropical Keratopathy, or atypical Keratopathy are reported to be common in tropical and subtropical areas. [199-204] Clinically the lesions appear as variably sized (up to 4 mm) round to irregular grey to white corneal opacities which are most dense in their centres and can be single or multiple, and unilateral or bilateral. The opacities are inactive, do not stain with fluorescein and, with slit-lamp examination, appear to be located in the anterior stroma. Their etiology is unknown although there are reports that they are due to infections with acid-fast bacteria [205] or fungi[206] local factors such as UV light and living outdoors, [203, 207] or because of fire-ant exposure [208, 209]. The condition does not respond to topical corticosteroids, antibiotics or antifungals although keratectomy is curative[206]. There are reports that the lesions resolve when affected animals are moved out of tropical areas[203, 210].

Clinically identical lesions to those described above are common in cats on Saint Kitts. Herein, we describe the gross, microscopic and synchrotron based small angle X-ray scattering (SAXS) abnormalities in 6 cats with typical "Florida spots".

Methods

Cats and samples. In 2016 and 2017 we sampled lesions macroscopically typical of Tropical Keratopathy (Florida spots) from six adult domestic short-haired cats (DSH) presented for necropsy at the Ross University School of Veterinary Medicine (RUSVM) Pathology Service after humane euthanasia for a variety of reasons not associated with the ocular lesions. Typical lesions were identified based on the available descriptions in the literature,[203, 206, 210-213] essential criteria being that the lesions were single, multifocal or coalescing, round to heterogeneous, leukomatous, corneal opacities of varying sizes that were located within the superficial stroma. The opacities had to have a dense white cotton-like obstructive centre with a less dense, respersive, and ill-defined periphery (Figure 58). Finally, the affected eyes had to have had normal tear production in the Schirmer Tear Test, negative fluorescein staining, and no evidence of corneal vascularization or oedema. As controls, we used samples from clinically normal areas adjacent to lesions in affected cats as well as samples from the corneas of a clinically normal cat necropsied at RUSVM and another one necropsied at Massey University School of Veterinary Medicine, New Zealand where Tropical Keratopathy is unknown. These cats had also been humanely euthanized for reasons unrelated to eye disease. Skin biopsy punches (3mm diameter) were used to obtain samples from the lesions and the normal areas of the corneas. The biopsy samples were divided into quarters of which two were placed in 10% formalin in phosphate buffered saline for light microscopy, one in modified Karnovsky's fixative (2.5% glutaraldehyde in 100nM phosphate buffer, pH7.0) for TEM and one in Triton X surfactant (0.25% Triton X-100, 0.25% sodium deoxycholate, 0.02% EDTA, 20mg/L RNase I and 200mg/L DNase I) for SAXS.

Figure 58. Tropical Keratopathy, eye, cat. (1) Case 3. The right cornea contains multifocal to coalescing leukomatous lesions of various sizes (arrows). The centre is denser than the periphery of the lesion; (2) Case 2. Bilateral corneal opacities.

Histology. To determine the microscopic features of the lesions, samples in formalin were dehydrated in graded ethanol solutions and embedded in paraffin before 5 µm thick sections were cut and routinely stained with hematoxylin and eosin (HE). In addition, several special stains were used: Periodic acid Schiff (PAS) to highlight and determine the integrity of the epithelial basal lamina (basement membrane) [28214] and Descemet's membrane;[215] acid fast stain to detect acid-fast organisms;[205] Alcian blue stain to detect abnormal accumulations of acid polysaccharide in the stroma.[216] Slides were examined using a conventional light microscope (Olympus BX 43) equipped with an Olympus DP 26 digital camera and the cellSense Standard image analysis software. Great care was taken during collection of samples to avoid compression due to handling. Tissues in our lab are routinely handled on the back/side edge to avoid sample damage. We paid particular attention to orientation when trimming the biopsies to ensure that perpendicular sections were obtained through the cornea, as close as possible to the centres of the lesion. As an internal quality control, we observed normal cornea on both sides of the lesions.

Transmission Electron Microscopy (TEM). To determine the ultrastructure of the lesions, samples fixed in glutaraldehyde were trimmed, washed three times in phosphate buffered saline (0.1M, pH 7.2), post fixed in osmium tetroxide (0.1M) for one hour, dehydrated in graded ethanol washes (from 25% to 100% in increments of 25), and embedded in epoxy resin (EponTM Epoxy Embedding Medium Kit, Merck, USA). Ultra-thin sections of 60 to 70 nm were cut with an ultra-microtome (Leica EM UC7, Leica, Germany) and mounted on a copper grid. Following negative staining with ammonium molybdate the sections were examined by transmission electron microscopy (Tecnai G^2 BioTWIN, FEI Company, Czech Republic).

Synchrotron based small angle X-ray scattering (SAXS). The SAXS beamline at the Australian Synchrotron was used to examine the collagen structure in the lesions (N=10) and normal (N=10) corneas (Table 1). Each of the punch biopsy quarters preserved in Triton X for SAXS analysis were divided in half and mounted flat-on to the X-ray beam to perform surface measurements where nine diffraction patterns were recorded using a three by three grid with 0.25 mm spacing. The diffraction patterns were recorded at the Australian Synchrotron SAXS/WAXS beamline. A high-intensity undulator source was utilized with an energy resolution of 10^{-4} from a cryo-cooled Si (111) double-crystal monochrometer. The beam size full width half maximum focused at the sample was 250 x 80 µm with a total photon flux of approximately 2 x 10^{12} photons s^{-1}. All diffraction patterns

were recorded with an X-ray energy of 11 keV using Pilatus 1M detector with an active area of 170 x 170 mm and a sample detector distance of 3371 mm. The exposure time for diffraction patterns was in the range of 1 – 5 seconds. Data processing on the 90 scatter patterns created from samples of lesions from 2 cats and samples of normal cornea from 3 cats was carried out using the Scatterbrain software. Intensities displayed are all absolute detector counts (one X-ray detected one detector count), except when stated otherwise (Figure 59).

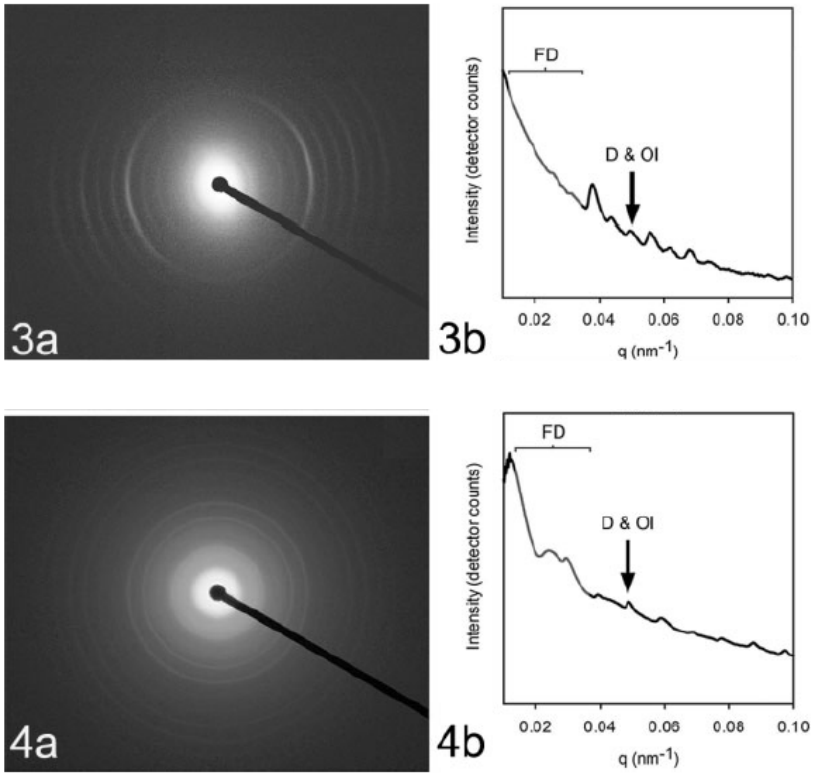

Figure 59. Photo images of the radial X-ray diffraction patterns produced by affected (3a) and normal (4a) collagen and graphs of the intensity of the diffraction at different radial distances from the beam (3b & 4b). The fibril diameter (FD) is determined by modelling the shape of the curve; D-spacing (D) and orientation index (OI) are determined from the fifth-order peak.

We would note that we were not able to perform focal SAXS measurements of just the lesion and not the surrounding normal collagen. Instead, we obtained total measurements across the entire anterior to posterior thickness of the cornea which contained collagen of both the lesion and adjacent normal cornea. We therefore selected biopsies from more severe lesions for the SAXS studies as these contained the highest ratios of abnormal to normal collagen, which would enable us to more readily characterize the collagen in the lesion.

Fibril Diameter and Size Distribution. The Irena software package running with Igor Pro [101] was used to calculate the fibril diameters from the SAXS data. The range of 0.01 – 0.04Å^{-1} was used to fit the wave vector, Q and at an azimuthal angle of 90° over a 5° segment to the long axis of most of the collagen fibrils. This azimuthal angle of the long axis was determined as the position for the maximum intensity when referring to the d-spacing diffraction peaks. The "cylinderAR" shape model (with an arbitrary aspect ratio of 100) was used for all fittings. The aspect ratio was not optimized for each individual fitting and it was noted as being possible for the collagen fibrils unbranched lengths to exceed the aspect ratio of 100. Fibril diameters were also determined from TEM images showing end-on collagen fibrils using ImageJ (National Institute of Health,

Bethesda, MD) with the Particle Analysis function having a circulatory threshold of 0.7– 1.0. We measured fibrils from 7 samples (4 normal corneas and 3 lesions) over a total area of 5.1 μm^2 (2.4 μm^2 for the normal tissue and 2.7 μm^2 for the lesions). *Orientation Index.* The collagen orientation was determined from the azimuthal angle for the maximum intensity of the d-spacing diffraction peaks. The orientation index (OI) was the primary measure used where OI is defined as (90° - OA)/90°, where OA is the minimal azimuthal angle range, centred at 180° that contains 50% of the micro fibrils. [109] The OI range is from perfect alignment, represented by an OI of one, through to isotropy where the OI is zero. The OI was calculated from the spread in the azimuthal angle of the d-spacing peak at 0.059 – 0.060 Å. Each OI value represents and average of 9 – 18 measurements of a single sample. *D-Spacing.* The central position of Gaussian approximations, fitted to the fifth order diffraction peak from the integrated intensity at the azimuthal angle range of 45 - 135°, was used to calculate the d-spacing according to Bragg's law.

Statistical Analysis. Analyses were performed using Minitab 17 Statistical Software (2010) (State College, PA: Minitab, Inc) using a two-sample t test for unequal variance. A P value of under 0.05 was regarded as significant.

Alumni survey. Previous students at RUSVM were approached through the RUSVM Alumni Association to anonymously complete an online Qualtrics (Qualtrics software, Version 122014, Provo, UT. http://www.qualtrics.com) survey which requested details on the outcome of Florida spots in cats adopted on Saint Kitts and returned to the USA. The survey was approved by the Institutional Review Board of RUSVM.

RESULTS

Cats and Samples. The cats used in the study (Table 16) were adults of both sexes with multiple lesions, 0.5 to 4 mm maximum dimension, multifocal to coalescing, in one or both eyes (Figure 58).

Table 16. Cases selected for the study.

Samples	Case No.	Year collected	Origin	Age	Sex	Breed	Lesion location
Cats with lesions	1	2016	SK	young adult	male	DSH*	Left eye
	2	2016	SK	adult	female	DSH	Bilateral
	3	2016	SK	3 years	male	DSH	Right eye
	4	2017	SK	27 years	female	DSH	Bilateral
	5	2017	SK	6 years	male	DSH	Bilateral
Controls	6	2016	NZ	-	male	DSH	-
	7	2017	SK	6 months	female	Siamese	-

*Domestic short hair, SK – Saint Kitts and NZ – New Zealand

Histology. All lesions that we studied had essentially the same histological changes although their extent and severity varied between cats. The major change in the epithelium (Figure 60 (5)) was progressive epithelial hyperplasia towards the centre of the lesion with up to 13-15 cell layers (Figure 60 (6) & (7)) compared to only 6-9 layers in the normal controls or in the unaffected areas adjacent to the lesions. No mitotic figures were

observed in the epithelial lesions examined. The major change in the stroma was in the subepithelial and superficial regions where there corneal stromal lamellae appeared more dense as evidenced by loss of artifactual stromal clefts that appears during normal histological processing[217]. The thickness of the irregular collagen also increased progressively towards the centres of the lesions. Measurements showed the overall thickness of the cornea in the centre of lesions was 4 to 18% less than that of the normal cornea on the edge of the lesions. This reduction in corneal thickness was due to a decrease in the thickness of the corneal stroma. In some cases (Figure 61 (9)) the lesion was much more subtle, with mild changes in the superficial stroma and minimal changes in the overlying epithelium compared with a nearby non-affected area (Figure 61 (10)). Still, this change or this stage of the lesion (Figure 61 (11)) can be observed on light microscopy, with patience and a slide of good quality.

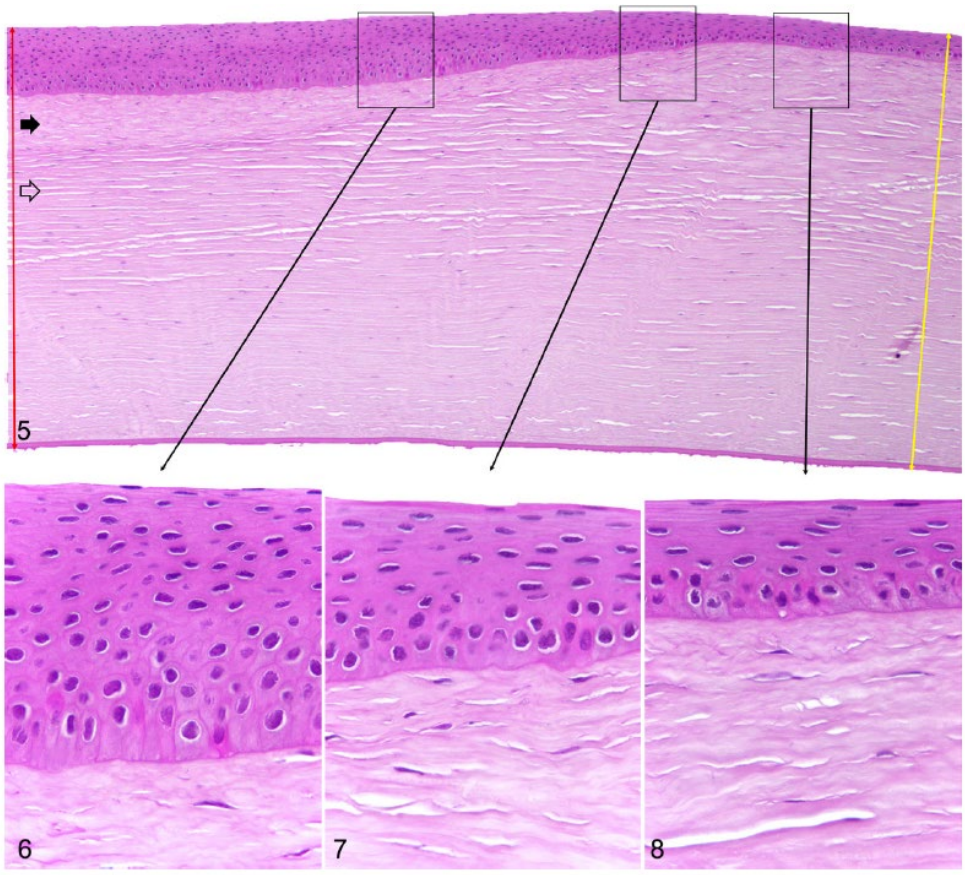

Figure 60. Typical histological changes seen in hematoxylin and eosin stained sections of the left eye of Case 2. (5) there is progressive corneal epithelial hyperplasia from right (normal area) to left (lesion) along with a progressive increase in the density of the superficial stroma with reduced spaces/clefts (thick black arrow) as opposed to the deeper corneal stroma (thick empty arrow). As a result of thinning of the stroma, the thickness of the cornea was reduced by up to 18% in lesions (red double arrow) as compared to the normal adjacent cornea (yellow double arrow). (6) centre of a lesion showing 13 to 15 cell layers in the corneal epithelium with a layer of dense collagen fibrils immediately beneath the lesion. (7) transition zone between the normal cornea and the lesion showing mild epithelial hyperplasia (up to 11 epithelial cell layers), some degree of irregularity in the basal lamina and, immediately beneath this, more densely packed collagen n the superficial stroma. (8) normal cornea adjacent to the lesion showing uniform epithelium with 6 to 9 cell layers and normal superficial stroma.

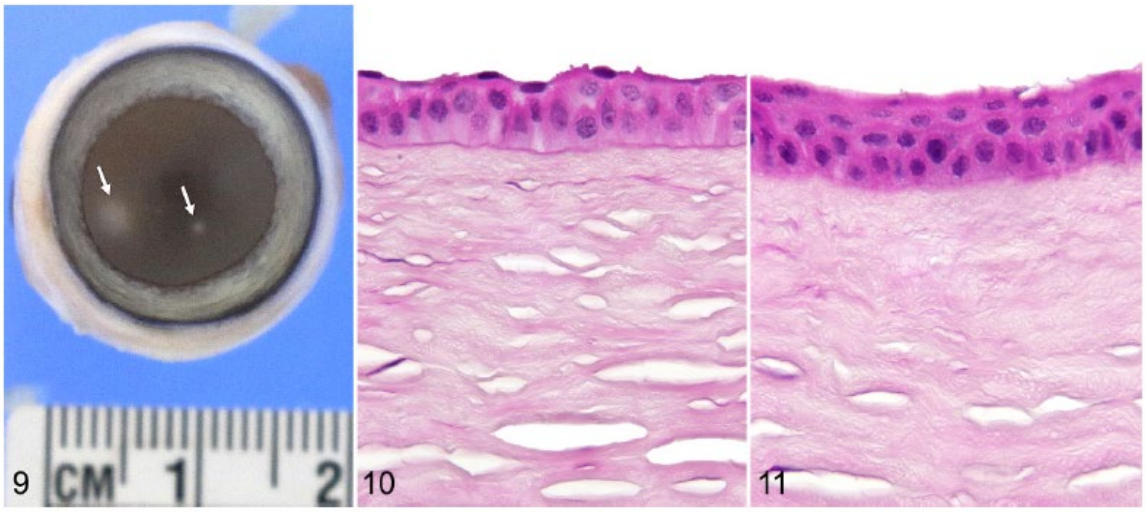

Figure 61. Tropical keratopathy, cornea (left eye), cat, case 6. (9) Several opacities ranging from under 1 mm to more than 3 mm are present. Two of them are more prominent (arrows) . (10) Unaffected area with normal corneal epithelium and stroma. Hematoxylin and eosin (HE). (11) The lesion in this case is subtle with minimal epithelial hyperplasia and increased density of the superficial stromal collagen with reduced clefts between fibrils. HE.

In routine HE stained sections the other corneal structures (deep stroma, Descemet's membrane and posterior epithelium) appeared normal and there was no evidence of inflammation, oedema, ulceration, stromal neovascularization or fibrosis associated with the lesions. Similarly, the PAS stain did not reveal any changes in the corneal epithelial basal lamina or in Descemet's membrane; no organisms were visualized with the acid-fast stain, and no accumulations of acid polysaccharides were observed with Alcian blue stain.

Transmission Electron Microscopy. The basal, wing and squamous cell layers of the epithelium at the site of the lesion were essentially identical to those in the normal corneas (Figure 61 (10) & (11)) and no inflammatory cells were seen. Increases in the numbers of polygonal basal cells were responsible for the epithelial hyperplasia (Figure 62 (12)). The numbers of mitotic figures in the hyperplastic epithelium were not increased and all the cells in this area had normal morphology, containing few organelles and being closely attached by numerous desmosomes. The basal surface of the epithelium appeared firmly attached to the corneal epithelium basement membrane with plentiful hemidesmosomes. In one of the lesions small vacuoles (< 1 µm) with no limiting membrane and sometimes bounded with osmium precipitates (probably lipids) were seen in the basement membrane and adjacent lamellae (Figure 62 (12)).

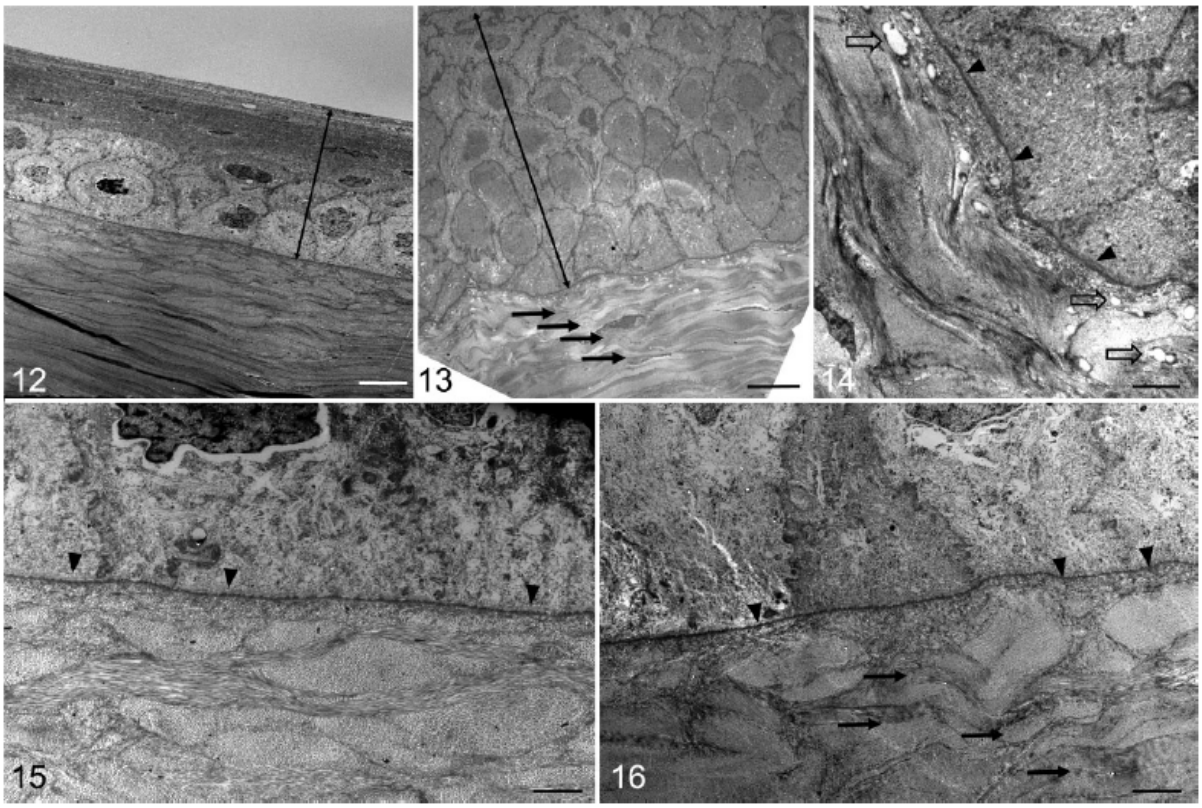

Figure 62. Cornea, cat. Transmission electron microscopy. (12) Case 7. Normal cornea (scale bar is 10 mm; double arrow, corneal epithelium). (13) Case 2. Hyperplastic epithelium (double arrow) in a lesion with vacuoles in the basement membrane (see also Fig. 12) and undulating densely packed collagen (arrows) in the superficial stroma (scale bar is 10 mm). (14) Tropical Keratopathy, case 2. Within the lesion, the basement membrane contains vacuoles (empty arrows), and the irregular, undulating, and tightly packed collagen of the superficial stroma under an intact epithelial basement membrane (arrowheads) (scale bar is 2 mm). (15) Case 4. Normal area of cornea adjacent to lesion (scale bar is 2 mm; arrowheads, basement membrane). (16) Case 4. Tropical Keratopathy. The superficial corneal stroma, beneath the area of epithelial hyperplasia, contains dense, undulating collagen fibrils (arrows) with intact epithelial basement membrane (arrowheads) (scale bar is 2 mm).

Collagen below the hyperplastic epithelium had a more undulating arrangement (Figure 62 (13), (14) & (15)) than the underlying collagen below the lesion which appeared normal[218], with regularly arranged, tightly packed, inter-branching collagen fibrils oriented in different planes. No neovascularization was seen in the stroma. The keratocytes between the collagen fibrils in both the lesion and normal areas of the stroma below the lesion were normal in number and morphology and Descemet's membrane was intact (data not shown on TEM but visible in histology images).

Computer measurement and analysis of the diameters of collagen fibrils seen end-on in electron microscope images revealed the average fibre diameter and range in size of the superficial stromal collagen of lesions (39.5 nm; SD 5.0 nm) (Figure 64 (17)) was greater than that of the underlying normal collagen (25.9 nm; SD 3.6 nm) ($P< 0.01$) (Figure 64 (18)).

Small angle X-ray scattering (SAXS). The averaged d-spacing in the lesion samples (63.6 nm; SD 1.0; range 2.4) were not significantly different from those of the normal corneas (64.9 nm; SD 0.4; range 0.9) ($P=0.18$) (Figure

64). The collagen fibril diameters and fibril diameter distributions were significantly larger in the lesion samples as compared to the samples of normal corneal tissue (35.5 nm, SD 2.6 nm versus 48.8 nm, SD 4.5 nm; P < 0.01). Similarly, there was an increase in the average orientation index of the collagen in the lesions as compared to that in normal areas (0.428, SD 0.06 versus 0.285, SD 0.03, respectively) (P< 0.01). This indicated a greater relative alignment of collagen fibrils in the lesions as compared with that in normal cornea (Figure 64).

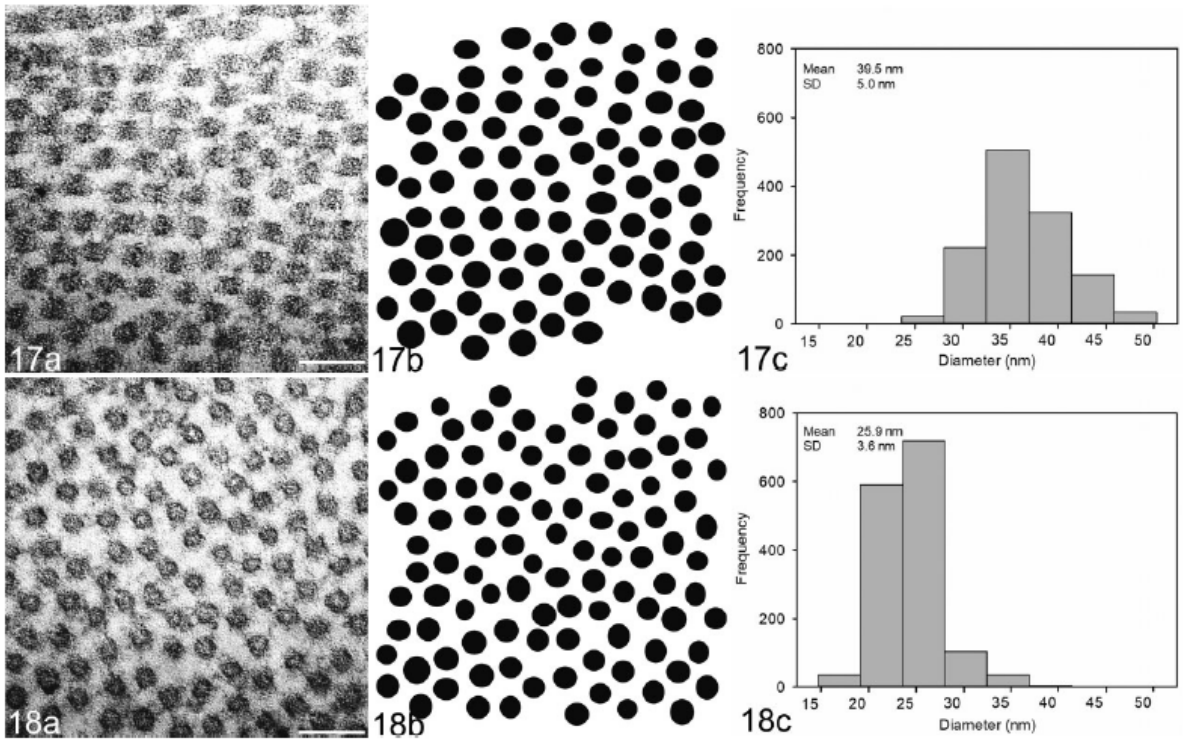

Figure 63. Collagen fibril size distribution in normal cornea (17) and in Tropical Keratopathy lesion (18). (a) Cornea, cat, case 3. Typical transmission electron micrograph of the stroma (scale bar is 100 nm). (b) The resulting binary image obtained using ImageJ software. (c) Frequency of different collagen fibril diameters in appropriately oriented transmission electron micrographs of the corneas studied. Collagen fibrils had significantly greater diameter in lesions of Tropical Keratopathy than in normal cornea (P < .01). SD, standard deviation.

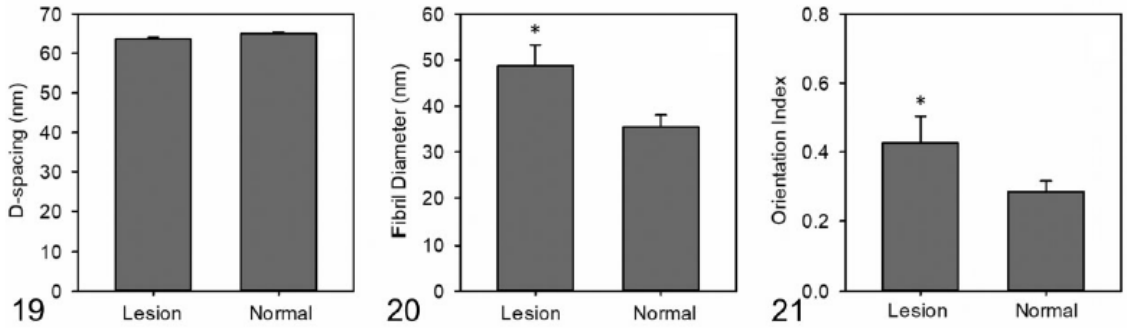

Figure 64. Collagen parameters measured by small-angle X-ray scattering (SAXS) in normal corneas and those with Florida spots. (19) D-spacing measured by SAXS in normal corneas and those with Florida spots. (20) Mean fibril diameter measured by SAXS in normal corneas and those with Florida spots. *P < .05 in a t-test for unequal variance. (21) Orientation index measured by SAXS in normal corneas and those with Florida spots. *P < .05 in a t-test for unequal variance.

Alumni survey. Six alumni reported they had adopted cats with Florida spots while on Saint Kitts and subsequently returned them to the USA from 2 to 25 years previously (mean 11.5 years). The lesions in one of the six cats was reported to have become less obvious but none totally regressed or became worse. The five cats with static lesions returned to, and lived in, a number of states in the USA including Minnesota (1 year), Maryland (5 years), Maine (1 year), New Jersey (7 years), Pennsylvania (1 year), New Hampshire (1 year), New York (14 years), Wisconsin (1 year), Oklahoma (1 year), Colorado (2 years), and Texas (1 year). These states are not in the south eastern USA, the region where Florida spots are most frequently reported[206].

Discussion

Although corneal opacities consistent with Florida spots and its aliases are reported to be common in tropical and subtropical areas, [203, 213] there have been few reports on their underlying pathology. An early study on radially symmetric light scattering opacities which occur in 10% of South Florida cats described innumerable granules, probably lipid, in the basement membrane of affected corneas. [207] These lesions seem grossly similar to those described in people with punctate Keratopathy (Rice's Keratopathy) [219] which is reported from the West Indies, and Central and South America[220-223]. Clinically, the human lesions are also non-active and asymptomatic but are very much smaller (under 1 mm in diameter)[219] than those we observed in cats (up to 4 mm). In one of the cases we examined with TEM, there were simple vacuoles in the epithelial basement membrane and immediately adjacent lamellae. They did not have a lining membrane (Figure 62 (13) and (14)) and were similar in location and morphology to some of the vacuoles described by Rice [220] in West Indians with punctate Keratopathy. It was suspected these empty simple vacuoles originally contained fat that was likely dissolved in the processing steps for electron microscopy. Although not observed in the cats in our study, Rice [220] found several other types of vacuoles including those with a lining membrane that formed villi, others in which the villi have become electron dense, and finally vacuoles almost filled with electron dense villi. It was suggested that these vacuoles, located under regions of epithelial detachment from Bowman's membrane due to epitheliolysis of basal cells, most likely contained lipid and calcium deposits[220].

Numerous round-to-oval vacuoles (30 – 200 microns) between normal collagen fibrils were seen in another early light microscopy study of keratectomy specimens from two cats and three dogs with Florida spots[224]. These were suggested to contain organisms similar to *Rhinosporidium*,[224] and there were no signs of inflammation or irritation. In 1987, Fischer et al. described a dog with acid-fast organisms within the stroma in a Florida spot lesion[205]. Transmission electron microscopy revealed a most likely lipoidal light staining material adjacent to keratocytes and 0.5 to 1 micron vacuoles scattered throughout the stroma. There were no alterations in the overlying corneal epithelium or stroma. In a study on 16 cats from Israel with Florida Keratopathy, one case was examined histopathologically and no changes were found in the cornea[208].

Although the Keratopathy we found in cats from St Kitts is clinically the same as the corneal opacities described in the veterinary reports above, its microscopic features are distinct. Previous reports and histopathology examination suggest that the lesion has no microscopic changes associated with it. [225] Our experience is that the lesions can be small so careful trimming of biopsies and proper placement in embedding media is needed to enable microscopic detection. Also, the extent of the epithelial hyperplasia and increase in

density of the subepithelial/superficial collagen varies in severity between lesions. In some cases, we struggled to identify subtle lesions and required careful examination of multiple serial sections. It is also possible there might be a number of underlying pathologies for the corneal opacities that are common in cats in the region are needed on cats in other areas to provide a better understanding of the lesions and enable a more appropriate name for the condition to be developed.

The most prominent feature of the condition in the cats on Saint Kitts is the abnormality in the collagen fibrils of the superficial stroma which is the site of the opacity seen with slit-lamp examination. Transparency of the cornea depends on the relatively regular parallel arrangement of collagen fibrils that are almost uniform in diameter and equally spaced (short-range ordering), under 1/2 the wavelength of visible light (400 - 700 nm)[4, 226, 227]. The large range in fibril diameters we found and the variability in spacing of the collagen fibrils in the abnormal stroma most likely account for the opacities seen clinically in the corneas we studied. As the collagen in the stroma is generally aligned to counteract shear stresses and thereby maintain corneal shape, it seems likely the greater alignment we observed in the lesions was induced by altered forces in the cornea. It remains to be elucidated at this stage whether or not the initial trigger for the lesion first affected the corneal epithelium or whether the hyperplasia most likely resulted from the stromal thinning we observed causing depressions in the cornea which became filled with epithelial cells. This basal cell proliferation and migration of epithelial cells from the limbus would have continued until the resulting hyperplastic epithelium became level with the adjacent corneal surface and therefore exposed to the palpebral 'snow plough' effect which maintains the smooth and uniform epithelial surface[228, 229].

It is noteworthy that although epithelial hyperplasia can be marked it does not contribute to corneal opacity and the epithelial layer is normal in slit-lamp examinations of affected eyes. The individual cells in the hyperplastic epithelia we observed appeared normal by both light and electron microscopy and thus provide the relatively small fluctuations between the refractive indices of the cell cytoplasm and organelles (short-range order) needed for transparency[192]. Also, the cells appeared to be functioning normally and providing a diffusion barrier to prevent fluid (tears) flow into the hydrophilic stroma: the cells were tightly attached to one another with large numbers of desmosomes, there were no obvious intracellular spaces, and there was no stromal oedema.

Although previous studies in cats and dogs also described vacuoles in lesions the ones we report in our case were not related to acid-fast organisms [205] and were far smaller than the vacuoles described which possibly contained *Rhinosporidium*[224]. Also, they were not visible as light scattering granules with HE staining [207] and were localized to the basement membrane or the area immediately beneath it, unlike the above vacuoles which were widely distributed in the stroma. The vacuoles described in human patients with Tropical Keratopathy were also mainly in the basement membrane but were considerably more numerous, forming dense aggregates. They also appeared in a variety of forms not seen in our study and were regarded as being evidence of fatty degeneration and calcification possibly induced by trauma[220, 223].

Our study did not show the cause of the lesions but we found no evidence they were caused by acid-fast organisms, as reported for Florida spots[205], or by fungi as reported with mycotic keratopathy[224]. Our results do show, however, that the primary problem is in the superficial stroma where collagen fibrils with a wide range of diameters and interfibrillar spacing were seen microscopically and confirmed by SAXS measurements. In the cases we examined, a corneal wound can be ruled out by the absence of its classical histological features, such as: oedema, stromal fibroblastic metaplasia of keratocytes or angiogenesis[230]. Further studies are needed to determine if these changes are due to the other suggested causes of the lesions, mainly exposure to UV light, [207] fire-ant (*Wasmania auropunctata*) venom[208, 209], or microtrauma as a result of dust or other air-borne pollutants[203, 220, 221]. Based on local experience we doubt that fire-ants are a significant cause of the lesions as, although these ants are present on Saint Kitts, we very rarely see fire-ant related skin lesions in cats let alone the severe acute keratitis associated with fire-ants[209].

There is one report that lesions in three cats from Martinique resolved when the cats returned to France, and that they recurred when the cats returned to the island[203]. In our survey, the lesions in only one of the cats was reported to improve but not resolve. The lesions in the other five cats, however, did not change even though most of the cats went to areas in the USA not associated with Florida spots and therefore presumably without the agents causing the lesions. This lack of resolution seems more consistent with the seemingly irreversible lesions we observed in the study.

It is of note that other species on Saint Kitts, with lesions clinically identical to the feline "Florida spots" we describe, have very similar histological changes. These include dogs, which have been previously reported to have "Florida spots"[9, 21, 23]. Indian mongooses (*Herpestes javanicus*), and vervet monkeys (*Chlorocebus aethiops sabaeus*). There are on-going studies at RUSVM investigating the histopathology and the pathogenesis of the corneal opacities in these other species.

Conclusion

In conclusion, our study represents the first detailed description of the corneal opacities seen commonly in cats on the Caribbean island of Saint Kitts. The major abnormality is the thinning of the corneal stroma and more aligned collagen fibrils in the superficial region that have a wide variety of fibril sizes and interfibrillar spacing. The other changes (various degree of overlying epithelium hyperplasia and occasional vacuoles in the basement membrane) do not appear to contribute to the opacification of the cornea. The lesions appear not to be associated with infectious or inflammatory processes and further studies are needed to determine the etiology of the lesions and the distribution of affected animals in the region.

Overall Conclusions

Small angle X-ray scattering (SAXS) has proven useful for measuring the shape and arrangement of collagen fibrils in the cornea and leather. SAXS is an X-ray diffraction technique where measurements of the scattered wave angles and intensities, produced by X-ray interactions with particles, provide nano-structural detail of particle sizes and shapes. In the case of leather and the cornea, where fibrous type I collagen is the main structural component; we can determine a range of parameters that characterize the size and arrangement of the collagen fibrils. These parameters include D-spacing, relative alignment (orientation index, OI), interfibrillar spacing, fibril diameter and intermolecular spacing.

SAXS was used in Chapters 3, 4, 5 and 6 to investigate collagen structures in leather.

In Chapter 3 we used SAXS to investigate leather from three species typically used for leather making (sheep, cattle and deer) to see the natural variation within and between their skins. Comparing the SAXS measurements with normalized tear strength measurements, we noted an unpredictable variability in collagen arrangement within each species but a significant difference in strength between species. There were no obvious regions of generally stronger or weaker skin within individual skins. The predominant collagen fibril direction (OI) was perpendicular to the backbone of all species, with the greatest alignment found in sheep followed by deer then cattle. These findings have important implications for manufacturers of leather products. They show there is no relationship between flat-on orientation measurements over the whole skin and with tear strength. The orientation maps presented here suggest that it is the selection of the species that should be considered first if strength is a priority, rather than the location within a skin.

In Chapter 4 we used SAXS to further investigate the correlation between leather strength and collagen fibril alignment (OI) by applying bi-axial strain to sheep skin during tanning to artificially aligning collagen fibrils. We found evidence to support a causal relationship between a high in-plane collagen fibril OI and tear strength. A relationship was also found between the amount of strain applied during tanning and tear strength. The tear strength depends on the relative direction of strain applied during tanning and the measured direction of tear strength. When a greater in-plane OI is achieved, it results in greater tear strength in both the parallel and perpendicular tear directions. Previously this relationship had been seen in a range of natural collagen materials, such as tendon, but in this instance, a material has been manufactured with improved properties. Since sheep leather is half the strength of cattle leather, it has limited commercial applications. The proposed method of artificially aligning collagen during tanning could be implemented at tanneries to increase sheep leather strength and value.

In Chapters 5 & 6 we use SAXS to characterize stiffness in leather and how water interacts with the collagen structure and what effect it has on leather stiffness. This follows on from findings presented in Chapter 4, where artificial collagen alignment increases leather strength but also the leather's stiffness. The stretch tanned leather was found to have more aligned slender fibrils in a more densely packed structure, seen as a reduction in sample thickness and an increase in D-spacing. With this structure the leather has a significantly greater Young's modulus (stiffness), compared to leather processed normally. Water is known to have a

mitigating effect on material stiffness. We investigated the effect of moisture content on the collagen structure and mechanical performance. The lateral intermolecular spacing and D-spacing both increased with increasing moisture content. The more predominate increases were seen in the lateral intermolecular spacing suggesting more water is incorporated laterally rather than longitudinally in the collagen molecule. Less remarkable effects were seen in changes to the fibril alignment as the moisture content varied. The moisture content did offer some mitigating effects to the leather stiffness by providing a lubricating effect from a thicker water layer that helped to reduce the internal friction between the fibrils. The dominant feature of material stiffness is fibril alignment and packing density which work in a synergistic manner to increase the material's stiffness. The primary swelling of the fibrils was in the lateral direction where the close packing of the fibrils did not appear to limit the lubricating effect the greater hydration shell appears to offer fibrils that are less well aligned. As such, the fully hydrated stretched leather is less stiff than fully hydrated non-stretched leather.

SAXS was then used to investigate corneal collagen structures in Chapters 6 & 7.

In Chapter 6 we show the effect of preservation for 5 days in 5% glutaraldehyde, 10% formalin, Triton X and 0.9% phosphate buffered saline (PBS) solutions on corneal collagen structures. All preservatives caused a significant change to the D-spacing, OI and fibril diameter of collagen in clinically normal sheep corneas compared to control, frozen samples. We reported a significant increase in the fibril diameter compared to the control cornea, while D-spacing increased significantly in corneas placed in Triton X but decreased significantly in those in 5% glutaraldehyde and 10% formalin. The collagen fibrils in corneas in 5% glutaraldehyde and 10% formalin had significantly greater orthogonal alignment (decreased OI). Overall, storage in PBS resulted in the least changes in collagen parameters measured by SAXS. Storage in Triton X and PBS reduced the tissue transparency. Essentially all the preservation media used in this study have a notable effect on collagen D-spacing, OI and fibril diameter. If tissue is analysed after preservation, understanding the effect the preservative has on the tissue structure is important to obtain comparable data from studies using SAXS.

In Chapter 7 we present the first detailed description of the corneal opacities (lesions) seen commonly in cats on the Caribbean island of St. Kitts. The major abnormality is the thinning of the corneal stroma and more aligned collagen fibrils in the superficial region that have a wide variety of fibre sizes and interfibrillar spacing. The other major lesions, an overlying hyperplastic epithelium and occasional vacuoles in the basement membrane, do not appear to contribute to the opacification of the cornea. The lesions appear not to be associated with infectious or inflammatory processes and further studies are needed to determine the aetiology of the lesions and the distribution of affected animals in the region.

The findings presented in this thesis have shown the usefulness of SAXS analysis of collagen structures which have added to the understanding of their structural function in skins, leather and the cornea for industrial and diagnostic applications.

References

1. Fratzl P and Weinkamer R, Nature's hierarchical materials. *Prog. Mater. Sci.* **52**:1263-1334 (2007).
2. Fratzl P, Ed., *Collagen: Structure and mechanics*. Springer Science, New York (2008).
3. Wells HC, Sizeland KH, Kirby N, Hawley A, Mudie S and Haverkamp RG, Collagen Fibril Structure and Strength in Acellular Dermal Matrix Materials of Bovine, Porcine and Human Origin. *ACS Biomat. Sci. Eng.* **1**:1026-1038 (2015).
4. Meek KM and Knupp C, Corneal structure and transparency. *Prog. Retin. Eye Res.* **49**:1-16 (2015).
5. Basil-Jones MM, Edmonds RL, Cooper SM and Haverkamp RG, Collagen fibril orientation in ovine and bovine leather affects strength: A small angle X-ray scattering (SAXS) study. *J. Agr. Food. Chem.* **59**:9972-9979 (2011).
6. Kelly SJ, Wells HC, Sizeland KH, Kirby N, Edmonds RL, Ryan T, Hawley A, Mudie S and Haverkamp RG, Artificially modified collagen fibril orientation affects leather tear strength. *J Sci Agric Food* (2017).
7. Yang W, Sherman VR, Gludovatz B, Schaible E, Stewart P, Ritchie RO and Meyers MA, On the tear resistance of skin. *Nat. Commun.* **6** (2015).
8. Di Lullo GA, Sweeney SM, Korkko J, Ala-Kokko L and San Antonio JD, Mapping the ligand-binding sites and disease-associated mutations on the most abundant protein in the human, type I collagen. *J. Biol. Chem.* **277**:4223-4231 (2002).
9. Gautieri A, Vesentini S, Redaelli A and Buehler MJ, Hierarchical Structure and Nanomechanics of Collagen Microfibrils from the Atomistic Scale Up. *Nano Letters* **11**:757-766 (2011).
10. Silver FH, Freeman JW and Seehra GP, Collagen self-assembly and the development of tendon mechanical properties. *J. Biomech.* **36**:1529-1553 (2003).
11. Basil-Jones MM, Edmonds RL, Allsop TF, Cooper SM, Holmes G, Norris GE, Cookson DJ, Kirby N and Haverkamp RG, Leather structure determination by small-angle X-ray scattering (SAXS): Cross sections of ovine and bovine leather. *J. Agric. Sci.* **58**:5286-5291 (2010).
12. Basil-Jones MM, Edmonds RL, Cooper SM, Kirby N, Hawley A and Haverkamp RG, Collagen Fibril Orientation and Tear Strength across Ovine Skins. *J Agric Sci* **61**:12327-12332 (2013).
13. Sizeland KH, Wells HC, Kelly SJR, Edmonds RL, Kirby NM, Hawley A, Mudie ST, Ryan TM and Haverkamp RG, The influence of water, lanolin, urea, proline, paraffin and fatliquor on collagen D-spacing in leather. *RSC Adv.* **7**:40658-40663 (2017).
14. Wells HC, Sizeland KH, Kelly SJR, Kirby N, Hawley A, Mudie S and Haverkamp RG, Collagen Fibril Intermolecular Spacing Changes with 2-Propanol: A Mechanism for Tissue Stiffness. *ACS Biomat. Sci. Eng.* **3**:2524-2532 (2017).
15. Kelly S, Edmonds, R., Cooper, S., Sizeland, K., Wells, H., Ryan, T., Kirby, N., Mudie S. and Haverkamp R., Mapping Tear Strength and Collagen Fibril Orientation in Bovine, Ovine and Cervine Hides and Skins. *J. Am. Chem. Soc.* **113**:1-11 (2018).
16. Kelly SJ, Weinkamer, R., Bertinetti, L., Edmonds, R.L., Sizeland, K. H., Wells, H. C. , Fratzl, P. and Haverkamp, R. G. , Effect of collagen packing and moisture content on leather stiffness, *J Mech Behav Biomed Mater* **90**:1-10 (2019).
17. Meek KM and Boote C, The organization of collagen in the corneal stroma. *Exp. Eye Res.* **78**:503-512 (2004).
18. Bolfa P, Kelly SJ, Wells HC, Sizeland KH, Scott EM, Kirby N, Mudie S, Armien AG, Haverkamp RG and Kelly PJ, Tropical Keratopathy (Florida Spots) in Cats. *Vet Path.*:0300985818789483 (2018).
19. Rich A and Crick FHC, The molecular structure of collagen. *J. Mol. Bio.* **3**:483-IN484 (1961).
20. Van Der Rest M and Garrone R, Collagen family of proteins. *The FASEB journal* **5**:2814-2823 (1991).
21. Lodish H, Berk A, Zipursky S, Matsudaira P, Baltimore D and Darnell J, Collagen: the fibrous proteins of the matrix. *Mol.Cell Bio.* **4** (2000).
22. Williams BR, Gelman RA, Poppke DC and Piez KA, Collagen fibril formation. Optimal in vitro conditions and preliminary kinetic results. *J. Bio. Chem.* **253**:6578-6585 (1978).
23. Chang S-W and Buehler MJ, Molecular biomechanics of collagen molecules. *Mat. Today* **17**:70-76 (2014).
24. Birk DE and Trelstad RL, Extracellular compartments in tendon morphogenesis: collagen fibril, bundle, and macroaggregate formation. *J. Cell Bio.* **103**:231-240 (1986).
25. Tanzer ML, Cross-linking of collagen. *Science* **180**:561-566 (1973).
26. Siegel RC and Martin G, Collagen Cross-Linking Enzymatic Synthesis of Lysine-Derived Aldehydes and the Production of Cross-Linked Components. *J. Bio. Chem.***245**:1653-1658 (1970).
27. Bowes JH and Cater CW, Crosslinking of collagen. *J. Appl. Chem.* **15**:296-304 (1965).

28. Kadler KE, Holmes DF, Trotter JA and Chapman JA, Collagen fibril formation. *Biochem. J.* **316**:1-11 (1996).
29. Petruska JA and Hodge AJ, A subunit model for the tropocollagen macromolecule. *Proc. Natl. Acad. Sci. USA* **51**:871-876 (1964).
30. Miller A, Collagen: the organic matrix of bone. *Phil. Trans. R. Soc. Lond. B* **304**:455-477 (1984).
31. Stinson RH and Sweeny PR, Skin collagen has an unusual d-spacing. *Biochem. Biophys. Acta.* **621**:158-161 (1980).
32. Diamant J, Keller A, Baer E, Litt M and Arridge RGC, Collagen; ultrastructure and its relation to mechanical properties as a function of ageing. *Proc. R. Soc. Lond. B* **180**:293-315 (1972).
33. Franchi M, Trire A, Quaranta M, Orsini E and Ottani V, Collagen structure of tendon relates to function. *Sci. World J.* **7**:404-420 (2007).
34. Haines BM and Barlow JR, The anatomy of leather. *J. Mater. Sci.* **10**:525-538 (1975).
35. Liao J and Vesely I, Skewness angle of interfibrillar proteoglycans increases with applied load on mitral valve chordae tendineae. *J. Biomech.* **40**:390-398 (2007).
36. Kayed HR, Sizeland KH, Kirby N, Hawley A, Mudie S and Haverkamp RG, Cross-Linking Collagen affects Fibril Orientation., in *Australian Synchrotron User Meeting, Melbourne, November 21–22, 2013*, Ed.
37. Sizeland KH, Wells HC, Higgins JJ, Cunanan CM, Kirby N, Hawley A and Haverkamp RG, Age Dependent Differences in Collagen Alignment of Glutaraldehyde Fixed Bovine Pericardium. *BioMed. Res. Int.* **2014**:189197 (2014).
38. Damink LHHO, Dijkstra PJ, Van Luyn MJA, Van Wachem PB, Nieuwenhuis P and Feijen J, Glutaraldehyde as a Crosslinking Agent for Collagen-based Biomaterials. *J. Mater. Sci-Mater.* **6**:460-472 (1995).
39. Meek KM and Chapman JA, Glutaraldehyde-induced Changes in the Axially Projected Fine Structure of Collagen Fibrils. *J. Mol. Bio.* **185**:359-370 (1985).
40. Harlan J and Feairheller S, Chemistry of the crosslinking of collagen during tanning, in *Protein Crosslinking*. Springer, pp 425-440 (1977).
41. Akhtar S, Effect of processing methods for transmission electron microscopy on corneal collagen fibrils diameter and spacing. *Microsc Res Techniq* **75**:1420-1424 (2012).
42. Sizeland KH, Basil-Jones MM, Edmonds RL, Cooper SM, Kirby N, Hawley A and Haverkamp RG, Collagen Orientation and Leather Strength for Selected Mammals. *J. Agric. Sci.* **61**:887-892 (2013).
43. Franchi M, Fini M, Quaranta M, De Pasquale V, Raspanti M, Giavaresi G, Ottani V and Ruggeri A, Crimp morphology in relaxed and stretched rat Achilles tendon. *J. Anat.* **210**:1-7 (2007).
44. Misof K, Rapp G and Fratzl P, A new molecular model for collagen elasticity based on synchrotron x-ray scattering evidence *Biophys. J.* **72**:1376-1381 (1997).
45. Shen ZL, Dodge MR, Kahn H, Ballarini R and Eppell SJ, Stress-strain experiments on individual collagen fibrils. *Biophys. J.* **95**:3956-3963 (2008).
46. Wenger MPE, Bozec L, Horton MA and Mesquida P, Mechanical Properties of Collagen Fibrils. *Biophys. J.* **93**:1255-1263 (2007).
47. Yu W, The mechanical properties of leather in relation to softness. *University of Leicester* (1999).
48. Wells HC, Sizeland KH, Kayed HR, Kirby N, Hawley A, Mudie ST and Haverkamp RG, Poisson's ratio of collagen fibrils measured by SAXS of strained bovine pericardium. *J. Appl. Phys.* **117**:044701 (2015).
49. Elliott DM, Narmoneva DA and Setton LA, Direct measurement of the Poisson's ratio of human patella cartilage in tension. *J. Biomech. Eng-T ASME* **124**:223-228 (2002).
50. Edelsten L, Jeffrey JE, Burgin LV and Aspden RM, Viscoelastic deformation of articular cartilage during impact loading. *Soft Matt.* **6**:5206-5212 (2010).
51. Montagna W, *The Structure and Function of Skin*. Elsevier (2012).
52. Winter DA, *Biomechanics and motor control of human movement*. John Wiley & Sons (2009).
53. Oxlund H, Manschot J and Viidik A, The role of elastin in the mechanical properties of skin. *J. Biomech.* **21**:213-218 (1988).
54. Oxlund H and Andreassen TT, The roles of hyaluronic acid, collagen and elastin in the mechanical properties of connective tissues. *J. Anat.* **131**:611-620 (1980).
55. Yang W, Sherman VR, Gludovatz B, Schaible E, Stewart P, Ritchie RO and Meyers MA, On the tear resistance of skin. *Nat. Comm.* **6** (2015).
56. Basil-Jones MM and Haverkamp RG, Fibrilar collagen structure determination of cross-sections of ovine leather using Small Angle X-ray Scattering (SAXS), in *Pacifichem 2010*, Ed, Honolulu, HI (2010).
57. Galarza B, Cavello I, Greco C, Hours R, Schuldt M and Cantera C, Alternative technologies for adding value to bovine hair waste. *J. Soc. Leather Tech. Chem.* **94**:26 (2010).
58. Weinstein GD and Boucek RJ, Collagen and Elastin of Human Dermis. *J. Investig. Derm.* **35**:227-229 (1960).
59. Tobin DJ, Introduction to skin aging. *J. Tissue Via.* **26**:37-46 (2017).

60. Sharphouse JH, *Leather Technician's Handbook*. Leather Producers' Association (1971).
61. Green G, Proteolysis of Collagen. *Nature* **180**:93-93 (1957).
62. Wells HC, Edmonds RL, Kirby N, Hawley A, Mudie ST and Haverkamp RG, Collagen fibril diameter and leather strength. *J. Agric. Food Chem.* **61**:11524-11531 (2013).
63. Basil-Jones MM, Edmonds RL, Norris GE and Haverkamp RG, Collagen fibril alignment and deformation during tensile strain of leather: A small-angle X-ray scattering study. *J Agric Food Chem* **60**:1201-1208 (2012).
64. Mutlu M, Ork, N., Yegin, O., Bas, S., Mapping the variations of tensile strength over the area os a sheep skin leather. *Annals of the University of Oradea Fasicle of Textiles, Leatherwork* **XV**:157-162 (2014).
65. Covington AD, Tanning Chemistry : The Science of Leather (2011).
66. Li Z, Paudecerf D and Yang J, Mechanical behaviour of natural cow leather in tension. *Acta Mechanica Solida Sinica* **22**:37-44 (2009).
67. Mallet JD and Rochette PJ, Ultraviolet light-induced cyclobutane pyrimidine dimers in rabbit eyes. *Photochemistry and photobiology* **87**:1363-1368 (2011).
68. Bashir H, Seykora JT and Lee V, Invisible Shield: Review of the Corneal Epithelium as a Barrier to UV Radiation, Pathogens, and Other Environmental Stimuli. *Journal of Ophthalmic & Vision Research* **12**:305-311 (2017).
69. West-Mays JA and Dwivedi DJ, The keratocyte: Corneal stromal cell with variable repair phenotypes. *The international journal of biochemistry & cell biology* **38**:1625-1631 (2006).
70. Bron AJ, The architecture of the corneal stroma. *British Journal of Ophthalmology* **85**:379-381 (2001).
71. Muller LJ, Pels E, Schurmans LR and Vrensen GF, A new three-dimensional model of the organization of proteoglycans and collagen fibrils in the human corneal stroma. *Exp Eye Res* **78**:493-501 (2004).
72. Benedek GB, Theory of Transparency of the Eye. *Appl Opt* **10**:459-473 (1971).
73. Komai Y and Ushiki T, The three-dimensional organization of collagen fibrils in the human cornea and sclera. *Invest Ophthalmol Vis Sci* **32**:2244-2258 (1991).
74. Cheng X and Pinsky PM, Mechanisms of self-organization for the collagen fibril lattice in the human cornea. *Journal of The Royal Society Interface* **10** (2013).
75. Fratzl P and Daxer A, Structural transformation of collagen fibrils in corneal stroma during drying. An x-ray scattering study. *Biophys J* **64**:1210-1214 (1993).
76. Cox J, Farrell R, Hart R and Langham M, The transparency of the mammalian cornea. *The Journal of physiology* **210**:601-616 (1970).
77. Maurice DM, The location of the fluid pump in the cornea. *J Physiol* **221**:43-54 (1972).
78. Qazi Y, Wong G, Monson B, Stringham J and Ambati BK, Corneal transparency: genesis, maintenance and dysfunction. *Brain Res Bull* **81**:198-210 (2010).
79. Meek KM, The Cornea and Sclera, in *Collagen: Structure and Mechanics*, ed. by Fratzl P. Springer US, Boston, MA, pp 359-396 (2008).
80. Jester JV, Corneal crystallins and the development of cellular transparency. *Seminars in Cell and Developmental Biology* **19**:82-93 (2008).
81. Meek KM and Fullwood NJ, Corneal and scleral collagens - a microscopist's perspective. *Micron* **32**:261-272 (2001).
82. Basil-Jones MM, Edmonds RL, Allsop TF, Cooper SM, Holmes G, Norris GE, Cookson DJ, Kirby N and Haverkamp RG, Leather structure determination by small angle X-ray scattering (SAXS): Cross sections of ovine and bovine leather. *J Agric Food Chem* **58**:5286-5291 (2010).
83. Bernado P, Mylonas E, Petoukhov MV, Blackledge M and Svergun DI, Structural characterization of flexible proteins using small-angle X-ray scattering. *Journal of the American Chemical Society* **129**:5656-5664 (2007).
84. Fratzl P, Jakob HF, Rinnerthaler S, Roschger P and Klaushofer K, Position-resolved small-angle X-ray scattering of complex biological materials. *Journal of Applied Crystallography* **30**:765-769 (1997).
85. Mertens HDT and Svergun DI, Structural characterization of proteins and complexes using small-angle X-ray solution scattering. *Journal of Structural Biology* **172**:128-141 (2010).
86. Paris O, From diffraction to imaging: New avenues in studying hierarchical biological tissues with x-ray microbeams (Review). *Biointerphases* **3**:FB16-FB26 (2008).
87. Glatter O and Kratky O, *Small angle X-ray scattering*. Academic press (1982).
88. Goodfellow JM, Elliott GF and Woolgar AE, X-ray diffraction studies of corneal stroma. *Journal of Molecular Biology* **119**:237-252 (1978).
89. Serra MJ, Genomics: The Science and Technology Behind the Human Genome Project. *Journal of Chemical Education* **77**:33 (2000).
90. Thomas JM and Sankar G, The Role of Synchrotron-Based Studies in the Elucidation and Design of Active Sites in Titanium− Silica Epoxidation Catalysts. *Accounts of Chemical Research* **34**:571-581 (2001).

91. Kempson IM, Paul Kirkbride K, Skinner WM and Coumbaros J, Applications of synchrotron radiation in forensic trace evidence analysis. *Talanta* **67**:286-303 (2005).
92. Heuberger A, X-ray lithography. *Microelectronic Engineering* **3**:535-556 (1985).
93. Henrich B, Bergamaschi A, Broennimann C, Dinapoli R, Eikenberry E, Johnson I, Kobas M, Kraft P, Mozzanica A and Schmitt B, PILATUS: A single photon counting pixel detector for X-ray applications. *Nuclear Instruments and Methods in Physics Research Section A: Accelerators, Spectrometers, Detectors and Associated Equipment* **607**:247-249 (2009).
94. Fournet AGaG, Small angle scattering of X-rays. *Journal of Polymer Science* **19**:594-594 (1956).
95. Ilavsky J and Jemian PR, Irena: tool suite for modeling and analysis of small-angle scattering. *J Appl Crystallogr* **42**:347-353 (2009).
96. Pro I, WaveMetrics Inc. *Lake Oswego, Oregon, USA Return to citation in text:[1]* (2011).
97. Kayed HR, Sizeland KH, Kirby N, Hawley A, Mudie ST and Haverkamp RG, Collagen Cross Linking and Fibril Alignment in Pericardium. *RSC Adv* **5**:3611-3618 (2015).
98. Wells HC, Sizeland KH, Kirby N, Hawley A, Mudie S and Haverkamp RG, Acellular dermal matrix collagen responds to strain by intermolecular spacing contraction with fibril extension and rearrangement. *J Mech Behav Biomed Mater* **79**:1-8 (2018).
99. Burger C, Zhou H-w, Wang H, Sics I, Hsiao BS, Chu B, Graham L and Glimcher MJ, Lateral Packing of Mineral Crystals in Bone Collagen Fibrils. *Biophysical Journal* **95**:1985-1992 (2008).
100. Vandenburgh HH and Karlisch P, Longitudinal growth of skeletal myotubes in vitro in a new horizontal mechanical cell stimulator. *In vitro cellular & developmental biology* **25**:607-616 (1989).
101. Pot MW, Faraj KA, Adawy A, van Enckevort WJ, van Moerkerk HT, Vlieg E, Daamen WF and van Kuppevelt TH, Versatile wedge-based system for the construction of unidirectional collagen scaffolds by directional freezing: practical and theoretical considerations. *ACS applied materials & interfaces* **7**:8495-8505 (2015).
102. Pot MW, Mihaila SM, Oosterwijk E, van Kuppevelt TH and Daamen WF, A comparison of cell distribution in anisotropic versus isotropic collagen scaffolds. *Towards regeneration of articular cartilage*:109 (2017).
103. Sacks MS, Smith DB and Hiester ED, A small angle light scattering device for planar connective tissue microstructural analysis. *Ann Biomed Eng* **25**:678-689 (1997).
104. Hermans JJ, Hermans PH, Vermaas D and Weidinger A, Quantitative evaluation of orientation in cellulose fibres from the X-ray fibre diagram. *Recueil des Travaux Chimiques des Pays-Bas* **65**:427-447 (1946).
105. Warrier J, Munshi V and Chidambareswaran P, Calculating Herman's Orientation Factor. *Textile Research Journal* **57**:554-555 (1987).
106. Collins TJ, ImageJ for microscopy. *Biotechniques* **43**:25-30 (2007).
107. Bertinetti L, Masic A, Schuetz R, Barbetta A, Seidt B, Wagermaier W and Fratzl P, Osmotically driven tensile stress in collagen-based mineralized tissues. *J Mech Behav Biomed Mater* **52**:14-21 (2015).
108. Masic A, Bertinetti L, Schuetz R, Chang SW, Metzger TH, Buehler MJ and Fratzl P, Osmotic pressure induced tensile forces in tendon collagen. *Nat Commun* **6** (2015).
109. Hoeve CAJ and Tata AS, The structure of water absorbed in collagen. *The Journal of Physical Chemistry* **82**:1660-1663 (1978).
110. Goldsmith LA, *Biochemistry and Physiology of the Skin*. Oxford University Press (1991).
111. Wilkes GL, Brown IA and Wildnauer RH, The biomechanical properties of skin. *Crit Rev Biotechnol* **1**:453-495 (1973).
112. Fratzl P, Misof K, Zizak I, Rapp G, Amenitsch H and Bernstorff S, Fibril structure and mechanical properties of collagen. *J Struct Biol* **122**:119-122 (1997).
113. Eppell SJ, Smith BN, Kahn H and Ballarini R, Nano measurements with micro-devices: mechanical properties of hydrated collagen fibrils. *J R Soc Interface* **3**:117-121 (2006).
114. Fratzl P, Collagen: Structure and Mechanics, an Introduction, in *Collagen: Structure and Mechanics*, ed. by Fratzl P. Springer US, Boston, MA, pp 1-13 (2008).
115. Kayed HR, Sizeland KH, Kirby N, Hawley A, Mudie ST and Haverkamp RG, Collagen Fibril Strain, Recruitment and Orientation for Pericardium under Tension and the Effect of Cross Links. *RSC Adv* **5**:103703-103712 (2015).
116. Kumar N, Kumar P, Nayak Badagabettu S, Prasad K, Kudva R and Vasudevarao RC, Surgical implications of asymmetric distribution of dermal collagen and elastic fibres in two orientations of skin samples from extremities. *Plastic surgery international* **2014**:364573 (2014).
117. Ní Annaidh A, Bruyère K, Destrade M, Gilchrist MD and Otténio M, Characterization of the anisotropic mechanical properties of excised human skin. *J Mech Behav Biomed Mater* **5**:139-148 (2012).
118. Pailler-Mattei C, Bec S and Zahouani H, In vivo measurements of the elastic mechanical properties of human skin by indentation tests. *Med Eng Phys* **30**:599-606 (2008).

119. Veronda DR and Westmann RA, Mechanical characterization of skin—Finite deformations. *J Biomech* **3**:111-124 (1970).
120. Langer K, On the anatomy and physiology of the skin. *J Plast Reconstr Aesthet Surg* **31**:3-8 (1978).
121. Kraissl CJ, The selection of appropriate lines for elective surgical incisions. *Plast Reconstr Surg* **8**:1-28 (1951).
122. Borges AF, Relaxed skin tension lines (RSTL) versus other skin lines. *Plast Reconstr Surg* **73**:144-150 (1984).
123. Emiroğlu M, Kuru B, Gülçelik MA, Atahan MK, Sezer AY, Karaali C and Güllüoğlu B, The Main Topics at the Oncoplastic Breast Surgery Course and Expert Panel. *J Breast Health* **13**:46-49 (2017).
124. Hellinger A, Roth I, Biber FC, Frenken M, Witzleb S and Lammers BJ, Surgical anatomy of the abdominal wall. *Arkh Anat Gistol Embriol* **87**:724-730 (2016).
125. Irwin DH, Tension lines in the skin of the dog. *The Journal of small animal practice* **7**:593-598 (1966).
126. Ní Annaidh A, Bruyère K, Destrade M, Gilchrist MD and Otténio M, Characterization of the anisotropic mechanical properties of excised human skin. *J Mech Behav Biomed Mater* **5**:139-148 (2012).
127. van Zuijlen PPM, Ruurda JJB, van Veen HA, van Marle J, van Trier AJM, Groenevelt F, Kreis RW and Middelkoop E, Collagen morphology in human skin and scar tissue: no adaptations in response to mechanical loading at joints. *Burns* **29**:423-431 (2003).
128. Nesbitt, Collagen Fibrils in Skin Orient in the Direction of Applied Uniaxial Load in Proportion to Stress while Exhibiting Differential Strains around Hair Follicles. *Funct Mater Lett* **8**:1841-1857 (2015).
129. Lynch B, Bancelin S, Bonod-Bidaud C, Gueusquin J-B, Ruggiero F, Schanne-Klein M-C and Allain J-M, A novel microstructural interpretation for the biomechanics of mouse skin derived from multiscale characterization. *Acta Biomater* **50**:302-311 (2017).
130. Tang Y, Ballarini R, Buehler MJ and Eppell SJ, Deformation micromechanisms of collagen fibrils under uniaxial tension. *J R Soc Interface* **7**:839-850 (2010).
131. Osaki S, Distribution map of collagen fiber orientation in a whole calf skin. *Anat Rec* **254**:147-152 (1999).
132. Osaki S, Yamada M, Takakusu A and Murakami K, A new approach to collagen fiber orientation in cow skin by the microwave method. *Cell Molec Bio* **39**:673-680 (1993).
133. Niitsuma K, Miyagawa S and Osaki S, Microwaves Determine the Orientational Distribution of Collagen Fibers in a Whole Cobra Skin. *Jap Polym J* **39**:181-186 (2006).
134. Aghamohammadzadeh H, Newton RH and Meek KM, X-ray scattering used to map the preferred collagen orientation in the human cornea and limbus. *Structure* **12**:249-256 (2004).
135. Fratzl P, Gupta H, Paschalis E and Roschger P, Structure and mechanical quality of the collagen–mineral nano-composite in bone. *Journal of materials chemistry* **14**:2115-2123 (2004).
136. Cookson D, Kirby N, Knott R, Lee M and Schultz D, Strategies for data collection and calibration with a pinhole-geometry SAXS instrument on a synchrotron beamline. *J Synchrotron Radiat* **13**:440-444 (2006).
137. Alexander EJ and Andriacchi TP, Correcting for deformation in skin-based marker systems. *J Biomech* **34**:355-361 (2001).
138. Holden JP, Orsini JA, Siegel KL, Kepple TM, Gerber LH and Stanhope SJ, Surface movement errors in shank kinematics and knee kinetics during gait. *Gait Posture* **5**:217-227 (1997).
139. Thorpe CT, Riley GP, Birch HL, Clegg PD and Screen HRC, Effect of fatigue loading on structure and functional behaviour of fascicles from energy-storing tendons. *Acta Biomater* **10**:3217-3224 (2014).
140. Dun R, The influence of selection and plane of nutrition on the components of fleece weight in Merino sheep. *Aust J Agr Res* **9**:802-818 (1958).
141. Lewis WS, Difference in weight between raw and clean wools. *J Franklin Inst* **180**:473 (1915).
142. Kokawa M, Yokoya N, Ashida H, Sugiyama J, Tsuta M, Yoshimura M, Fujita K and Shibata M, Visualization of Gluten, Starch, and Butter in Pie Pastry by Fluorescence Fingerprint Imaging. *Food Bio Tech* **8**:409-419 (2015).
143. Kang JJP, G. S. Ryu, S. W. Kim, Fiber Alignment of Steel Fiber Reinforced High Strength Concrete (SFR-HSC) in Flexural Members and its Effect on the Flexural Strength. *Key Eng Mat* **385-387**:789-792 (2008).
144. Michna H, Morphometric analysis of loading-induced changes in collagen-fibril populations in young tendons. *Cell Tissue Res* **236**:465-470 (1984).
145. Sizeland KH, Edmonds RL, Basil -Jones MM, Kirby N, Hawley A, Mudie S and Haverkamp RG, Changes to collagen structure during leather processing. *J Agric Food Chem* **63**:2499-2505 (2015).
146. Wright DM and Attenburrow GE, The set and mechanical behaviour of partially processed leather dried under strain. *J Mater Sci* **35**:1353-1357 (2000).
147. Boote C, Sturrock EJ, Attenburrow GE and Meek KM, Psuedo-affine behaviour of collagen fibres during the uniaxial deformation of leather. *J Mat Sci* **37**:3651-3656 (2002).
148. Ward AG, The mechanical properties of leather. *Rheo Acta* **13**:103-112 (1974).

149. Sturrock EJ, Boote C, Attenburrow GE and Meek KM, The effect of the biaxial stretching of leather on fibre orientation and tensile modulus. *J Mater Sci* **39**:2481-2486 (2004).
150. Kayed HR, Sizeland KH, Wells HC, Kirby N, Hawley A, Mudie S and Haverkamp RG, Age differences with glutaraldehyde treatment in collagen fibril orientation of bovine pericardium. *J Biomat Tissue Eng* **6** (2016).
151. Merkel RC, Liu CK, Latona N, Elamma A and Goetsch AL, Effects of level and length of supplementation on leather characteristics of yearling Boer and Spanish wethers. *J Am Chem Soc* **108**:139-145 (2013).
152. Liu CK, Latona NP and DiMaio GL, Lubrication of leather with polyethylene glycol. *J Am Chem Soc* **97**:355-368 (2002).
153. Liu CK and Dimaio GL, Effects of vacuum drying variables on the mechanical properties of leather. *J Am Chem Soc* **96**:243-254 (2001).
154. O'leary DN and Attenburrow GE, Differences in strength between the grain and corium layers of leather. *J Mat Sci* **31**:5677-5682 (1996).
155. Kayed HR, Sizeland KH, Wells HC, Kirby N, Hawley A, Mudie S and Haverkamp RG, Age differences with glutaraldehyde treatment in collagen fibril orientation of bovine pericardium. *J Biomat Tissue Eng* **6**:992-997 (2016).
156. Kelly SJ, Kelly PJ, Wells HC, Sizeland KH, Haverkamp RG, Armien A and Bolfa P, Corneal Epithelial Hyperplasia Combined with a Superficial Corneal Stromal Collagen Disorder as the Main Underlying Changes in Tropical Keratopathy (Florida Spots) in Cats. *J Comp Pathol* **158**:95 (2018).
157. Wells HC, Holmes G, Jeng US, Wu WR, Kirby N, Hawley A, Mudie S and Haverkamp RG, A small angle X-ray scattering study of the structure and development of looseness in bovine hides and leather. *J Sci Agric Food* **97**:1543-1551 (2017).
158. Evans WD and Critchfield CL, The effects of atmospheric moisture on the physical properties of vegetable and chrome tanned calf leathers. *J Res Natl Bur Stand* **11**:147-162 (1933).
159. Sizeland KH, Holmes G, Edmonds RL, Kirby N, Hawley A, Mudie ST and Haverkamp RG, Fatliquor Effects on Collagen Fibril Orientation and D-spacing in Leather during Tensile Strain. *J Am Leather Chem Assoc* **110** (2015).
160. Sizeland KH, Holmes G, Edmonds RL, Kirby N, Hawley A, Mudie ST and Haverkamp RG, Fatliquor effects on collagen fibril orientation and d-spacing in leather during tensile strain. *J Am Leather Chem Assoc* **110**:355-362 (2015).
161. Wess TJ and Orgel JP, Changes in collagen structure: drying, dehydrothermal treatment and relation to long term deterioration. *Thermochim Acta* **365**:119-128 (2000).
162. Turunen MJ, Khayyeri H, Guizar-Sicairos M and Isaksson H, Effects of tissue fixation and dehydration on tendon collagen nanostructure. *J Struct Biol*:Ahead of Print (2017).
163. Bertinetti L, Masic A, Schuetz R, Barbetta A, Seidt B, Wagermaier W and Fratzl P, Osmotically driven tensile stress in collagen-based mineralized tissues. *J Mech Behav Biomed* **52**:14-21 (2015).
164. Wells HC, Sizeland KH, Kelly SJR, Kirby N, Hawley A, Mudie S and Haverkamp RG, Collagen Fibril Intermolecular Spacing Changes with 2-Propanol: A Mechanism for Tissue Stiffness. *ACS Biomat Sci Eng* **3**:2524–2532 (2017).
165. Varma S, Orgel Joseph PRO and Schieber Jay D, Nanomechanics of Type I Collagen. *Biophys J* **111**:50-56 (2016).
166. Fratzl P, Fratzl-Zelman N and Klaushofer K, Collagen packing and mineralization: an x-ray scattering inverstigation of turkey leg tendon. *Biophys J* **64**:260-266 (1993).
167. Benecke G, Wagermaier W, Li C, Schwartzkopf M, Flucke G, Hoerth R, Zizak I, Burghammer M, Metwalli E, Muller-Buschbaum P, Trebbin M, Forster S, Paris O, Roth SV and Fratzl P, A customizable software for fast reduction and analysis of large X-ray scattering data sets: applications of the new DPDAK package to small-angle X-ray scattering and grazing-incidence small-angle X-ray scattering. *J Appl Crystallogr* **47**:1797-1803 (2014).
168. Basil-Jones MM, Edmonds RL, Allsop TF, Cooper SM, Holmes G, Norris GE, Cookson DJ, Kirby N and Haverkamp RG, Leather structure determination by small-angle X-ray scattering (SAXS): Cross sections of ovine and bovine leather. *J Agric Food Chem* **58**:5286-5291 (2010).
169. Wells HC, Sizeland KH, Kelly SJR, Kirby N, Hawley A, Mudie S and Haverkamp RG, Acellular dermal matrix collagen responds to strain by intermolecular spacing contraction with fibril extension and rearrangement *J Mech Behav Biomed* **79**:1-8 (2018).
170. Fullerton GD and Amurao MR, Evidence that collagen and tendon have monolayer water coverage in the native state. *Cell Biol Int* **30**:56-65 (2006).
171. Bella J, Brodsky B and Berman HM, Hydration structure of a collagen peptide. *Structure* **3**:893-906 (1995).
172. Cusack S and Miller A, Determination of the elastic-constants of collagen by Brillouin light scattering. *J Mol Biol* **135**:39-51 (1979).

173. McDaniel DP, Shaw GA, Elliott JT, Bhadriraju K, Meuse C, Chung KH and Plant AL, The stiffness of collagen fibrils influences vascular smooth muscle cell phenotype. *Biophys J* **92**:1759-1769 (2007).
174. Sizeland KH, Wells HC, Norris GE, Edmonds RL, Kirby N, Hawley A, Mudie S and Haverkamp RG, Collagen D-spacing and the effect of fat liquor addition. *J Am Leather Chem Assoc* **110**:66-71 (2015).
175. Price RI, Lees S and Kirschner DA, X-ray diffraction analysis of tendon collagen at ambient and cryogenic temperatures: Role of hydration. *Int J Biol Macromol* **20**:23-33 (1997).
176. Boote C, Kamma-Lorger CS, Hayes S, Harris J, Burghammer M, Hiller J, Terrill NJ and Meek KM, Quantification of collagen organization in the peripheral human cornea at micron-scale resolution. *Biophys J* **101**:33-42 (2011).
177. de la Cuesta FB, Wenger MPE, Bean RJ, Bozec L, Horton MA and Robinson IK, Coherent X-ray diffraction from collagenous soft tissues. *Proc Natl Acad Sci USA* **106**:15297-15301 (2009).
178. McCally RL and Farrell RA, Structural implications of small-angle light scattering from cornea. *Exp Eye Res* **34**:99-113 (1982).
179. Quantock AJ, Boote C, Young RD, Hayes S, Tanioka H, Kawasaki S, Ohta N, Iida T, Yagi N, Kinoshita S and Meek KM, Small-angle fibre diffraction studies of corneal matrix structure: A depth-profiled investigation of the human eye-bank cornea. **40**:s335-s340 (2007).
180. Meek KM and Quantock AJ, The use of X-ray scattering techniques to quantify the orientation and distribution of collagen in the corneal stroma. *Prog Retin Eye Res* **20**:95-137 (2001).
181. Gyi TJ, Meek KM and Elliott GF, Collagen interfibrillar distances in corneal stroma using synchrotron X-ray diffraction: a species study. *Int J Biol Macromol* **10**:265-269 (1988).
182. Fullwood N and Meek K, A synchrotron X-ray study of the changes occurring in the corneal stroma during processing for electron microscopy. *J Microsc* **169**:53-60 (1993).
183. Turunen MJ, Khayyeri H, Guizar-Sicairos M and Isaksson H, Effects of tissue fixation and dehydration on tendon collagen nanostructure. *J Struct Biol* (2017).
184. Craig AS, Robertson JG and Parry DAD, Preservation of corneal collagen fibril structure using low-temperature procedures for electron microscopy. *J Ultrastruct Mol Struct Res* **96**:172-175 (1986).
185. Jester JV, Corneal crystallins and the development of cellular transparency, in *Semin Cell Dev Biol*, Ed. Elsevier, pp 82-93 (2008).
186. Grauss RW, Hazekamp MG, Oppenhuizen F, van Munsteren CJ, Gittenberger-de Groot AC and DeRuiter MC, Histological evaluation of decellularised porcine aortic valves: matrix changes due to different decellularisation methods. *Eur J Cardiothorac Surg* **27**:566-571 (2005).
187. Dahl SL, Koh J, Prabhakar V and Niklason LE, Decellularized native and engineered arterial scaffolds for transplantation. *Cell transplantation* **12**:659-666 (2003).
188. Cartmell JS and Dunn MG, Development of cell-seeded patellar tendon allografts for anterior cruciate ligament reconstruction. *Tissue Eng* **10**:1065-1075 (2004).
189. Meek K, Fullwood N, Cooke P, Elliott G, Maurice D, Quantock A, Wall R and Worthington C, Synchrotron x-ray diffraction studies of the cornea, with implications for stromal hydration. *Biophys J* **60**:467-474 (1991).
190. Mazzotta C, Balestrazzi A, Traversi C, Baiocchi S, Caporossi T, Tommasi C and Caporossi A, Treatment of progressive keratoconus by riboflavin-UVA-induced cross-linking of corneal collagen: ultrastructural analysis by Heidelberg Retinal Tomograph II in vivo confocal microscopy in humans. *Cornea* **26**:390-397 (2007).
191. Meek KM, Dennis S and Khan S, Changes in the Refractive Index of the Stroma and Its Extrafibrillar Matrix When the Cornea Swells. *Biophys J* **85**:2205-2212 (2003).
192. Barros PSd and Safatle AMV, Florida spots in dogs and cats. A clinical study in Sao Paulo – Brazil. *Brazilian Journal of Veterinary Research and Animal Science*:276-277 (1977).
193. Gilger BC, Bentley E and Ollivier FJ, Diseases and surgery of the canine cornea and sclera, in *Veterinary ophthalmology*. Blackwell Publishing, Ames, IA, pp 690-752 (2007).
194. Michaud B, Kératopathie atypique chez 3 chats d'un même propriétaire. *Le Point Vétérinaire* **303**:59-60 (2010).
195. Moore PA, Feline corneal disease. *Clin Tech Small Anim Pract* **20**:83-93 (2005).
196. Roze M, Plisnier M, Sottovia J and Cloet P, Etude de la keratopathie tropicale a la Martinique. *Revue de médecine vétérinaire* **155**:598-601 (2004).
197. Whitley R and Gilger B, Diseases of the canine cornea and sclera. *Veterinary ophthalmology* **3**:635-673 (1999).
198. Fischer CS and Peiffer J, R., Acid fast organism associated with corneal opacities in a dog, in *Transactions of the Eighteenth Annual Scientific Program of the American College of Veterinary Ophthalmologists*, Ed, Fort Worth, pp 241-243 (1978).
199. Peiffer Jr R and Jackson W, Mycotic keratopathy of the dog and cat in the southeastern United States: a preliminary report. *Journal American Animal Hospital Association* (1979).

200. Tucker G, Karpinski L and Fuseler J, Morphology and distribution of light-scattering granules in the corneas of South Florida cats. *Journal of Cell Biology* **83**:479A (1979).
201. Sarfaty H, Florida keratopathy in sixteen cats and a dog in Israel, in *International Society of Veterinary Ophthalmology*, Ed, Versailles, Paris, France (2008).
202. Theron L, Hypothese de la keratopathie liée a wasmannia auropunctata-le modele polynesien, Ed. Université de Liège, Belgium (2007).
203. Michaud B, Kératopathie atypique chez 3 chats d'un même propriétaire. *Point vétérinaire* **41** (2010).
204. de Moraes Barros PS and Safatle AMV, Florida spots in dogs and cats. A clinical study in São Paulo-Brazil. *Braz J vet Res cinim Sci* **34**:276-277 (1997).
205. Moore PA, Feline corneal disease. *Clinical techniques in small animal practice* **20**:83-93 (2005).
206. Gilger BC, Bentley E and Ollivier FJ, Diseases and surgery of the canine cornea and sclera. *Veterinary ophthalmology* **4**:690-752 (2007).
207. Torricelli AA, Singh V, Santhiago MR and Wilson SE, The corneal epithelial basement membrane: structure, function, and disease. *Invest Ophthalmol Vis Sci* **54**:6390-6400 (2013).
208. Obata H and Tsuru T, Corneal wound healing from the perspective of keratoplasty specimens with special reference to the function of the Bowman layer and Descemet membrane. *Cornea* **26**:S82-89 (2007).
209. Weiss JS, Orlando F and Albert DM, The usefulness of routine alcian blue staining of corneal specimens. *Cornea* **7**:127-132 (1988).
210. Cookson D, Kirby N, Knott R, Lee M and Schultz D, Strategies for data collection and calibration with a pinhole-geometry SAXS instrument on a synchrotron beamline. *J Synchrotron Radiat* **13**:440-444 (2006).
211. Treuting PM and Dintzis SM, *Comparative anatomy and histology: a mouse and human atlas (expert consult)*. Academic Press (2011).
212. Cullen CL, Wadowska DW, Singh A and Melekhovets Y, Ultrastructural findings in feline corneal sequestra. *Veterinary ophthalmology* **8**:295-303 (2005).
213. Galvis V, Tello A, Jaramillo LC, Paredes D and Camacho PA, Prevalence of Punctate Keratopathy of West Indians in a Colombian Referral Center and a New Name Proposed: Rice s Keratopathy. *Open Ophthalmol J* **9**:12-16 (2015).
214. Rice N, Jones BR and Ashton N, Punctate keratopathy of West Indians. *The British journal of ophthalmology* **52**:865 (1968).
215. McLendon BF, Kunesh MT, Graig EL and Makley TE, West Indian punctate keratopathy. *Cornea* **12**:406-412 (1993).
216. Waller SG, Proano R and Guderian R, West Indian punctate keratopathy in Ecuador. *Cornea* **13**:377-378 (1994).
217. Tietze B, Kasper B, Guthoff R and Geerling G, West Indian (Caribbean) punctate keratopathy: Clinical and in vivo confocal microscopical findings. *Cornea* **30**:1270-1272 (2011).
218. Dubielzig RR, Ketring K, McLellan GJ and Albert DM, *Veterinary ocular pathology, a comparative review*. Saunders, Elsevier, China (2010).
219. Farrell RA and McCally RL, Corneal transparency. *Principles and Practice of Ophthalmology* **2**:629-644 (2000).
220. Doutch JJ, Quantock AJ, Joyce NC and Meek KM, Ultraviolet light transmission through the human corneal stroma is reduced in the periphery. *Biophysical journal* **102**:1258-1264 (2012).
221. Lemp MA and Mathers WD, Renewal of the Corneal Epithelium. *Eye & Contact Lens* **17**:258-266 (1991).
222. Dillon EC, Eagle RC and Laibson PR, Compensatory epithelial hyperplasia in human corneal disease. *Ophthalmic Surgery, Lasers and Imaging Retina* **23**:729-732 (1992).
223. Njaa LB and Wilcock BP, The ear and eye, in *Pathologic basis of veterinary disease*, ed. by Zachary JF and McGavin MD. Elsevier, St. Louis, Missouri, p 1206 (2012).

Appendix A. List of Publications

Journal Articles

Kelly, S. J., R. Weinkamer, L. Bertinetti, R. L. Edmonds, K. H. Sizeland, H. C. Wells, H. C. , P. Fratzl and R. G. Haverkamp. 2018. Effect of collagen packing and moisture content on leather stiffness, *J Mech Behav Biomed Mater* **90**:1-10 (2019).

Kelly, S. J., R. Weinkamer, L. Bertinetti, R. L. Edmonds, K. H. Sizeland, H. C. Wells, H. C. , P. Fratzl and R. G. Haverkamp. 2018. Data on collagen structures in leather with varying moisture contents from small angle X-ray scattering and three point bend testing. *Data in Brief* **21**:1220-1226 (2018).

Bolfa, P., **S. J. Kelly**, H. C. Wells, K. H. Sizeland, E. M. Scott, N. Kirby, S. Mudie, A. G. Armien, R. G. Haverkamp, and P. J. Kelly. 2018. Tropical Keratopathy (Florida Spots) in Cats. Vet. Path.0300985818789483.

Kelly, S. J., H. C. Wells, K. H. Sizeland, N. Kirby, R. L. Edmonds, T. Ryan, A. Hawley, S. Mudie, and R. G. Haverkamp. 2018. Artificially modified collagen fibril orientation affects leather tear strength. J. Sci. Food Agric. 98(9):3524-3531.

Kelly, S. J., Edmonds, R. L., Cooper, S., Sizeland, K. H., Wells, H. C., Ryan, T., Kirby, N., Mudie S. and Haverkamp R. 2018. Mapping Tear Strength and Collagen Fibril Orientation in Bovine, Ovine and Cervine Hides and Skins. J. Am. Chem. Soc. 113(1):1-11.

Wells H. C., K. H. Sizeland, **S. J. Kelly**, M. M. Basil-Jones, R. L. Edmonds, R. G. Haverkamp. 2018. Fibril orientation and strength in collagen materials and adaptation to strain. Adv. Mat. Letters 9(6):411-418.

Sizeland, K. H., H. C. Wells, **S. J. Kelly**, K. E. Nesdale, B. C. H. May, S. G. Dempsey, C. H. Miller, N. Kirby, A. Hawley, S. Mudie, T. Ryan, D. Cookson, and R. G. Haverkamp. 2017. Collagen Fibril Response to Strain in Scaffolds from Ovine Forestomach for Tissue Engineering. ACS Biomat. Sci. Eng. 3(10):2550-2558.

Wells, H. C., K. H. Sizeland, **S. J. Kelly**, N. Kirby, A. Hawley, S. Mudie, and R. G. Haverkamp. 2017. Collagen Fibril Intermolecular Spacing Changes with 2-Propanol: A Mechanism for Tissue Stiffness. ACS Biomat. Sci. Eng. 3(10):2524-2532.

Sizeland, K. H., H. C. Wells, **S. J. Kelly**, R. L. Edmonds, N. M. Kirby, A. Hawley, S. T. Mudie, T. M. Ryan, and R. G. Haverkamp. 2017. The influence of water, lanolin, urea, proline, paraffin and fatliquor on collagen D-spacing in leather. RSC Adv. 7(64):40658-40663. 10.1039/C7RA05560A.

Conference Papers, Presentations and Posters

Kelly, **S. J.,** R. Weinkamer, L. Bertinetti, P. Fratzl and R. G. Haverkamp. Stiffness of modified collagen structures manipulated by moisture content. Australian Synchrotron User Meeting, Melbourne, Australia, November 2018. Oral Presentation.

Haverkamp, R.G., **S. J. Kelly**, R.L. Edmonds, K.H. Sizeland and H.C. Wells. Modifying collagen fibril structural arrangement to increase strength. International Conference on Materials Engineering and Nano Science (ICMENS) Conference, Hong Kong, January 2018. Oral Presentation.

Wells, H.C., K.C. Sizeland, **S. J. Kelly** and R.G. Haverkamp. The effect of 2-propanol and acid on collagen structure and stiffness in acellular dermal matrix materials. International Conference on Materials Engineering and Nano Science (ICMENS) Conference, Hong Kong, January 2018. Oral Presentation.

Sizeland, K. H., H. C. Wells, **S. J. Kelly**, N. M. Kirby, A. Hawley, S. T. Mudie, T. M. Ryan and R. G. Haverkamp. Nanostructure and micromechanical response of collagen in tissue for medical applications. 7th International

Conference on Mechanics of Biomaterials and Tissue (ICMOBT), Waikoloa, Hawaii, December 2017. Oral Presentation.

Sizeland, K. H., H. C. Wells, **S. J. Kelly**, N. M. Kirby, A. Hawley, S. T. Mudie, T. M. Ryan, R. G. Haverkamp. The Architecture of Collagen and its Biomechanical Response- Small Angle X-ray Scattering Studies. User Meeting, Australian Synchrotron, Melbourne, Australia, November 2017. Oral Presentation.

Kelly, **S. J.,** R. Weinkamer, L. Bertinetti, P. Fratzl and R. G. Haverkamp. Effect of collagen alignment and moisture content on leather stiffness. Monday Seminar, Max Planck Institute for Colloids and Interfaces, Golm, Germany, October 2017. Oral Presentation.

Haverkamp, R. G., H. C. Wells, **S. J. Kelly**, K. H. Sizeland and H. R. Kayed. Structure and Strength in Collagen Materials. Max Planck Institute, Potsdam, Germany, August 2016. Invited Lecture. Oral Presentation.

Kelly, S. J., P. J. Kelly, H. C. Wells, K. H. Sizeland, R. G. Haverkamp, A. Armien and P. Bolfa. Corneal epithelial hyperplasia combined with a superficial corneal stromal collagen disorder as the main underlying changes in Tropical Keratopathy (Florida Spots) in Cats. 13th European Pathology Congress in Milan, Italy, August 2017. Oral Presentation.
(*Conference Proceeding:* **Kelly, S. J.**, P. J. Kelly, H. C. Wells, K. H. Sizeland, R. G. Haverkamp, A. Armien, and P. Bolfa. 2018. Corneal Epithelial Hyperplasia Combined with a Superficial Corneal Stromal Collagen Disorder as the Main Underlying Changes in Tropical Keratopathy (Florida Spots) in Cats. J. Comp. Pathol. 158:95).

Kelly, S. J., K. H. Sizeland, H. C. Wells, R. L. Edmonds, C. Cole, N. Kirby, A. Hawley, S. Mudie and R. G. Haverkamp. Artificially induced collagen fiber orientation affects tear propagation in leather". IULTCS Congress in Chennai, India, February 2017. Oral Presentation.

Conference Posters

Kelly, S. J., H. C. Wells, K. H. Sizeland and R. G. Haverkamp. The effect of water on collagen nano-structure and mechanics. User Meeting, Australian Synchrotron, Melbourne, Australia, November 2017. Poster Presentation.

Sizeland, K. H., H. C. Wells, **S. J. Kelly**, N. M. Kirby, A. Hawley, S. T. Mudie, T. M. Ryan, and R. G. Haverkamp. Synchrotron SAXS of Collagen Biomaterials for Industrial Applications. User Meeting, Australian Synchrotron, Melbourne, Australia, November 2017. Poster Presentation.

Sizeland, K. H., H.C. Wells, **S. J. Kelly**, H.R. Kayed, N.M Kirby, S.T Mudie, A. Hawley, T.M. Ryan, and R.G. Haverkamp. Synchrotron SAXS of Collagen Biomaterials for Industrial Applications. Australian X-ray Analytical Association Conference, Melbourne, Australia, February 2017. Poster Presentation.

Kelly, S. J., H. C. Wells, K. H. Sizeland and R. G. Haverkamp. "Artificially induced collagen fibril orientation affects tear propagation in leather. User Meeting, Australian Synchrotron, Melbourne, Australia, November 2016. Poster Presentation.

Kelly, S. J., P. Bolfa, H. C. Wells, K. H. Sizeland, R. G. Haverkamp and P. J. Kelly. Pathology of Tropical Keratopathy in the Cat. Annual OneHealth Day, St Kitts, November 2016. Poster Presentation.

Appendix B. Poster Presentations

A list of poster deliveries from June 2016 - October 2017.

1. Poster presented at the One Health Symposium, Ross University, St Kitts, November 2016.

Pathology of Tropical Keratopathy in a Cat

S. J. Kelly[¥], P. Bolfa[#], T. E. Weronko[#], D. Hilchie[#], H. C. Wells[¥], K. H. Sizeland^, R. G. Haverkamp[¥] and P. J. Kelly[#]

[¥]School of Engineering and Advanced technology, Massey University, Private Bag 11222, Palmerston North, New Zealand 4442, [#]Ross University School of Veterinary Medicine, St Kitts, [^]Australian Synchrotron, 800 Blackburn Road, Clayton, VIC 3168, Australia.

Tropical keratopathy (Florida or Caribbean keratopathy, Florida spots) is a common eye lesion of dogs and cats in tropical and subtropical areas which is also sometimes seen in people[1], horses and birds[2]. Lesions consist of variably sized grey to grey-white corneal opacities which can be single or multiple and are most dense in their centres. The opacities are inactive and their aetiology is unknown although it has been suggested they are due to infections with acid-fast bacteria[3], fungi[4] and as a result of fire-ant exposure[5]. Treatments including antibiotics, corticosteroids and antifungals have been unsuccessful. There is little data on the pathology of the lesions with a study in people indicating the opacities resulted from sharply circumscribed areas of fatty degeneration and vacuole formation in Bowman's membrane in particular, and also to some extent, in the underlying stroma [6]. Epithelia were normal. A study in cats indicated there were light scattering granules in the corneas of affected animals[7]. To provide further information on the pathology of tropical keratopathy in cats we carried out histology, electron-microscopy and Synchrotron-based small and X-ray scattering (SAXS) imaging on a typical lesion in a cat.

---

[1] Rice N, Jones BR and Ashton N, Punctate keratopathy of West Indians. *The British journal of ophthalmology* **52**:865 (1968).
[2] Whitley R and Gilger B, Diseases of the canine cornea and sclera. *Veterinary ophthalmology* **3**:635-673 (1999).
[3] Fischer C and Poulter R, Acid-fact organism associated with corneal opacities in a dog, in *Proc Am Coll Vet Ophthalmol*, Ed, p 241 (1987).
[4] Peiffer Jr R and Jackson W, Mycotic keratopathy of the dog and cat in the southeastern United States: a preliminary report. *Journal* [1] *American Animal Hospital Association* (1979).
[5] Theron L, Hypothese de la keratopathie liée a wasmannia auropunctata-le modele polynesien, Ed. Université de Liège, Belgium (2007).
[6] Meek KM and Knupp C, Corneal structure and transparency. *Progress in Retinal and Eye Research* **49**:1-16 (2015).

2. Poster presented at the Australian Synchrotron User Meeting, Melbourne, Australia, November 2016.

ARTIFICIALLY INDUCED COLLAGEN FIBRE ORIENTATION AFFECTS TEAR PROPAGATION IN LEATHER

S. J. Kelly[†], K. H. Sizeland[†¥], H. C. Wells[†], R. L. Edmonds[§], C. Cole[§], N. Kirby[¥], A. Hawley[¥], S. Mudie[¥], and R. G. Haverkamp[†].

[†]School of Engineering and Advanced Technology, Massey University, Palmerston North, 4442 New Zealand, ‡Institute of Fundamental Sciences, Massey University, Private Bag 11222, Palmerston North 4442, New Zealand §Leather and Shoe Research Association, Palmerston North, 4442 New Zealand, ¥Australian Synchrotron, Clayton, Vic 3168, Australia.

Skins have a natural collagen orientation that lays parallel to the backbone of the animal[1]. In this region, collagen fibres are found to be most aligned allowing for functional stretching and strength while on the animal. When stretch forces are applied, collagen fibres tend to align themselves from head to tail in the direction of the force. This configuration allows the fibres to display their greatest strength[2] and resistance to tear propagation[3].

[1] Fratzl P and Weinkamer R, Nature's hierarchical materials. Prog Mater Sci 52:1263-1334 (2007).
[2] Fratzl P, Ed., Collagen: Structure and mechanics. Springer Science, New York (2008).
[3] Wells HC, Sizeland KH, Kirby N, Hawley A, Mudie S and Haverkamp RG, Collagen Fibril Structure and Strength in Acellular Dermal Matrix Materials of Bovine, Porcine and Human Origin. ACS Biomat Sci Eng 1:1026-1038 (2015).

3. Poster presented at the Australian Synchrotron User Meeting, Melbourne, Australia, November 2017.

THE EFFECT OF WATER ON COLLAGEN NANO-STRUCTURE AND MECHANICS

S. J. Kelly[†], L. Bertinetti[¥], R. Weinkamer[¥], K. H. Sizeland[§], H. C. Wells[†], R. L. Edmonds[‡], P. Fratzl[¥] and R. G. Haverkamp[†]

[†]School of Engineering and Advanced Technology, Massey University, Palmerston North, 4442 New Zealand, [¥]Department of Biomaterials, Max Planck Institute of Colloids and Interfaces, Research Campus Potsdam-Golm, 14424 Potsdam Germany. [§]Australian Synchrotron, Clayton, Vic 3168, Australia, [‡]Leather and Shoe Research Association, Palmerston North, 4442 New Zealand.

Biological materials utilize water to control properties. Moisture content in collagen rich tissue, such as tendons, has been linked to reduced elasticity due to aging[1]. In processed collagen materials, such as extracellular matrix materials and leather, the moisture content has been linked to material stiffness[2,3] and changes in the collagen structure[4,5]. Here we investigate the effects of water, incorporated through relative humidity conditioning (40, 60 and 80%), on the collagen structure and mechanics of flexible and stiff ovine leather.

---

[1] Fratzl P and Weinkamer R, Nature's hierarchical materials. Prog Mater Sci 52:1263-1334 (2007).
[2] Fratzl P, Ed., Collagen: Structure and mechanics. Springer Science, New York (2008).
[3] Wells HC, Sizeland KH, Kirby N, Hawley A, Mudie S and Haverkamp RG, Collagen Fibril Structure and Strength in Acellular Dermal Matrix Materials of Bovine, Porcine and Human Origin. ACS Biomat Sci Eng 1:1026-1038 (2015).
[4] Meek KM and Knupp C, Corneal structure and transparency. Prog Retin Eye Res 49:1-16 (2015).
[5] Basil-Jones MM, Edmonds RL, Cooper SM and Haverkamp RG, Collagen fibril orientation in ovine and bovine leather affects strength: A small angle X-ray scattering (SAXS) study. J Agr Food Chem 59:9972-9979 (2011).

Appendix C. Oral Presentations

A list of conferences presentations involving this work from June 2016- November 2018.

1. Presentation delivered at the Australian Synchrotron User Meeting, Australia, November 2018.

Stiffness of modified collagen fibril structures manipulated by moisture content.

S J. Kelly[†], R. Weinkamer[‡], L. Bertinetti[‡], H. C. Wells[†], K. H. Sizeland[§], P. Fratzl‡ and R.G. Haverkamp[*]

[†]School of Engineering and Advanced Technology, Massey University, Palmerston North, New Zealand 4442, [‡]Department of Biomaterials, Max Planck Institute of Colloids and Interfaces, Research Campus Potsdam-Golm, 14424 Potsdam Germany. [§]Australian Synchrotron, Clayton, Vic 3168, Australia

Flexibility and strength are both desirable characteristics in skin derived collagen materials, like leather. Dehydration of skin during production of leather transforms tissue into a stiffer material. The hydration state is a key parameter in leather production controlling the material strength and flexibility. The structural basis for flexibility in leather was investigated and the moisture content varied. Mechanical properties of collagen are known to change with moisture content. Leather produced by tanning under strain increases the leather strength through increased fibril alignment but also reduces flexibility. Small angle X-ray scattering was used to determine collagen structures and three point bend tests to measure flexibility. Results show how the interplay between moisture content and fibril alignment can be used to optimize properties in leather.

2. Presentation delivered at the Max Plank Institute for Colloids and Interfaces, Germany, October 2017.

Effect of Collagen Alignment and Moisture Content on Leather Stiffness

S. J. Kelly[†], R. Weinkamer[‡], L. Bertinetti[‡], P. Fratzl[‡] and R. G. Haverkamp[†]

[†]School of Engineering and Advanced Technology, Massey University, Palmerston North, 4442 New Zealand, [‡] Max Planck Institute of Colloids and Interfaces, Research Campus Potsdam-Golm, 14424 Potsdam Germany.

Leather can be made from a variety of animals, each of which present different strengths and therefore use cases. Type 1 collagen is a major structural component of skin and in turn contributes significant properties to skin derived products such as leather. Analysing collagen structures in a variety of animal leather has revealed a link between fibril alignment and material strength, where a greater in-plane alignment results in stronger leather. Previous experiments, based on this concept, have shown that we can artificially align collagen fibrils to increase material strength. However, in the process of enhancing this property we compromise the materials flexibility. Since both flexibility and strength are desirable properties we want to better understand the relationship between structure, strength, stiffness and the mediating effects of moisture content.

3. Presentation delivered at the IULTCS Congress in Chennai, India, February 2017.

ARTIFICIALLY INDUCED COLLAGEN FIBRIL ORIENTATION AFFECTS TEAR PROPAGATION IN LEATHER

S. J. Kelly[†], K.H. Sizeland[†§], H.C. Wells[†], R. L. Edmonds[‡], C. Cole[‡], T. Ryan[§], N. Kirby[§], A. Hawley[§], S. Mudie[§], and R. G. Haverkamp[†]

[†]School of Engineering and Advanced Technology, Massey University, Palmerston North, 4442 New Zealand, [‡]Leather and Shoe Research Association, Palmerston North, 4442, New Zealand, [§]Australian Synchrotron, Clayton, Vic 3168, Australia.

Ovine leather has around half the strength of bovine leather and is therefore not suitable for high value applications such as shoes. For leather from a variety of animals, it has been found that the extent of collagen fibril alignment (orientation index) is closely correlated with the strength of the leather. We tested whether biaxial stretching for the duration of tanning or compressing pickled pelts prior to tanning, the ovine skins could increase the orientation index of the collagen fibrils and the strength of the final product. Control and test ovine skins were tanned using conventional chrome tanning methods. After the pickling and bating, the test skins were compressed between rollers before tanning or stretched bi-axially during the tanning process. The stretch applied was between 2.3%, 10% and 15% of the pickled pelts original length, either uniformly (10% and 10%) in both directions or with 2.3% in one direction and 7.5% in the other. Tear strengths were measured by standard methods in two directions, normal to one another relative to the backbone of the skin. Collagen fibril orientation was measured using synchrotron based small angle X-ray scattering, both edge on to the leather and flat on to the leather. The in-plane collagen fibril orientation index rose from ca. 0.45 to ca. 0.70 both with compression with rollers and biaxial stretching. With non-uniform biaxial stretching, there was an increase in the flat-on orientation index. Tear strengths are affected by both the in-plane fibril orientation. Tear propagation is resisted by collagen fibrils arranged at right angles to the tear front but propagates more readily along the direction of fibril. While it was possible to increase the collagen fibril orientation, this led to a direction specific tear strength increase rather than an overall increase in the skins tear strength, which has a more complex but rational behaviour.

4. Presentation delivered during the Australian Synchrotron User Meeting, November 2016.

Creating alignment for stronger leather

S. J. Kelly[†], H. C. Wells[†], K. H. Sizeland[‡] and R. G. Haverkamp[†]

[†] School of Engineering and Advanced Technology, Massey University, 4442, New Zealand and [‡] Australian Synchrotron, Clayton, Vic 3168, Australia.

Leather is essentially preserved skin with a few properties changed by the tanning process. Skin is made up of a layer of cells – the epidermis – which is supported by a collagen network that gives skin its structural strength. Structural strength requirements vary from place to place on the skin in the live animal – for example, linear strength is required over the limbs and along the body while flexible skin is required over joints. For structural strength, the collagen fibres in skin all need to be aligned in the same direction - something like a rope which is elastic and strong in one direction. For areas where skin needs to be flexible, the collagen fibres need to point in all directions, as in a mesh which forms a sort of net which has strength and flexibility in all directions. When skin is tanned to make leather, the strength and flexibility of the final product depends on the natural collagen alignment in the region of the hide from where the leather was obtained. We applied bi-axial stretching forces to sheep skins during the tanning process to see whether we could induce more parallel alignment of collagen fibres and hence increase the strength of the leather. We used SAXS analysis of normal and stretched sheep skins to determine if we had in fact changed the collagen fibre orientation and we used industry standard tear testing to compare the strength of the two products. Our results showed we could re-orient the collagen fibres and that the resultant product had greater strength and anisotropic qualities. Our studies indicate that we might not have to use certain parts of hides for certain leather products, for example, shoes from areas with great linear strength and clothes from more flexible areas. Instead, we can alter the natural collagen structure of skin during tanning and produce leather products with customized strength and flexibility characteristics.

Appendix D. Statement(s) of Contribution towards Publication

MASSEY UNIVERSITY

GRADUATE RESEARCH SCHOOL

STATEMENT OF CONTRIBUTION
TO DOCTORAL THESIS CONTAINING PUBLICATIONS

We, the candidate and the candidate's Principal Supervisor, certify that all co-authors have consented to their work being included in the thesis and they have accepted the candidate's contribution as indicated below in the Statement of Originality.

Name of Candidate: Susyn Kelly

Name/Title of Principal Supervisor: Professor Richard Haverkamp

Name of Published Research Output and full reference:

Mapping Tear Strength and Collagen Fibril Orientation in Bovine, Ovine and Cervine Hides and Skins

Kelly S., Edmonds, R., Cooper, S., Sizeland, K., Wells, H., Ryan, T., Kirby, N., Mudie S. and Haverkamp R., Mapping Tear Strength and Collagen Fibril Orientation in Bovine, Ovine and Cervine Hides and Skins. Journal of the American Leather Chemists Association 113 (1):1-11 (2018).

In which Chapter is the Published Work: Chapter 3.

Please indicate either:

- The percentage of the Published Work that was contributed by the candidate: **90%**

and/ or

- Describe the contribution that the candidate has made to the Published Work:

Candidate's Signature — November 2017 (Date)

Principal Supervisor's signature — 10 September 2018 (Date)

MASSEY UNIVERSITY

GRADUATE RESEARCH SCHOOL

STATEMENT OF CONTRIBUTION
TO DOCTORAL THESIS CONTAINING PUBLICATIONS

We, the candidate and the candidate's Principal Supervisor, certify that all co-authors have consented to their work being included in the thesis and they have accepted the candidate's contribution as indicated below in the Statement of Originality.

Name of Candidate: Susyn Kelly

Name/Title of Principal Supervisor: Professor Richard Haverkamp

Name of Published Research Output and full reference:

Artificially modified collagen fibril orientation affects leather tear strength.

Kelly S. J., Wells H. C., Sizeland K. H., Kirby N., Edmonds R. L., Ryan T., Hawley A., Mudie S. and Haverkamp
R. G., Artificially modified collagen fibril orientation affects leather tear strength. Journal of the Science of Food and Agriculture: DOI: 10.1002/jsfa.8863.

In which Chapter is the Published Work: Chapter 4.

Please indicate either:

- The percentage of the Published Work that was contributed by the candidate: 7**0%**

  and/ or

- Describe the contribution that the candidate has made to the Published Work:

Candidate's Signature

November 2017
Date

Principal Supervisor's signature

10 September 2018
Date

MASSEY UNIVERSITY

GRADUATE RESEARCH SCHOOL

STATEMENT OF CONTRIBUTION
TO DOCTORAL THESIS CONTAINING PUBLICATIONS

We, the candidate and the candidate's Principal Supervisor, certify that all co-authors have consented to their work being included in the thesis and they have accepted the candidate's contribution as indicated below in the Statement of Originality.

Name of Candidate: Susyn Kelly

Name/Title of Principal Supervisor: Professor Richard Haverkamp

Name of Published Research Output and full reference:

Effect of moisture content on collagen packing and stiffness in stretch-tanned leather.

Kelly S. J., Weinkamer R., Bertinetti L., Edmonds R. L., Sizeland K. H., Wells H. C., Fratzl P. and Haverkamp R. G., Effect of collagen packing and moisture content on leather stiffness, *Journal of the Mechanical Behavior of Biomedical Materials,* vol. 90, pp. 1-10, 2019/02/01/ 2019.

In which Chapter is the Published Work: Chapter 5.

Please indicate either:

- The percentage of the Published Work that was contributed by the candidate: 8**0%**

  and/ or

- Describe the contribution that the candidate has made to the Published Work:

Candidate's Signature

August 2018
Date

Principal Supervisor's signature

10 September 2018
Date

MASSEY UNIVERSITY

GRADUATE RESEARCH SCHOOL

STATEMENT OF CONTRIBUTION
TO DOCTORAL THESIS CONTAINING PUBLICATIONS

We, the candidate and the candidate's Principal Supervisor, certify that all co-authors have consented to their work being included in the thesis and they have accepted the candidate's contribution as indicated below in the Statement of Originality.

Name of Candidate: Susyn Kelly

Name/Title of Principal Supervisor: Professor Richard Haverkamp

Name of Published Research Output and full reference:

Data on collagen structures in leather with varying moisture contents from small angle X-ray scattering and three point bend testing.

S.J. Kelly, R. Weinkamer, L. Bertinetti, R.L. Edmonds, H.C. Wells, K.H. Sizeland, P. Fratzl:j: and R.G. Haverkamp. Data on collagen structures in leather with varying moisture contents from small angle X-ray scattering and three point bend testing. Submitted to Data in Brief, August 2018.

In which Chapter is the Published Work: Chapter 6.

Please indicate either:

- The percentage of the Published Work that was contributed by the candidate: **80%**

  and/ or

- Describe the contribution that the candidate has made to the Published Work:

Candidate's Signature — August 2018 (Date)

Principal Supervisor's signature — 10 September 2018 (Date)

MASSEY UNIVERSITY

GRADUATE RESEARCH SCHOOL

STATEMENT OF CONTRIBUTION
TO DOCTORAL THESIS CONTAINING PUBLICATIONS

We, the candidate and the candidate's Principal Supervisor, certify that all co-authors have consented to their work being included in the thesis and they have accepted the candidate's contribution as indicated below in the Statement of Originality.

Name of Candidate: Susyn Kelly

Name/Title of Principal Supervisor: Professor Richard Haverkamp

Name of Published Research Output and full reference:

Tropical keratopathy (Florida Spots) in Cats.

Bolfa P., Kelly S. J., Wells H. C., Sizeland K. H., Scott E. M., Kirby N., Mudie S., Armien A. G., Haverkamp R. G., and Kelly P. J., Tropical keratopathy (Florida Spots) in Cats. Journal of Veterinary Pathology: DOI: 10 .1177/0300985818789483.

In which Chapter is the Published Work: Chapter 8.

Please indicate either:

- The percentage of the Published Work that was contributed by the candidate: **40%**

and/ or

- Describe the contribution that the candidate has made to the Published Work:

Candidate's Signature

August 2018
Date

Principal Supervisor's signature

10 September 2018
Date